4.4.9.3 Bending moment weak axis

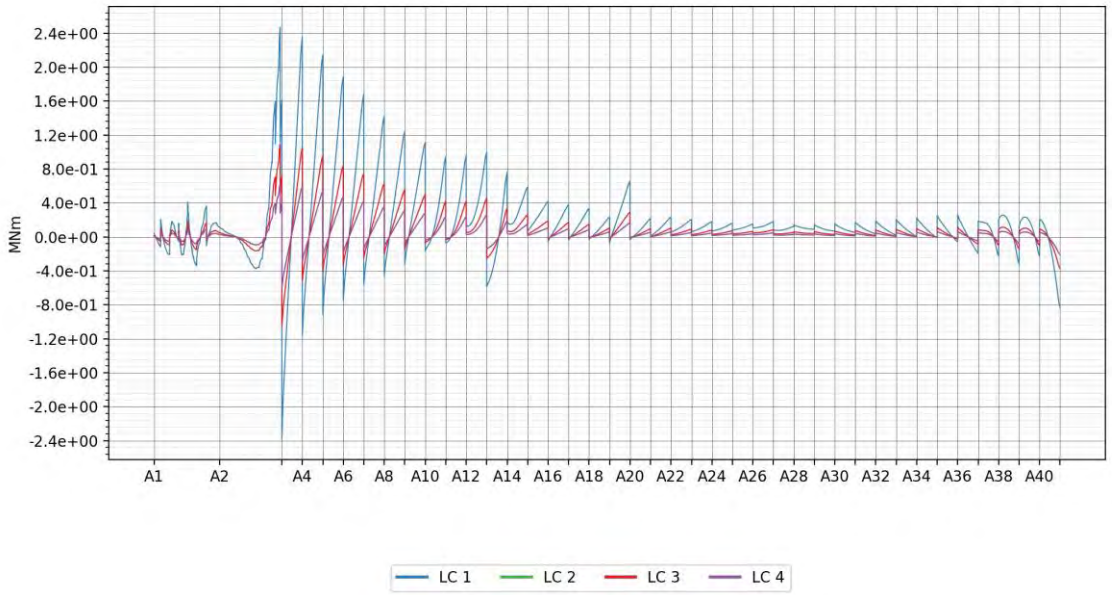

4.4.9.4 Torsional moment

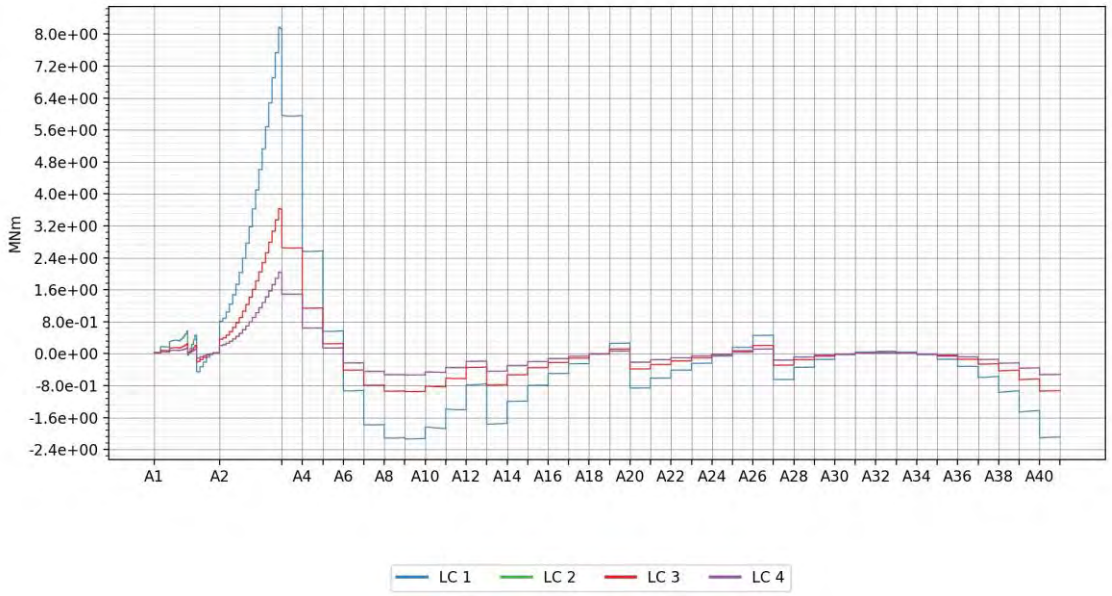

4.4.9.5 Vertical shear force

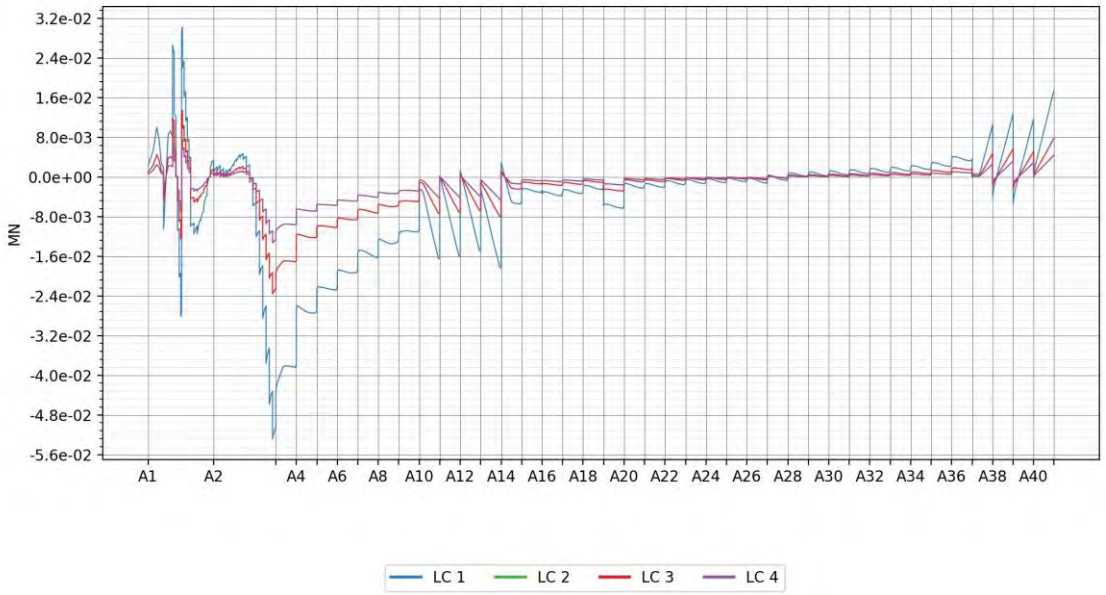

4.4.9.6 Transverse shear force

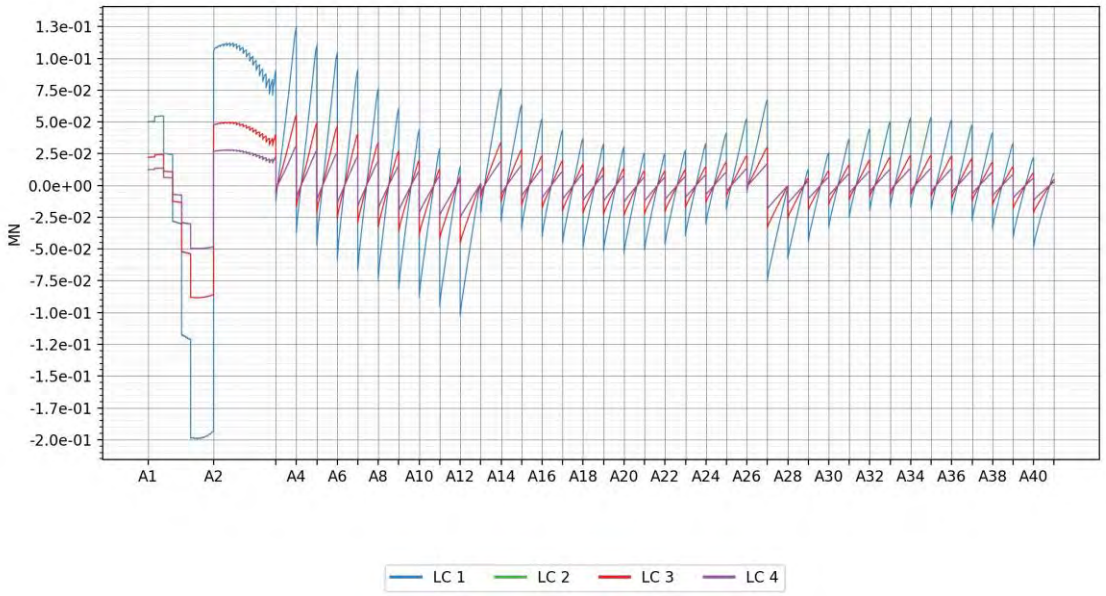

4.4.10 Tide

4.4.10.1 Axial force

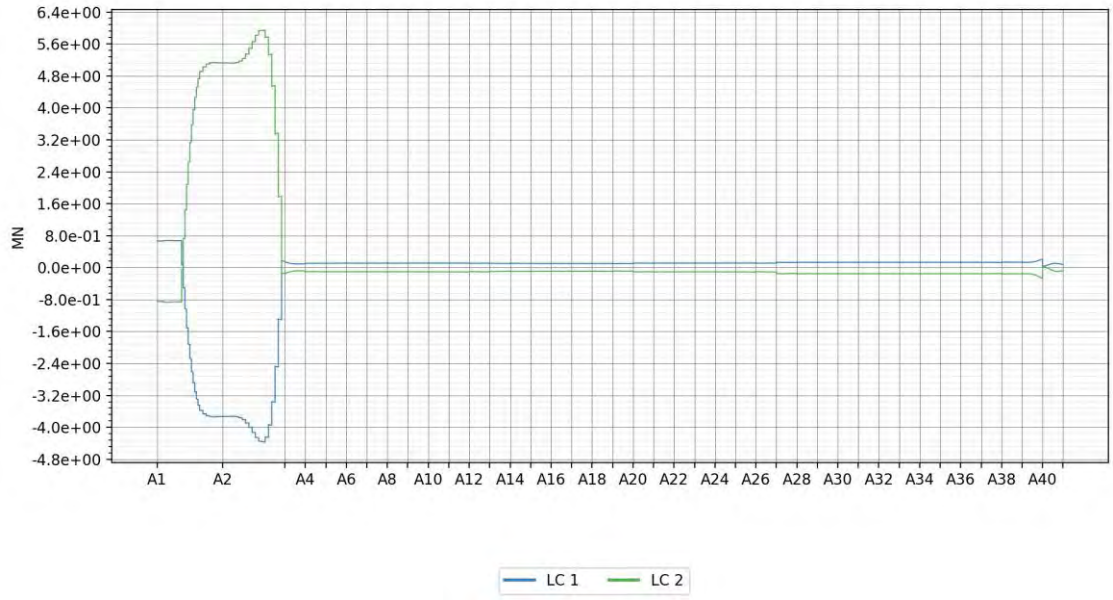

4.4.10.2 Bending moment strong axis

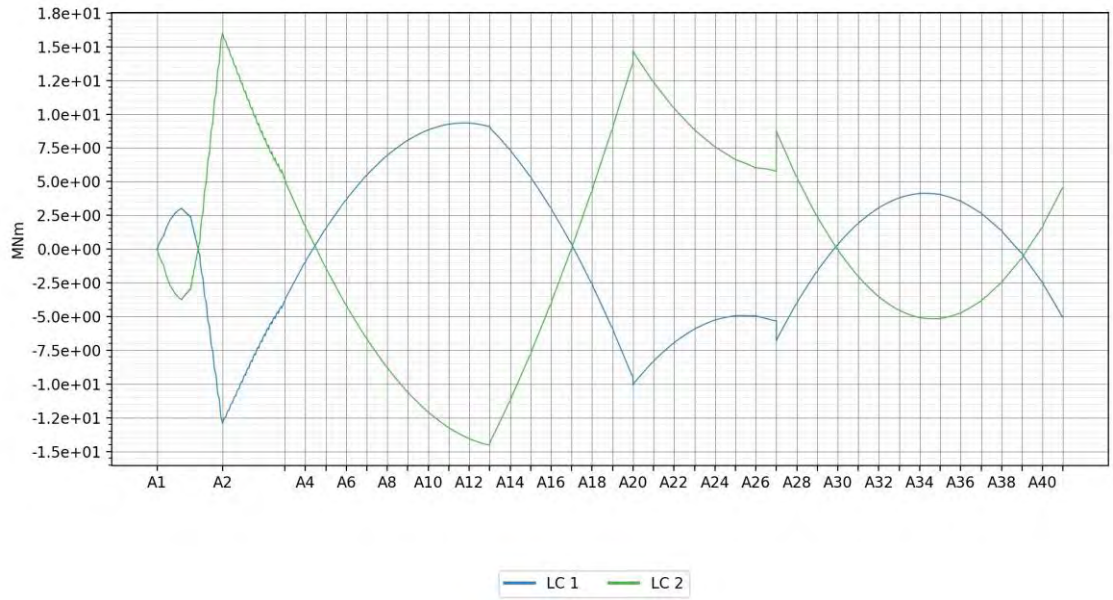

4.4.10.3 Bending moment weak axis

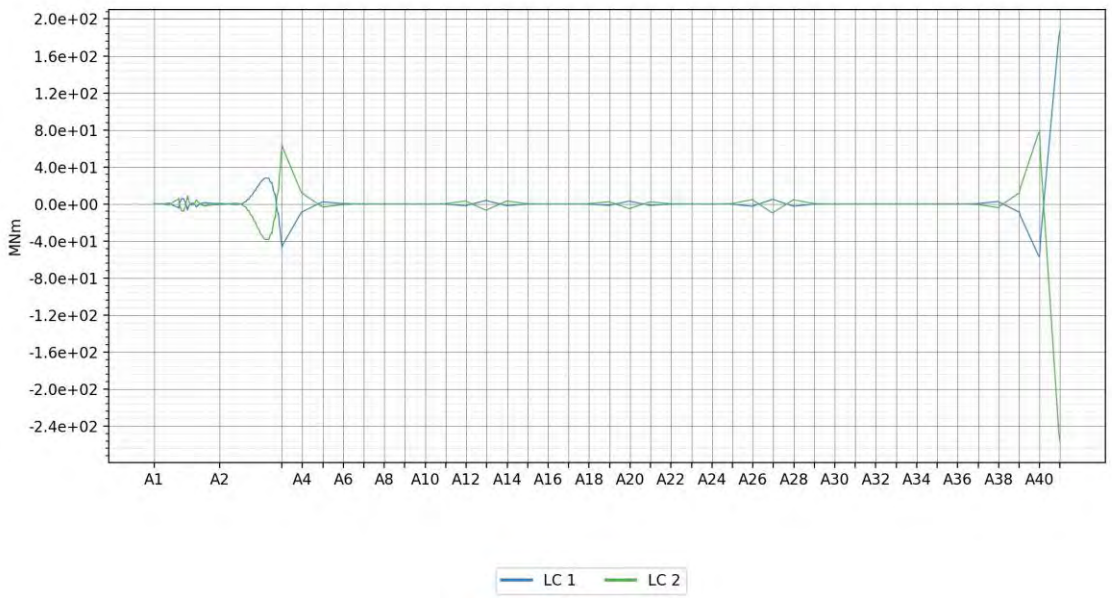

4.4.10.4 Torsional moment

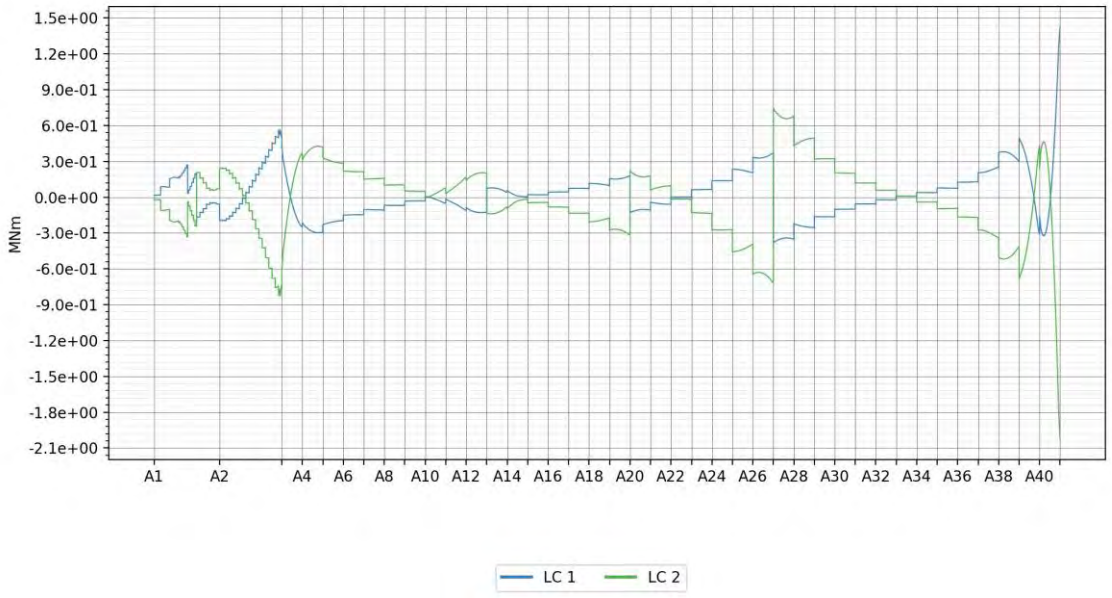

4.4.10.5 Vertical shear force

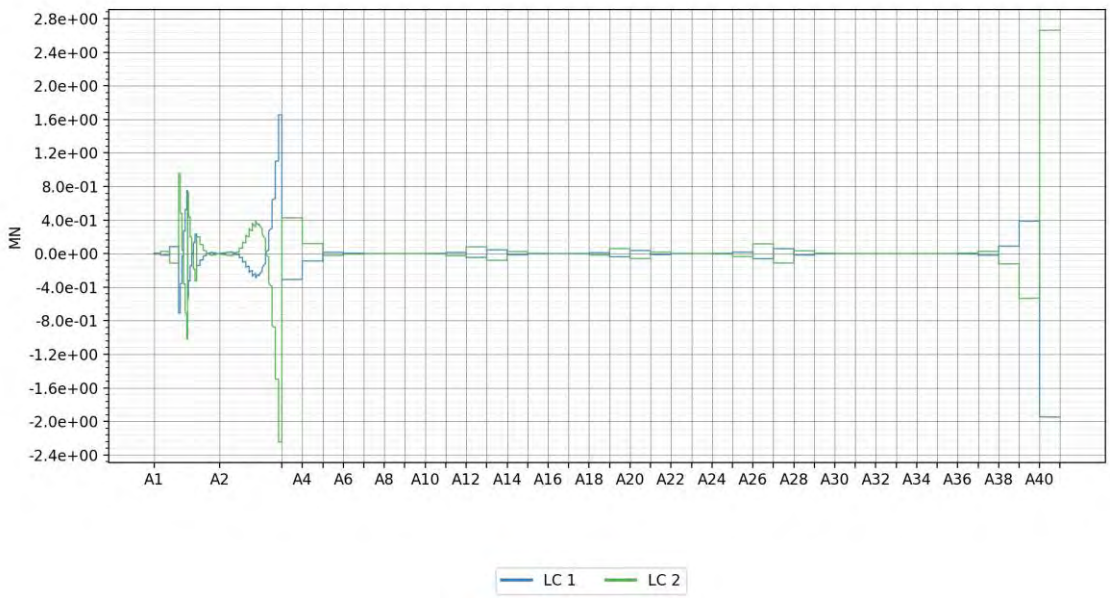

4.4.10.6 Transverse shear force

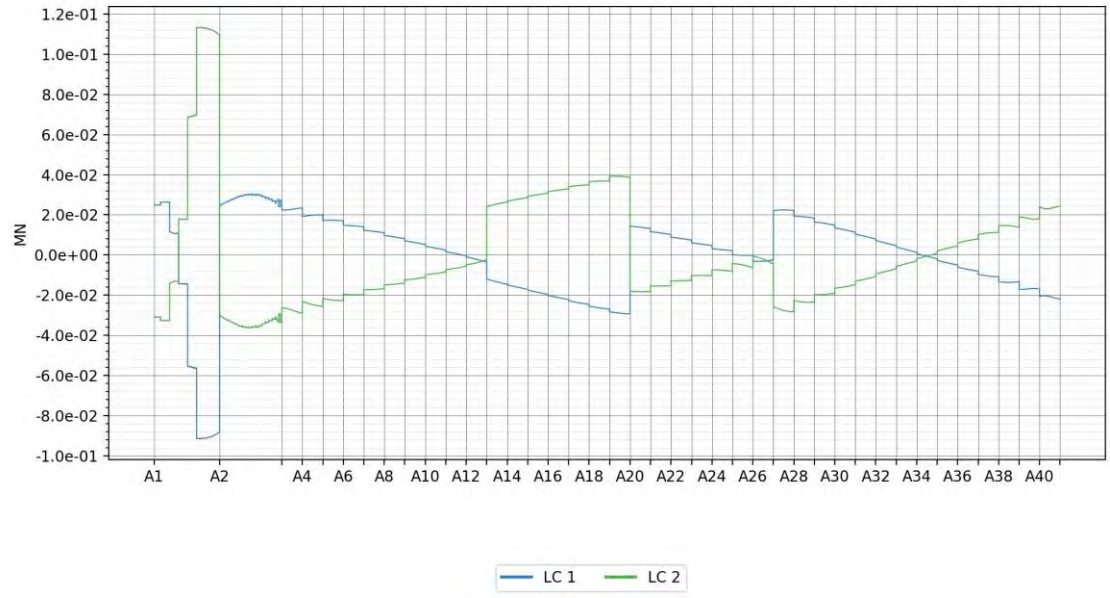

5 Comfort evaluation

As per Design Basis, ref. [9], the driver comfort while driving across the bridge shall be assessed considering the Overall Total Vibration Value (OVTV) as described in ISO 2631, ref. [10]. The below sections further detail the requirement, the methods applied, and the resulting OVTV values for each of the bridge concepts.

The evaluation was performed for the K12_05 iteration of the concept in which the mooring system different from the K12_07 iteration. Spot checks indicate that the motions in a one-year condition was fairly similar between the two iterations, and the results are thus considered valid.

5.1 Method

5.1.1 Requirements

The driver comfort shall be assessed based on the formula below as per ref. [9].

$$OVTV = \sqrt{k_{vs}^2 RMS_{vs}^2 + k_{ls}^2 RMS_{ls}^2 + k_{ps}^2 RMS_{ps}^2 + k_{rs}^2 RMS_{rs}^s + k_{vb}^2 RMS_{vb}^2 + k_{lb}^2 RMS_{lb}^2 + k_{vf}^2 RMS_{vf}^2 + k_{lf}^2 RMS_{lf}^2}$$

- RMS-values are based on accelerations in vertical and lateral directions experienced by the driver, as well as roll and pitch rotations. Longitudinal direction and yaw rotation are not to be included.
- k-values are multiplication factors as specified in [9].

In addition to the above terms, a frequency weighting function shall be applied on the acceleration spectra prior to calculating the RMS values, ref. [9].

For the assessment, a vehicle model accounting for the stiffness, mass and damping characteristics of representative vehicles shall be considered implemented in the analyses. An evaluation should be performed to assess the importance of modelling the vehicle as compared to basing the accelerations on the girder accelerations directly. Vehicle properties have been provided by SVV in [11].

The following response contributions shall be considered to establish vehicle response:

- Dynamic response of bridge
    - The forward speed of the vehicle shall be accounted for.
- Wind actions on the vehicle. Vehicle wind coefficients have been provided by SVV in [11].

The following acceptance criteria applies to the driver comfort assessment:

- OVTV shall not exceed 0.315 m/s^2 in 1-year environmental conditions, at a driving speed of 70 km/h.

If this criterion is not fulfilled, an uptime assessment shall be documented, where the necessary reduced speed limit during the year shall be reflected.

5.1.2 Assumptions

The following assumptions are considered:

- In accordance with the Design Basis, ref. [9], only one point in the vehicle is considered to represent the floor, seat and backrest accelerations. It is however assumed that the

multiplication factors and frequency weighting functions applicable to each point shall still be used.

- Only 1 off vehicle model is required to be established and checked in the analyses. This vehicle should represent a typical size sedan, the parameters of which were given by SVV [12, 13].
- The acceptance criteria shall be assessed as an average OVTV value for the entire bridge.

5.1.3 Approach

5.1.3.1 Complete assessment

For complete assessment of the comfort criteria, analyses including the following effects are required:

- Time domain analyses of bridge dynamics due to environmental loads
- Vehicle model analyses where the vehicle is subject to the dynamics of the bridge and the wind loading corresponding to the wind loading applied on the bridge

For the analysis setup applied in this project, such analyses require time domain analyses to get correspondence between wind applied on the bridge and on the vehicle. Time domain analyses are time consuming, and an alternative approach has therefore been applied for the current stage of the project.

5.1.3.2 Alternative approach

The following alternative approach is considered:

- Wave induced bridge dynamics are obtained based on Frequency Domain (FD) analyses in Orcaflex.
- Wind induced bridge dynamics are obtained based on FD analyses in Novaframe.
- Wind loading on vehicle is obtained as realizations of the wind field along the bridge using WindSim.

Based on these analyses, the OVTV is obtained from three separate contributions, where it is assumed that there is no dynamic amplification of vehicle accelerations when exposed to bridge dynamics. Forward speed of the vehicle is considered in each of the analyses.

- OVTV based on wave induced bridge dynamics.
- OVTV based on wind induced bridge dynamics.
- OVTV based on wind loading on vehicle model.

The total OVTV value is obtained as the sum of each contribution. The level of conservatism in this approach remains to be investigated by comparing with the complete assessment.

5.1.4 Bridge dynamics

Bridge dynamics based on both Orcaflex and Novaframe are calculated in the frequency domain. Built in functionality in each software is used to generate synthesized timeseries of the response at each node along the bridge girder, accounting for the relative phase information between nodes.

Having obtained the response in each node of the bridge girder, this data is further processed to account for the offset position of the vehicle relative to the reference node. The offset is accounted for by the below equations,

$$Y_{dynamic,offset} = Y_{dynamic} + \Delta y \cos\left(Roll_{dynamic}\right) - \Delta z \sin\left(Roll_{dynamic}\right) - \Delta y$$
$$Z_{dynamic,offset} = Z_{dynamic} + \Delta z \cos\left(Roll_{dynamic}\right) + \Delta y \sin\left(Roll_{dynamic}\right) - \Delta z$$

where $Z_{dynamic,offset}$ is the new vertical motion timeseries, $Z_{dynamic}$ is the original vertical motion timeseries, Δy and Δz are the lateral and vertical offsets from the node, and $Roll_{dynamic}$ is the roll timeseries. Further, Y describes the lateral motion.

For calculation of the OVTV, the forward speed of the vehicle is included. With respect to bridge dynamics, the effect of forward speed is important to account for the encounter frequency, which leads to a shift in frequencies associated with the energy in the power spectrum.

The nodal bridge dynamic timeseries are thereafter used to establish vehicle timeseries as motion timeseries the vehicle experiences as it crosses the bridge. These timeseries are obtained by interpolating the node motion timeseries at the position of the vehicle at each timestep of the crossing duration. The following steps are taken to obtain the vehicle timeseries:

- Establish the vehicle positions along the bridge profile at each timestep as function of vehicle speed
- For each vehicle position, identify the closest nodes before and after the vehicle position
- Interpolate the node motion timeseries at each timestep with respect to the vehicle position relative to the closest nodes. The following equation shows the linear interpolation applied for vertical motion

$$Z_{vehicle\ pos} = \frac{Z_{node\ after} - Z_{node\ before}}{P_{node\ after} - P_{node\ before}} \left(P_{vehicle\ pos} - P_{node\ before}\right) + Z_{node\ before}$$

where $Z_{vehicle\ pos}$ is the vertical motion of the vehicle at a given timestep, $Z_{node\ after}$ and $Z_{node\ before}$ is the vertical motion of the nodes after and before the position of the vehicle, $P_{node\ after}$ and $P_{node\ before}$ is the position of the nodes along the bridge profile, and $P_{vehicle\ pos}$ is the vehicle position along the bridge profile.

The same interpolation is applied also for the other degrees of freedom; lateral, roll and pitch. The resulting vehicle timeseries will have a duration defined by the length of the bridge profile and the vehicle speed. Further, the vehicle timeseries will change when varying the vehicle start time. Multiple realizations are therefore established by obtaining the vehicle timeseries starting at different timesteps of the input timeseries.

5.1.5 Vehicle dynamics

Vehicle dynamics are obtained using Python to establish a vehicle model and solve the equation of motion as the vehicle travels across the bridge. For the alternative approach considered at this stage, the loading on the vehicle is obtained by combining the wind field along the bridge with the forward speed of the vehicle as it crosses the bridge to generate the relative wind speed and relative heading.

For the full time domain approach, also the relative speed and displacement between the bridge girder and the vehicle suspension would be included.

The wind field along the bridge is obtained using WindSim to model the field and assigning wind speed timeseries to selected nodes along the bridge. The approach used to establish these wind timeseries is the same as used for other wind analyses in Orcaflex, with the same input parameters.

To establish the wind loading on the vehicle, the following steps are taken:

1. Obtain the position of the vehicle at each timestep of the wind timeseries. This is found by multiplying the vehicle speed with the timesteps, until the vehicle has covered the full arc length.
2. Wind timeseries of the global x- and y-component wind speeds are established as a continuous timeseries for the position of the vehicle during crossing. This is obtained using the same interpolation scheme as given in section 5.1.4. Based on these wind component timeseries, the total wind and wind heading is established.
3. The vehicle heading while crossing the bridge is obtained by assessing the angle between each node of the bridge in the global x- and y-coordinate system. For convenience the vehicle headings are established at the same timesteps as used for wind heading.
4. The wind direction on vehicle, α, is found by combining the wind heading and vehicle heading at each timestep.
5. The relative wind velocity and heading is found by combining the wind direction on the vehicle with the wind speed and vehicle speed. In this, the vehicle speed is constant, while the wind direction on vehicle and the wind speed will vary for each timestep. The equation is given in [11].
6. Based on the relative wind heading, the corresponding aerodynamic coefficients are found based on regression coefficients given in [11]. However, note that the given regression coefficients are non-zero for 0 degrees relative wind heading. For sway and roll, this leads to steps in the loading when crossing from +0 to -0 deg relative wind heading, as the sign of the non-zero wind load changes. To omit this the regression coefficients are modified by removing the non-zero constant term, and factorizing the coefficients to arrive at the original maximum coefficient. The change is shown in Figure 5-1.

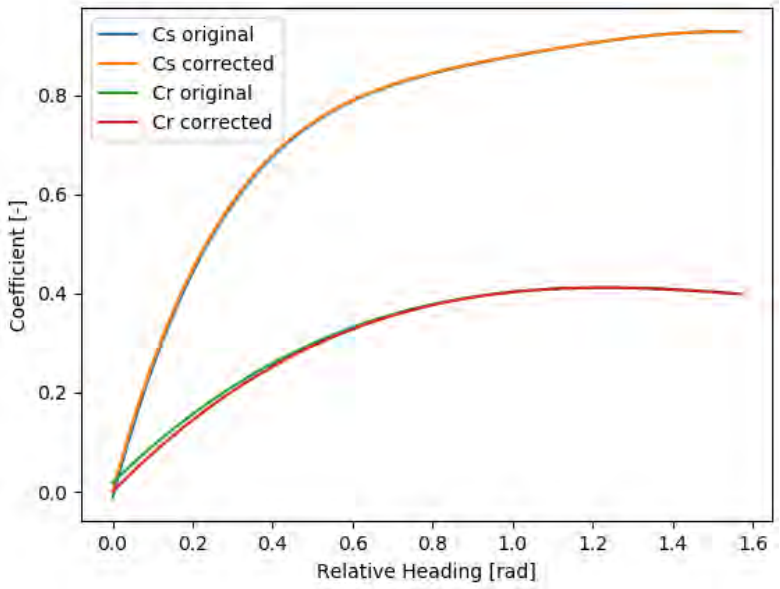

Figure 5-1 Corrected aerodynamic coefficients

7. The wind loading is finally obtained for sway, lift and roll as functions of the aerodynamic coefficients and the relative wind speed, as detailed in [11]. The sign of the relative wind heading is used to determine the load direction for sway and roll.
    a. To include the effect of aerodynamic damping, the relative wind speed is corrected by including the relative velocity of the vehicle while solving the equation set described below. This is done by first obtaining the lateral component of the relative wind speed, and then combine this with the lateral speed of the vehicle, to obtain a relative velocity accounting for the wind induced lateral motions of the vehicle. The lateral velocity of the vehicle is very small compared to the relative wind speed and is therefore assumed not to affect the relative wind heading. However, the effect of accounting for the wind-induced vehicle motions provides an important damping contribution to the model.

The vehicle model is established using the data provided by SVV, ref. [11], as input to the equation of motion:

$$\boldsymbol{M\ddot{u} + C\dot{u} + Ku = F}$$

where M, C and K are the vehicle mass, damping and stiffness matrices, $\ddot{u}$, $\dot{u}$ and u are the acceleration, velocity and displacement vectors, and F is the external force vector.

This equation is solved as a differential equation, using the Python function "solve_ivp" from the Scipy library, by defining the following equations from the equation of motion:

$$\boldsymbol{y = \dot{u}}$$

$$\boldsymbol{\dot{y} = FM^{-1} - CM^{-1}\dot{u} - KM^{-1}u}$$

Note that the timestep used when solving this set of equations is defined within the "solve_ivp" function. The wind loading $\boldsymbol{F}$ is found as a function within "solve_ivp", where the relative wind headings are interpolated to obtain the wind coefficients, and the wind loading is obtained accounting for the instantaneous lateral velocities of the vehicle. The same approach would apply for road velocity and displacement when including these effects in the full time domain approach.

5.1.6 Calculation of OVTV

To evaluate the OVTV criteria, acceleration spectra are required. These are needed to apply the frequency weighting functions prior to finding the RMS value. The frequency weighting functions are established based on the equations given in ISO 2631-1, ref. [10].

Before establishing the spectra, the timeseries are pre-processed first by subtracting the mean value, and secondly by applying a Tukey window, ramping the first and last 0.5% of the timeseries from a factor of 0 to 1.

The motion spectra are obtained using Fast Fourier transformation, and converting the spectra to one-sided. To ensure that the variance of the spectra correspond to the variance of the original timeseries, the variance of the timeseries prior to applying the Tukey window is obtained, in addition to the variance of the generated spectra. Thereafter, the spectra amplitudes are corrected by the factor $\frac{Var_{Original}}{Var_{Spectra}}$. This factor typically shows < 1% difference.

To convert the motion spectra to acceleration spectra, the following derivation is used:

Considering $z = Asin(\omega t)$, then the corresponding acceleration is be $\ddot{z} = -\omega^2 Asin(\omega t)$. The amplitudes of a harmonic vibration are related to the spectrum by:

$$A^2 = 2S_z(\omega)d\omega$$
$$(\omega^2 A)^2 = 2S_{\ddot{z}}(\omega)d\omega$$

The acceleration spectrum can be expressed as a function of the motion spectrum:

$$S_{\ddot{z}}(\omega) = \omega^4 S_z(\omega)$$

The equation for determining OVTV consist of RMS results and factors for 8 different combinations of position and degree of freedom (DOF). Table 5-1 below shows how each position and DOF is combined, weighted and factored.

Combination number, i	DOF	Position	Weighting Function	Multiplication Factor	RMS name
1	Vertical	Seat	Wk	kvs	RMSvs
2	Lateral	Seat	Wd	kls	RMSls
3	Pitch	Seat	We	kps	RMSps
4	Roll	Seat	We	krs	RMSrs
5	Vertical	Backrest	Wd	kvb	RMSvb
6	Lateral	Backrest	Wd	klb	RMSlb
7	Vertical	Floor	Wk	kvf	RMSvf
8	Lateral	Floor	Wk	klf	RMSlf

Table 5-1 OVTV Combination Matrix

The following steps are taken to assess the OVTV criteria based on the established spectra:

- Establish the frequency weighted acceleration spectrum for each combination:

  $$S_{i,weighted}(f) = S_i(f) * W_i(f)$$

  where $S_i(f)$ is the acceleration spectrum for combination number i, and $W_i(f)$ is the corresponding frequency weighting function

- Obtain the RMS value of the weighted spectrum, by the square root of the spectral area / variance:

$$RMS_i = \sqrt{\sum_{j=1}^{N} S_{i,weighted}(f_j) df_j}$$

where N is the total number of frequencies in the spectrum, j is the frequency number, and df_j is the frequency band for the considered spectral amplitude. Note that the frequency band is determined for each spectral amplitude, to account for the possibility of unequal frequency steps.

- Finally, the OVTV value is obtained:

$$OVTV = \sqrt{\sum_{i}^{n} RMS_i^2 \, k_i^2}$$

where n is the total number of combinations and k_i is the corresponding multiplication factor.

5.2 Load input

The basic requirement for OVTV is to be below 0.315 m/s^2 in 1-year environmental conditions. For the alternative approach considered at this stage, 1-year values for both wind and wave have been applied, meaning that joint-probability considerations have not been accounted for. Table 5-2 shows the applied environmental conditions.

Table 5-2 Applied environmental conditions

Heading - Coming from	Hs	Tp	Wind Speed
[deg]	[m]	[s]	[m/s]
0			
30			
60	0.45	3.2	15
90	1	4	18.2
120	0.85	3.8	18.2
150	0.94	3.5	18.2
180	0.8	3.2	18.2
210	0.85	3.8	18.2
240	0.8	3.2	19.3
270	1	3.5	21.4
300	1.2	4.3	21.4
330	0.65	3.8	21.4

Wave data is based on the 1-year contour plots provided in Metocean, ref. [5]. Sensitivity analyses have been performed along the contours, showing that the highest periods give the highest OVTV, when combined with high waves. The sensitivity was done in steps of 0.5 s from 1 s, and shows that high frequent wave loading is not governing based on the current models. Sensitivities are also done with the peak enhancement factor and spreading exponent, resulting in 2.3 and 3 respectively as the most critical.

Wind data is obtained as the 1-year wind from ref. [5].

Note that contour data for waves from 0 and 30 degrees is not provided in ref. [5]. These headings are therefore omitted in the analyses herein.

For the analyses based on bridge motions, a vehicle offset from the result nodes of 8.5 m laterally and 2.5 m vertically is applied in the analyses to account for the position of the vehicle relative to the bridge girder neutral axis. Further, 500 vehicle crossings are simulated for each driving direction, starting from north and south. A vehicle speed of 70 km/h and a timestep of 0.2 s is used.

For the wind on vehicle model analyses, 30 off crossings are simulated for each environmental heading, driving from south to north only. The limited extent of this is due to the computational time, and the observed results showing that further work will be needed on this. A timestep of 0.1 s is used.

5.3 Results

Considering the alternative approach applied herein, the OVTV is obtained by combining the contribution from each of the three analyses. However, as will be shown, the OVTV obtained from wind loading on the vehicle is very high, exceeding the OVTV criteria significantly. Results will therefore be presented for the wind and wave induced bridge motions separately, and thereafter for the vehicle.

OVTV based on wave induced bridge motions is seen to behave as expected, where combinations of high Hs and high Tp gives the governing results. Results are presented in Figure 5-2, where a maximum OVTV of 0.059 m/s^2 is seen.

OVTV based on wind induced bridge motions is also seen to behave as expected, where the highest wind speeds from the northwestern sector governs results. A maximum OVTV of 0.055 m/s^2 is seen.

The overall OVTV results considering bridge motions only is also presented. A maximum OVTV of 0.114 m/s^2 is obtained for K12 for environmental loading from 300 degrees.

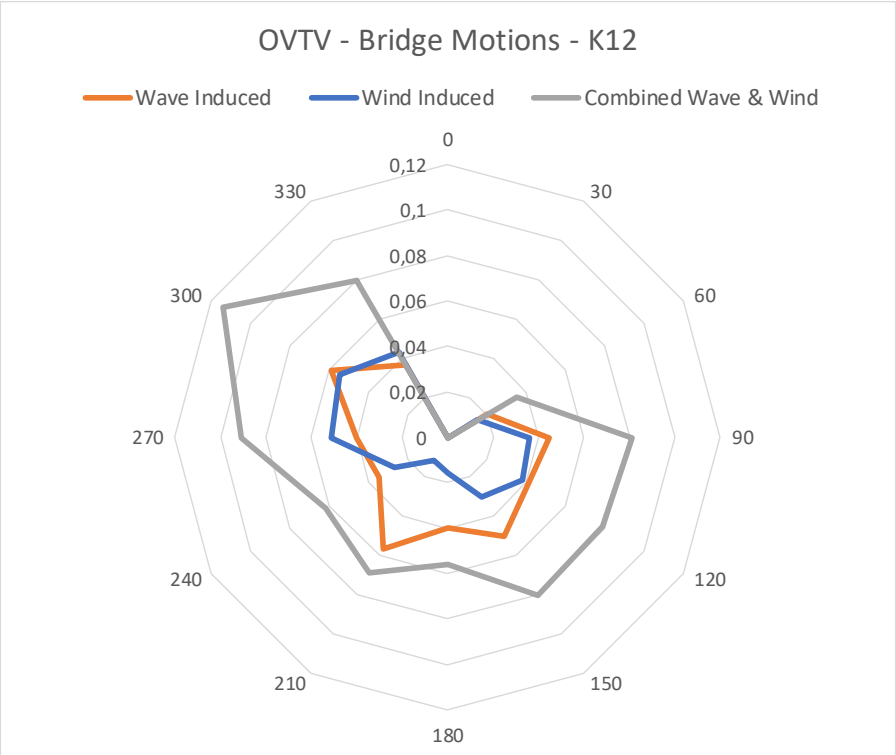

Figure 5-2 OVTV – Wave & Wind Induced Bridge Motions

For the results of the wind acting on the vehicle directly, the results significantly exceed the OVTV requirement. The results are presented in Figure 5-3, showing a maximum OVTV of approximately 0.95 m/s^2 when accounting for aerodynamic damping. Comparing these results with analyses performed without aerodynamic damping, it is found that the most critical heading improves by approximately 25%, while for the pure lateral wind headings the results improve even further. This trend is as expected and demonstrates the importance of the aerodynamic damping for the local vehicle response.

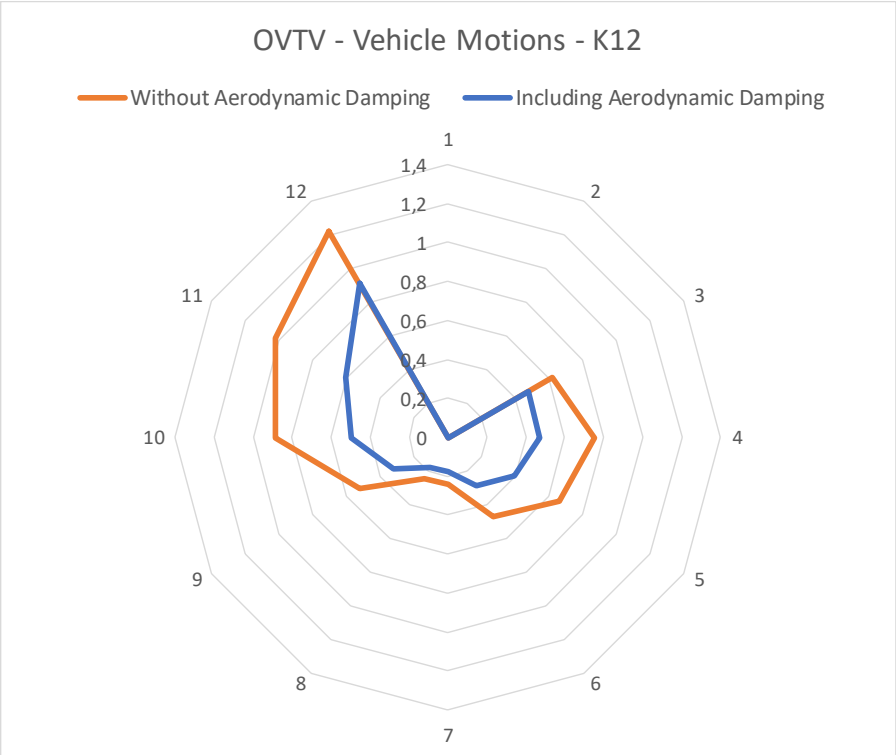

Figure 5-3 OVTV – Wind on vehicle model

Investigating the vehicle timeseries, shown in Figure 5-4, it is found that the sway motion of the vehicle has significant high frequent content. These results include the aerodynamic damping, but still the high frequent energy in the wind spectrum results in vibrations throughout the timeseries. The results are however much better than without aerodynamic damping, as shown in Figure 5-5. Aerodynamic damping is seen to reduce the maxima and give more rapid decays. This shows that properly determining all vehicle damping contributions in sway is very important for the overall results.

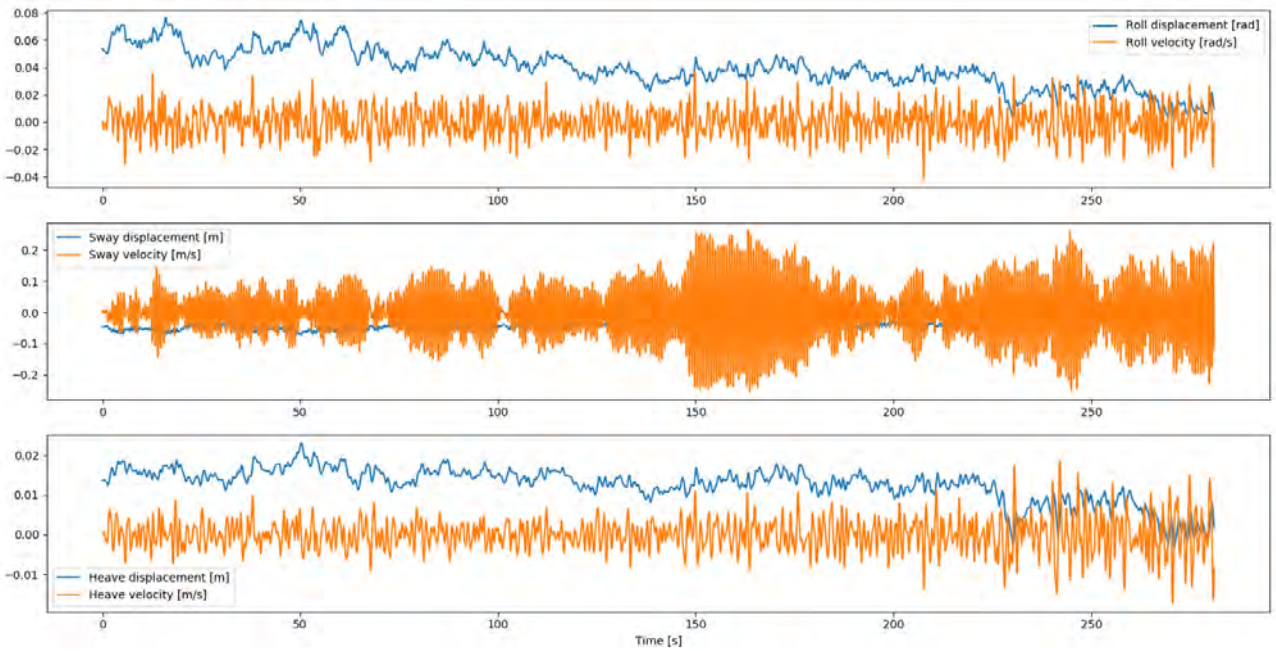

Figure 5-4 Timeseries of vehicle response during one bridge crossing – wind from 330 degrees

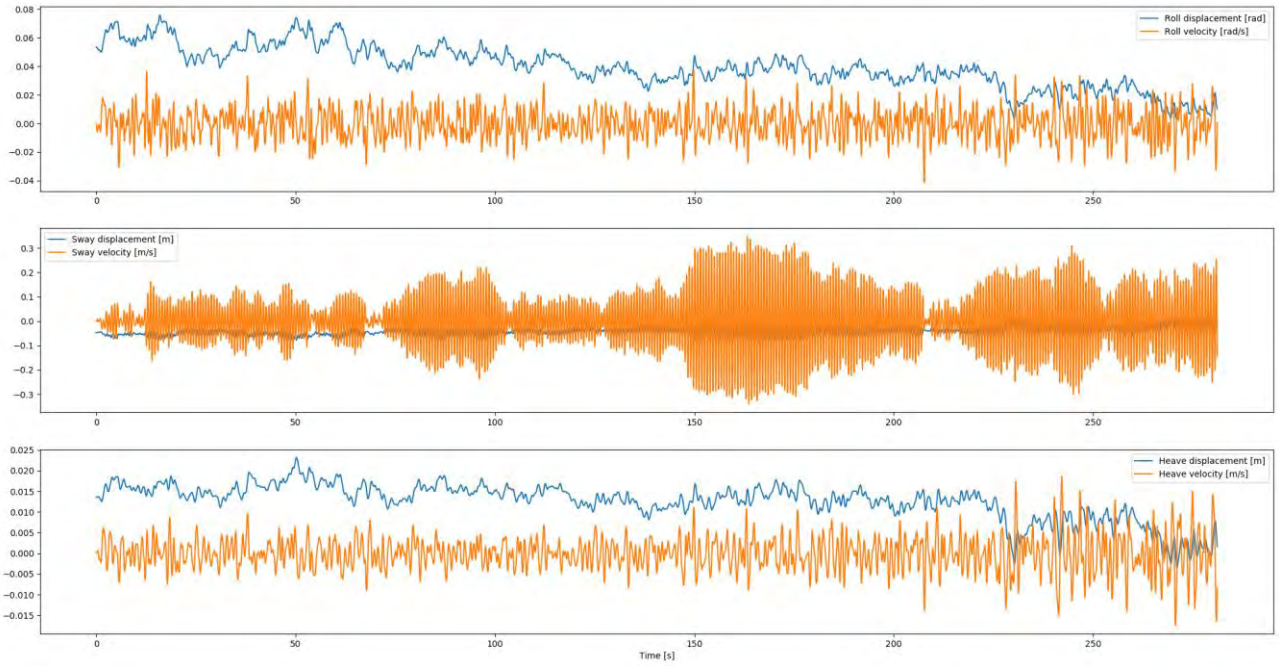

Figure 5-5 Timeseries of vehicle response during one bridge crossing – wind from 330 degrees – Without aerodynamic damping

5.4 Discussion

The OVTV criterion serving as basis for assessing the driving comfort is in an early phase of being implemented for floating bridges, and hence a proper threshold value correctly representing drivable conditions remains to be defined following further initiatives currently undertaken by SVV. The results presented herein are compared with the current threshold, but future findings could well lead to a different threshold value to be applied.

As a general comment, the reduction of wave condition from the metocean design basis in phase 3 to phase 5 of the project gives a significant reduction of bridge motions, and it is expected that the same would be observed if comparing OVTV results of the two phases.

Evaluation of the OVTV criterion for the K12_05 concept shows that the utilization from bridge motion alone is low, in the range of 1/3 of the allowable value. When including wind loading on the vehicle the OVTV contribution from dynamic bridge response is about 12% of the total OVTV utilization. Based on the OVTV evaluation for wind on a stationary vehicle it is observed that the vehicle damping level in sway is very important for the overall results. If the assumed sway damping is correct, the findings show that the OVTV criterion is dominated by the local wind loads on vehicle.

A few effects could be considered in further work, possibly reducing the lateral accelerations:

- Time-dependent aerodynamic coefficients accounting for the time required to get stable drag and lift coefficients
- Effect of forward speed on vehicle response parameters

6 Ultimate limit state capacity

6.1 General

The bridge is designed in ULS using the partial factor method according to Eurocode. Load combination factors are taken from Table 8 in the Design basis [9].

Three load combinations were considered for the design in ULS:

- **ULS1: Dominating permanent load (G-EQ$_K$).** Traffic is included with 1 year environmental load.
- **ULS2: Dominating traffic (Q-Trf$_K$)**. Traffic is included with 1 year environmental load.
- **ULS3: Dominating environmental load (Q-E$_{env(100y)}$).** 100 years environmental load is included. Bridge is closed for traffic.

It is also possible to develop additional load combinations by other load groups as dominant loads. However, based on previous experience these combinations will not be governing. The bridge girder is mainly governed by ULS3 for strong-axis response and ULS2 for weak-axis response. ULS1 was not considered dimensioning and is not reported further herein.

In the following sections combination info is given for each ULS combination along with summarized design forces in the different parts of the bridge. Detailed results are given in the enclosures to this report, both for the factorized and direct method.

In the combinations, dynamic environmental loads have been estimated to the expected maximum value for a 1-hour storm. The estimation is based on a single 1-hour realization, with the individual dynamic load groups analyzed separately and combined in the postprocessing. Hence, there is an uncertainty in the extreme response level that should be considered when using the results. A comparison of uncoupled combined results and coupled environmental conditions with all load components are shown in section 0, and shows that for the simulated conditions the combination factors used for uncoupled simulations are acceptable.

Mooring line response is assessed using both uncoupled and coupled simulations. Due to the nonlinear stiffness of the mooring clusters the coupled approach yields the most accurate results.

6.2 ULS response

Two iterations of the concept were used in the results reported in the following. The bridge girder response (section 6.2.3) was documented with the latest model iteration, the K12_07 model, but the tables for response for the other structural elements (section 6.2.4 to 6.2.11) were not updated from K12_06. The difference between the two model iterations were minor stiffness changes in the bridge girder, and the K12_06 results are considered valid for the other structural elements.

6.2.1 Load group info ULS2

The ULS2 combination contains 1-year environmental conditions together with traffic. Wind loading on the bridge is calculated based on drag coefficients without traffic on the bridge and may thus be somewhat underestimated. See section 8.5 for a separate sensitivity study on ULS response with traffic loading. ULS2 yields the dimensioning weak-axis moment due to the weight of traffic.

Table 6-1 Combination into – ULS2

Load group	Load_factor	Return_period [years]	Software system	Result type
Permanent	1.20	N/A	RM Bridge	Static
Temperature	0.84	N/A	RM Bridge	Static
Traffic	1.35	N/A	RM Bridge	Static
Tide	1.12	100	Orcaflex	Static
Dynamic wind 1 y	1.12	1	Orcaflex	Time series
Static wind 1y	1.12	1	Orcaflex	Static
Wave 1 y	1.12	1	Orcaflex	Time series
Swell 1 y	1.12	1	Orcaflex	Time series
Current	1.12	100	Orcaflex	Static

The mooring line response is given as characteristic values, not including load factors.

6.2.2 Load group info ULS3

Table 6-2 Combination into – ULS3

Load group	Load_factor	Return_period [years]	Software system	Result type
Permanent	1.20	N/A	RM Bridge	Static
Temperature	0.84	N/A	RM Bridge	Static
Tide	1.60	100	Orcaflex	Static
Dynamic wind 100 y	1.60	100	Orcaflex	Time series
Static wind 100 y	1.60	100	Orcaflex	Static
Wave 100 y	1.60	100	Orcaflex	Time series
Swell 100 y	1.60	100	Orcaflex	Time series
Current	1.60	100	Orcaflex	Static

6.2.3 Bridge girder

The amplitude of the ULS3 strong-axis bending moment is somewhat less than the moment from ship collisions. Towards the Northern abutment ULS3 response is less than that from ship collisions. Torsional moments in the bridge girder are higher for ULS3 than ship collision for all concepts. See [14] for details on ship collision response.

The weak-axis bending moment at the north abutment are relatively high, but this is a very local effect that has been accounted for in the structural design of the bridge girder.

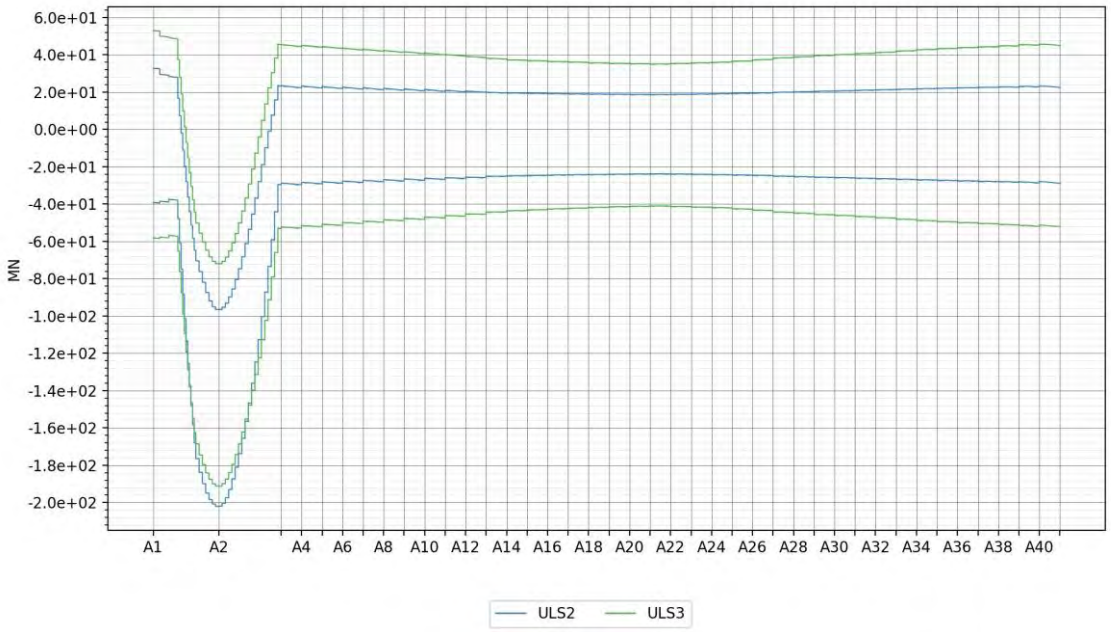

Figure 6-1 Bridge girder axial force – ULS

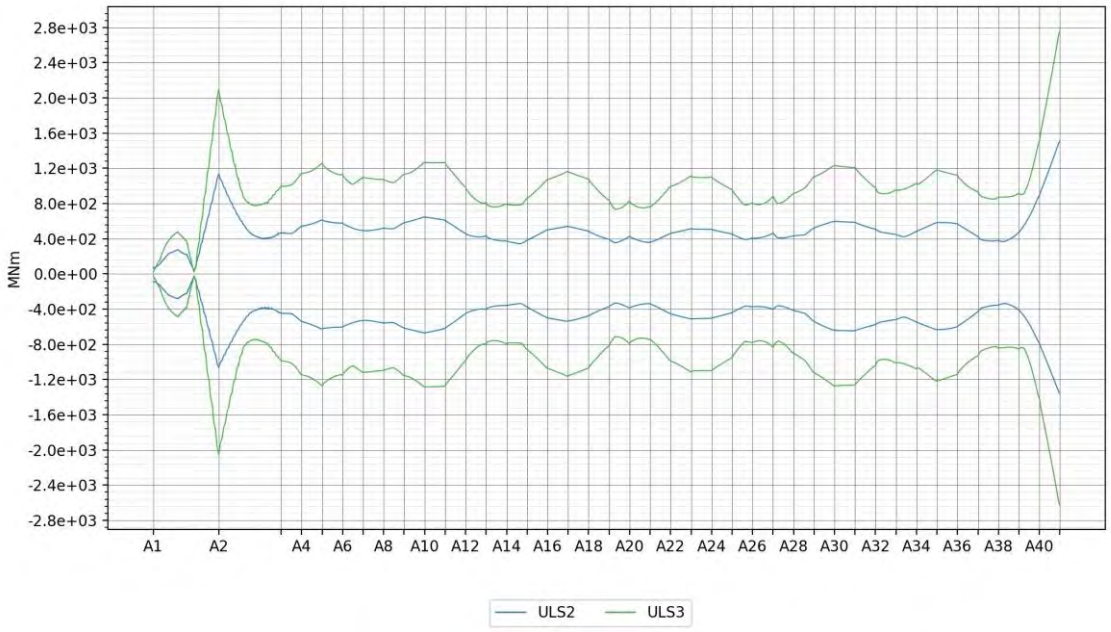

Figure 6-2 Bridge girder bending moment about strong axis – ULS

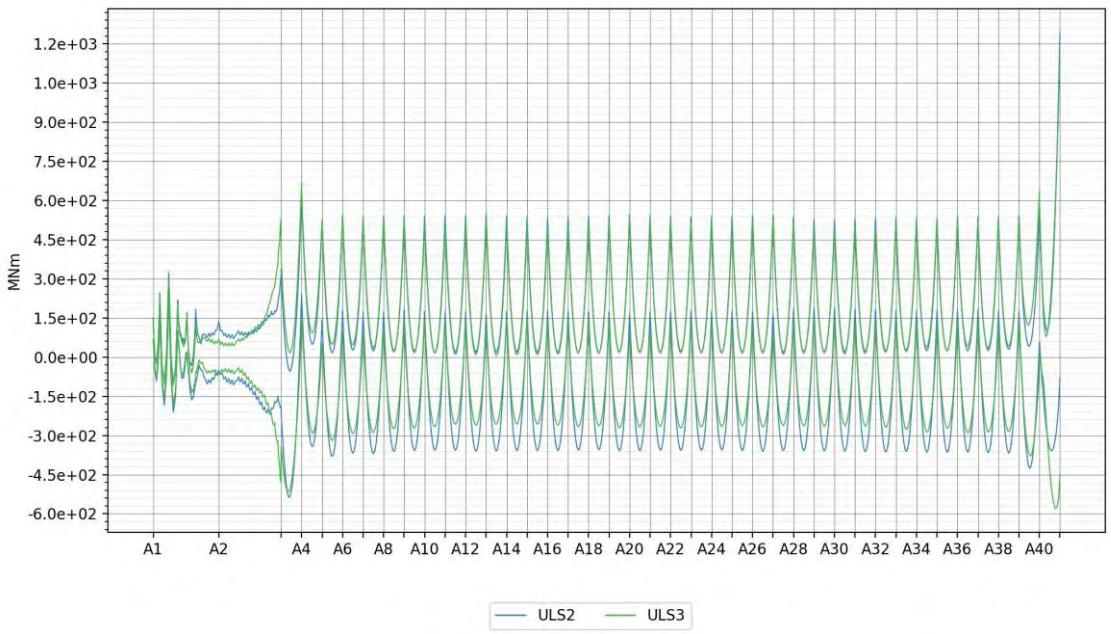

Figure 6-3 Bridge girder bending moment about weak axis – ULS

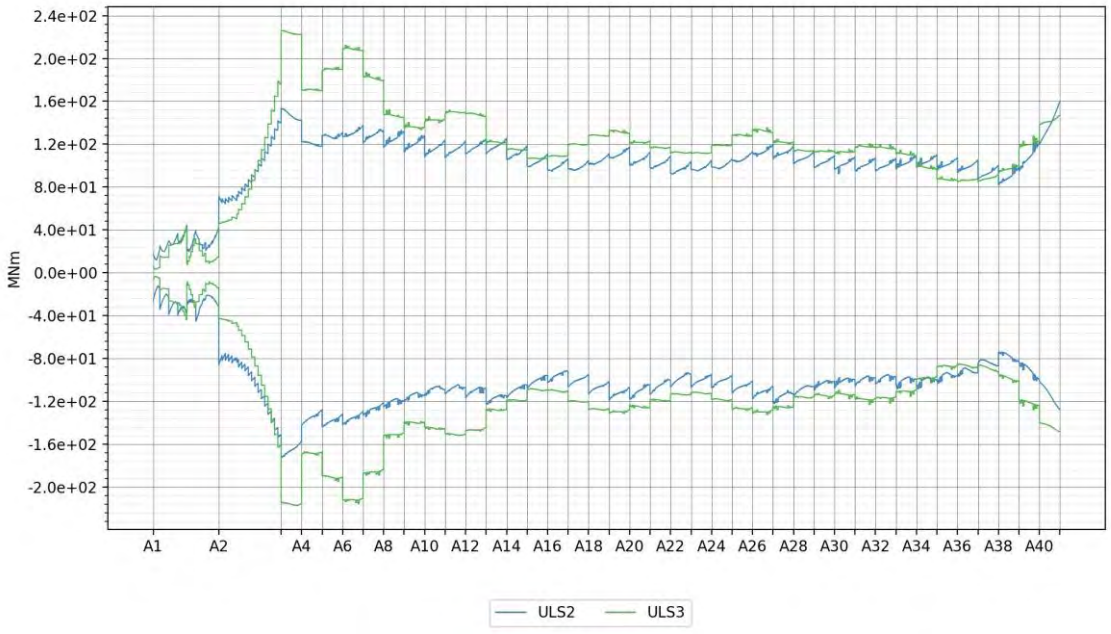

Figure 6-4 Bridge girder torsional moment – ULS

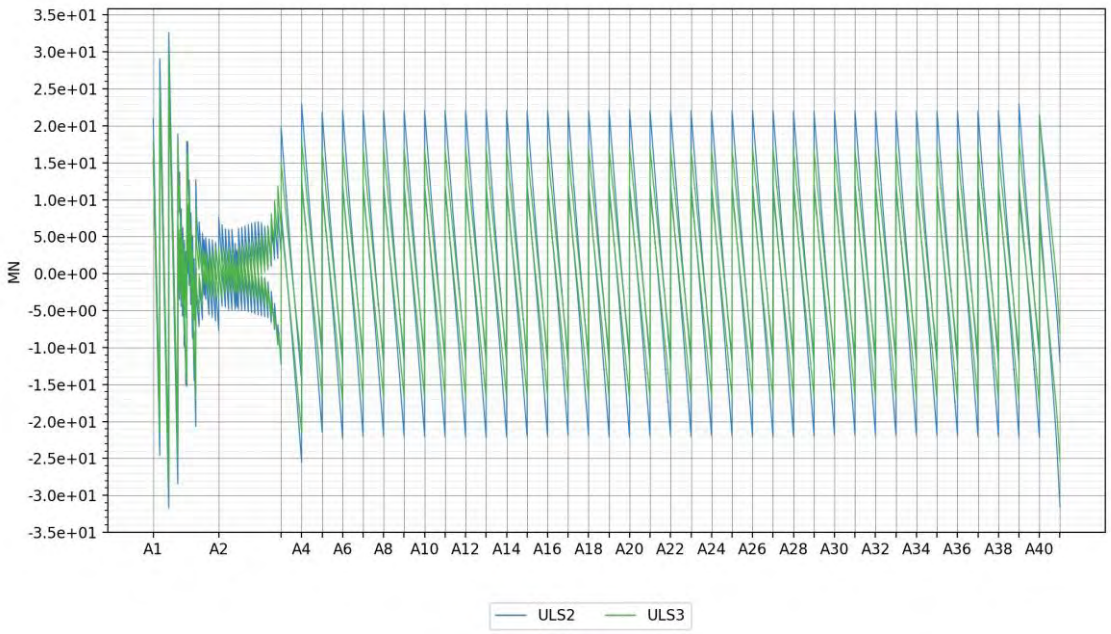

Figure 6-5 Bridge girder vertical shear force – ULS

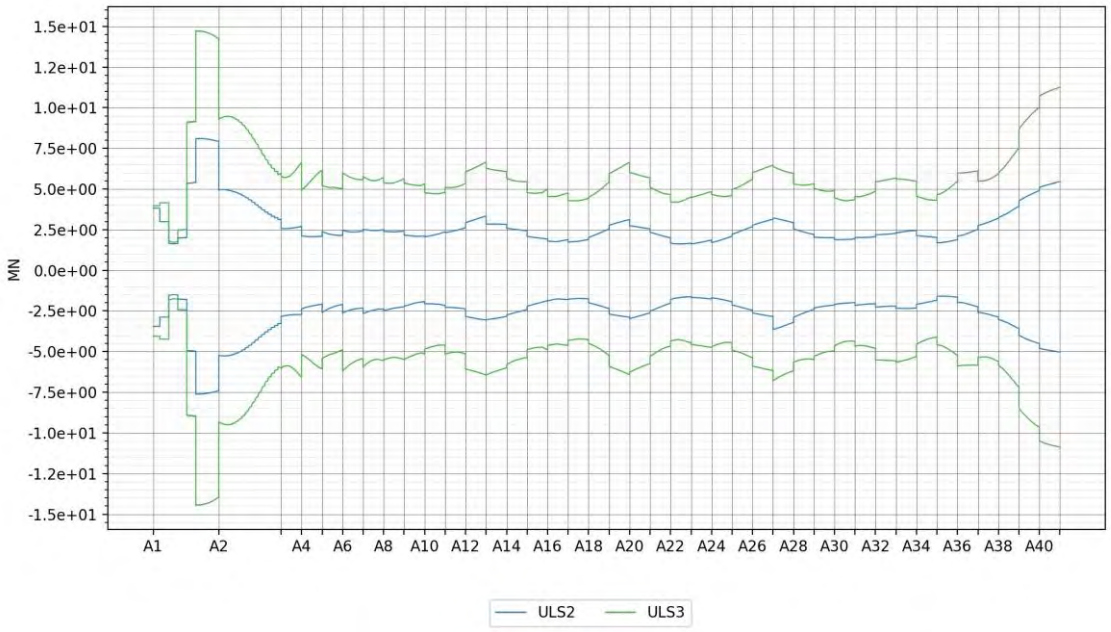

Figure 6-6 Bridge girder transverse shear force – ULS

6.2.4 Floating bridge columns

Table 6-3 Axial force [MN] – ULS

	ULS2		ULS3	
	Min	**Max**	**Min**	**Max**
A3 bottom	-32.8	-13.1	-27.4	-9.7
A3 top	-28.0	-8.2	-23.0	-4.4
A4 bottom	-49.2	-33.8	-41.0	-31.2
A4 top	-44.8	-29.2	-36.4	-27.0
A20 bottom	-41.7	-26.4	-32.9	-24.6
A20 top	-41.0	-25.6	-32.1	-23.7

Table 6-4 Bending moment about longitudinal axis [MNm] – ULS

	ULS2		ULS3	
	Min	**Max**	**Min**	**Max**
A3 bottom	-51.9	52.2	-76.1	66.1
A3 top	-107.9	115.1	-296.3	296.1
A4 bottom	-41.3	37.5	-81.5	73.6
A4 top	-82.9	89.1	-172.6	178.9
A20 bottom	-50.3	62.3	-55.8	55.4
A20 top	-60.7	74.2	-79.8	81.5

Table 6-5 Bending moment about transverse axis [MNm] – ULS

	ULS2		ULS3	
	Min	**Max**	**Min**	**Max**
A3 bottom	-16.0	11.6	-55.3	51.4
A3 top	-106.6	102.5	-524.5	521.2
A4 bottom	-8.6	8.9	-28.3	29.0
A4 top	-68.0	71.3	-291.7	296.6
A20 bottom	-15.5	15.8	-50.1	50.5
A20 top	-37.2	37.9	-129.2	130.2

Table 6-6 Torsional moment [MNm] – ULS

	ULS2		ULS3	
	Min	**Max**	**Min**	**Max**
A3 bottom	-16.6	16.6	-89.7	89.7
A3 top	-16.6	16.6	-89.7	89.7
A4 bottom	-16.2	16.2	-90.6	90.6
A4 top	-16.2	16.2	-90.6	90.6
A20 bottom	-25.4	25.1	-88.1	87.7
A20 top	-25.4	25.1	-88.1	87.7

Table 6-7 Longitudinal shear force [MN] – ULS

	ULS2		ULS3	
	Min	**Max**	**Min**	**Max**
A3 bottom	-2.0	2.0	-10.2	10.2
A3 top	-2.0	2.0	-10.3	10.3
A4 bottom	-1.5	1.4	-6.4	6.2
A4 top	-1.5	1.4	-6.4	6.3
A20 bottom	-2.1	2.1	-7.6	7.6
A20 top	-2.1	2.1	-7.6	7.6

Table 6-8 Transverse shear force [MN] – ULS

	ULS2		ULS3	
	Min	**Max**	**Min**	**Max**
A3 bottom	-1.9	2.1	-6.0	6.2
A3 top	-1.9	2.1	-6.0	6.2
A4 bottom	-1.9	2.1	-4.3	4.7
A4 top	-2.0	2.2	-4.5	4.8
A20 bottom	-1.8	1.9	-4.9	5.1
A20 top	-1.8	1.9	-4.9	5.1

6.2.5 Back span columns

Table 6-9 Axial force [MN] – ULS

	ULS2		ULS3	
	Min	**Max**	**Min**	**Max**
BCE1 bottom	-56.4	-48.5	-51.3	-48.3
BCE1 top	-51.4	-43.4	-46.3	-43.3
BCE2 bottom	-70.9	-61.4	-65.1	-61.1
BCE2 top	-62.4	-52.9	-56.6	-52.5
BCE3 bottom	-52.2	-32.2	-50.4	-33.2
BCE3 top	-39.6	-19.6	-37.8	-20.6
BCE4 bottom	-46.4	-21.8	-46.0	-25.0
BCE4 top	-30.8	-6.1	-30.4	-9.4
BCE5 bottom	-48.7	-23.2	-42.5	-28.4
BCE5 top	-27.7	-2.1	-21.5	-7.3

Table 6-10 Bending moment about longitudinal axis [MNm] – ULS

	ULS2		ULS3	
	Min	**Max**	**Min**	**Max**
BCE1 bottom	-14.0	17.8	-7.7	7.9
BCE1 top	-22.8	30.5	-12.2	12.2
BCE2 bottom	-44.9	50.7	-62.9	63.3
BCE2 top	-26.9	35.1	-17.1	17.2
BCE3 bottom	-73.8	79.3	-128.7	129.3
BCE3 top	-23.2	31.0	-10.5	10.6
BCE4 bottom	-115.4	121.3	-219.2	220.1
BCE4 top	-30.2	37.4	-23.5	23.7
BCE5 bottom	-121.3	120.9	-230.0	230.8
BCE5 top	-48.1	56.5	-47.2	47.5

Table 6-11 Bending moment about transverse axis [MNm] – ULS

	ULS2		ULS3	
	Min	**Max**	**Min**	**Max**
BCE1 bottom	-12.4	26.0	-12.7	25.3
BCE1 top	-31.8	7.9	-29.5	7.0
BCE2 bottom	-16.2	17.8	-15.8	17.1
BCE2 top	-19.9	16.6	-17.7	14.8
BCE3 bottom	-18.5	8.1	-17.8	8.1
BCE3 top	-5.8	24.7	-5.2	22.8
BCE4 bottom	-9.6	13.9	-9.1	13.3
BCE4 top	-17.2	9.2	-15.4	7.3
BCE5 bottom	-11.6	6.6	-11.4	5.2
BCE5 top	-6.4	15.8	-2.3	13.8

Table 6-12 Torsional moment [MNm] – ULS

	ULS2		ULS3	
	Min	**Max**	**Min**	**Max**
BCE1 bottom	-0.35	0.42	-0.31	0.31
BCE1 top	-0.34	0.41	-0.31	0.31
BCE2 bottom	-0.68	0.75	-1.08	1.09
BCE2 top	-0.68	0.74	-1.08	1.09
BCE3 bottom	-0.94	0.99	-1.72	1.73
BCE3 top	-0.94	0.99	-1.72	1.73
BCE4 bottom	-1.15	1.18	-2.20	2.21
BCE4 top	-1.15	1.18	-2.20	2.21
BCE5 bottom	-0.95	0.95	-1.85	1.86
BCE5 top	-0.96	0.96	-1.87	1.88

Table 6-13 Longitudinal shear force [MN] – ULS

	ULS2		ULS3	
	Min	**Max**	**Min**	**Max**
BCE1 bottom	-1.52	4.32	-1.46	4.09
BCE1 top	-1.51	4.32	-1.46	4.09
BCE2 bottom	-1.44	1.65	-1.34	1.52
BCE2 top	-1.44	1.65	-1.33	1.52
BCE3 bottom	-1.28	0.41	-1.20	0.39
BCE3 top	-1.28	0.41	-1.19	0.38
BCE4 bottom	-0.45	0.74	-0.40	0.69
BCE4 top	-0.45	0.74	-0.39	0.68
BCE5 bottom	-0.50	0.25	-0.50	0.19
BCE5 top	-0.50	0.24	-0.49	0.17

Table 6-14 Transverse shear force [MN] – ULS

	ULS2		ULS3	
	Min	**Max**	**Min**	**Max**
BCE1 bottom	-1.49	1.92	-0.61	0.60
BCE1 top	-1.48	1.92	-0.60	0.59
BCE2 bottom	-1.92	2.14	-2.19	2.17
BCE2 top	-1.92	2.15	-2.20	2.19
BCE3 bottom	-2.39	2.57	-3.64	3.63
BCE3 top	-2.40	2.57	-3.66	3.64
BCE4 bottom	-3.24	3.36	-5.77	5.75
BCE4 top	-3.25	3.37	-5.79	5.77
BCE5 bottom	-2.87	3.00	-4.89	4.88
BCE5 top	-2.87	3.00	-4.89	4.88

6.2.6 Tower legs lower part

Table 6-15 Axial force [MN] – ULS

		ULS2		ULS3	
		Min	**Max**	**Min**	**Max**
east	**bottom**	-262.8	-203.5	-255.3	-187.2
	top	-206.6	-147.3	-199.1	-131.0
west	**bottom**	-263.3	-205.2	-251.7	-189.9
	top	-207.2	-149.1	-195.5	-133.8

Table 6-16 Bending moment about longitudinal axis [MNm] – ULS

		ULS2		ULS3	
		Min	**Max**	**Min**	**Max**
east	**bottom**	-215.4	-72.1	-261.3	-14.2
	top	180.3	497.7	75.0	560.0
west	**bottom**	75.5	219.9	14.3	259.8
	top	-511.0	-186.5	-559.4	-73.1

Table 6-17 Bending moment about transverse axis [MNm] – ULS

		ULS2		ULS3	
		Min	**Max**	**Min**	**Max**
east	**bottom**	-231.9	389.7	-248.2	234.4
	top	-92.1	184.5	-96.9	84.4
west	**bottom**	-228.9	393.8	-250.5	231.7
	top	-92.3	186.0	-96.8	83.7

Table 6-18 Torsional moment [MNm] – ULS

		ULS2		ULS3	
		Min	**Max**	**Min**	**Max**
east	**bottom**	-27.2	36.5	-26.8	27.3
	top	-27.2	36.5	-26.8	27.3
west	**bottom**	-40.8	23.6	-25.0	28.0
	top	-40.8	23.6	-25.0	28.0

Table 6-19 Longitudinal shear force [MNm] – ULS

		ULS2		ULS3	
		Min	**Max**	**Min**	**Max**
east	**bottom**	-2.9	4.1	-3.1	3.1
	top	-2.8	4.0	-2.9	2.8
west	**bottom**	-2.9	4.2	-3.2	3.1
	top	-2.8	4.1	-2.9	2.8

Table 6-20 Transverse shear force [MNm] – ULS

		ULS2		ULS3	
		Min	**Max**	**Min**	**Max**
east	**bottom**	9.9	18.6	6.8	20.7
	top	0.1	8.8	-2.9	10.8
west	**bottom**	-19.0	-10.1	-20.7	-6.8
	top	-9.2	-0.3	-10.8	2.9

6.2.7 Tower legs upper part

Table 6-21 Axial force [MN] – ULS

		ULS2		ULS3	
		Min	**Max**	**Min**	**Max**
east	**bottom**	-192.4	-149.0	-179.0	-139.1
	top	-57.7	-34.9	-55.9	-28.0
west	**bottom**	-193.8	-149.3	-180.3	-137.1
	top	-57.9	-35.2	-56.1	-27.8

Table 6-22 Bending moment about longitudinal axis [MNm] – ULS

		ULS2		ULS3	
		Min	**Max**	**Min**	**Max**
east	**bottom**	-128.8	-90.6	-153.0	-61.0
	top	-91.0	-70.4	-95.8	-59.7
west	**bottom**	90.4	129.0	60.2	153.1
	top	70.2	90.5	60.5	95.9

Table 6-23 Bending moment about transverse axis [MNm] – ULS

		ULS2		ULS3	
		Min	**Max**	**Min**	**Max**
east	**bottom**	-89.0	178.0	-94.4	83.5
	top	-125.2	82.1	-89.8	80.4
west	**bottom**	-89.0	184.1	-95.8	81.7
	top	-118.6	83.8	-95.9	82.3

Table 6-24 Torsional moment [MNm] – ULS

		ULS2		ULS3	
		Min	**Max**	**Min**	**Max**
east	**bottom**	-25.1	20.7	-21.0	22.5
	top	-25.3	20.4	-21.3	22.3
west	**bottom**	-24.1	20.5	-19.9	22.0
	top	-23.8	20.7	-19.9	22.3

Table 6-25 Longitudinal shear force [MNm] – ULS

		ULS2		ULS3	
		Min	**Max**	**Min**	**Max**
east	**bottom**	-2.8	4.1	-2.8	2.8
	top	-6.7	6.8	-6.2	6.2
west	**bottom**	-2.8	4.2	-2.9	2.8
	top	-7.4	6.6	-5.8	6.6

Table 6-26 Transverse shear force [MNm] – ULS

		ULS2		ULS3	
		Min	**Max**	**Min**	**Max**
east	**bottom**	3.6	4.7	2.8	5.4
	top	-4.4	-3.6	-4.5	-3.2
west	**bottom**	-4.7	-3.6	-5.4	-2.8
	top	3.6	4.4	3.2	4.5

6.2.8 Tower crown

Table 6-27 Axial force [MN] – ULS

	ULS2		ULS3	
	Min	**Max**	**Min**	**Max**
tag				
bottom	-95.5	-61.5	-95.8	-46.9
top	0.0	0.0	0.0	0.0

Table 6-28 Bending moment about longitutinal axis [MNm] – ULS

	ULS2		ULS3	
	Min	**Max**	**Min**	**Max**
tag				
bottom	-12.8	10.9	-15.1	16.0
top	0.0	0.0	0.0	0.0

Table 6-29 Bending moment about transverse axis [MNm] – ULS

	ULS2		ULS3	
	Min	**Max**	**Min**	**Max**
tag				
bottom	-212.4	142.7	-176.4	157.0
top	0.0	0.0	0.0	0.0

Table 6-30 Torsional moment [MNm] – ULS

	ULS2		ULS3	
	Min	**Max**	**Min**	**Max**
tag				
bottom	-11.7	10.1	-11.8	12.9
top	0.0	0.0	0.0	0.0

Table 6-31 Longitudinal shear force [MN] – ULS

	ULS2		ULS3	
	Min	**Max**	**Min**	**Max**
tag				
bottom	-9.5	7.9	-8.7	9.1
top	0.0	0.0	0.0	0.0

Table 6-32 Transverse shear force [MN] – ULS

	ULS2		ULS3	
	Min	**Max**	**Min**	**Max**
tag				
bottom	-0.41	0.49	-0.70	0.68
top	0.00	0.00	0.00	0.00

6.2.9 Tower cross beam

Table 6-33 Axial force [MN] – ULS

	ULS2		ULS3	
	Min	**Max**	**Min**	**Max**
tag				
east	-17.4	-6.0	-21.5	-0.8
mid	-17.4	-6.0	-21.5	-0.8
west	-17.3	-5.9	-21.5	-0.8

Table 6-34 Bending moment about longitudinal axis [MNm] – ULS

	ULS2		ULS3	
	Min	**Max**	**Min**	**Max**
tag				
east	-162.3	-25.8	-207.7	33.3
mid	-95.9	-70.5	-90.2	-65.5
west	-158.3	-21.2	-209.0	33.5

Table 6-35 Bending moment about vertical axis [MNm] – ULS

	ULS2		ULS3	
	Min	**Max**	**Min**	**Max**
tag				
east	-3.0	3.1	-3.0	2.9
mid	-1.7	1.7	-2.1	2.0
west	-3.2	2.8	-3.0	2.9

Table 6-36 Torsional moment [MNm] – ULS

	ULS2		ULS3	
	Min	**Max**	**Min**	**Max**
tag				
east	-21.7	22.8	-18.5	17.1
mid	-21.7	22.8	-18.5	17.1
west	-21.7	22.8	-18.5	17.1

Table 6-37 Longitudinal shear force [MN] – ULS

	ULS2		ULS3	
	Min	**Max**	**Min**	**Max**
tag				
east	-0.28	0.31	-0.31	0.31
mid	-0.28	0.31	-0.30	0.30
west	-0.28	0.31	-0.30	0.30

Table 6-38 Vertical shear force [MN] – ULS

	ULS2		ULS3	
	Min	**Max**	**Min**	**Max**
tag				
east	-7.1	13.4	-15.4	21.0
mid	-9.9	10.7	-18.2	18.2
west	-12.7	7.9	-21.0	15.4

6.2.10Stay cables

Table 6-39 Axial force [MN] – ULS

	ULS2		ULS3	
	Min	Max	Min	Max
cable_BW_1	2.0	3.1	2.1	2.6
cable_BW_2	2.2	3.8	2.2	2.8
cable_BW_3	2.6	4.2	2.5	3.1
cable_BW_4	2.9	4.7	2.8	3.6
cable_BW_5	3.1	5.0	2.9	4.0
cable_BW_6	3.3	5.3	2.9	4.5
cable_BW_7	3.3	5.8	3.0	4.9
cable_BW_8	3.8	6.3	3.4	5.5
cable_BW_9	4.1	6.7	3.6	5.9
cable_BW_10	4.3	7.0	3.7	6.3
cable_BW_11	4.6	7.4	3.8	6.8
cable_BW_12	4.8	7.7	3.9	7.2
cable_BW_13	4.8	7.8	3.8	7.3
cable_BW_14	5.0	8.2	3.9	7.8
cable_BW_15	5.3	8.7	4.1	8.4
cable_BW_16	5.3	8.9	4.0	8.7
cable_BW_17	5.3	8.9	3.8	8.7
cable_BW_18	5.2	8.9	3.7	8.9
cable_FW_1	2.1	3.3	2.3	2.7
cable_FW_2	2.1	3.9	2.1	2.9

	ULS2		ULS3	
	Min	Max	Min	Max
cable_FW_3	2.4	4.6	2.4	3.4
cable_FW_4	2.7	5.2	2.5	3.8
cable_FW_5	2.9	5.7	2.7	4.2
cable_FW_6	3.2	6.2	2.9	4.6
cable_FW_7	3.4	6.7	3.0	5.0
cable_FW_8	3.6	7.0	3.2	5.4
cable_FW_9	3.8	7.5	3.4	5.7
cable_FW_10	4.0	7.9	3.6	6.0
cable_FW_11	4.2	8.2	3.8	6.3
cable_FW_12	4.4	8.4	3.9	6.6
cable_FW_13	4.5	8.5	3.7	7.1
cable_FW_14	4.5	8.8	3.3	7.9
cable_FW_15	4.4	9.2	2.9	8.7
cable_FW_16	4.2	9.5	2.5	9.4
cable_FW_17	4.0	9.7	2.2	9.8
cable_FW_18	3.3	9.7	1.8	9.8
cable_BE_1	2.0	3.1	2.1	2.6
cable_BE_2	2.2	3.7	2.2	2.9
cable_BE_3	2.5	4.2	2.4	3.2
cable_BE_4	2.9	4.6	2.7	3.7
cable_BE_5	3.1	4.9	2.8	4.1
cable_BE_6	3.2	5.3	2.9	4.6
cable_BE_7	3.2	5.9	2.9	5.0
cable_BE_8	3.7	6.3	3.3	5.5
cable_BE_9	4.0	6.7	3.6	5.9
cable_BE_10	4.3	6.9	3.7	6.2
cable_BE_11	4.6	7.4	3.9	6.7
cable_BE_12	4.8	7.7	4.0	7.1
cable_BE_13	4.8	7.7	3.9	7.2
cable_BE_14	5.1	8.1	4.0	7.7
cable_BE_15	5.4	8.7	4.1	8.3
cable_BE_16	5.4	8.9	4.0	8.6
cable_BE_17	5.3	8.9	3.9	8.7
cable_BE_18	5.2	8.9	3.8	8.8
cable_FE_1	2.1	3.3	2.2	2.7
cable_FE_2	2.0	3.8	2.1	2.9
cable_FE_3	2.4	4.5	2.4	3.4
cable_FE_4	2.6	5.1	2.5	3.8
cable_FE_5	2.9	5.6	2.7	4.3
cable_FE_6	3.1	6.1	2.9	4.7
cable_FE_7	3.3	6.7	3.0	5.2
cable_FE_8	3.6	7.0	3.2	5.5

	ULS2		ULS3	
	Min	Max	Min	Max
cable_FE_9	3.7	7.4	3.4	5.8
cable_FE_10	3.9	7.8	3.6	6.1
cable_FE_11	4.1	8.1	3.8	6.4
cable_FE_12	4.4	8.3	4.0	6.6
cable_FE_13	4.5	8.4	3.8	7.2
cable_FE_14	4.4	8.7	3.5	7.9
cable_FE_15	4.3	9.1	3.0	8.7
cable_FE_16	4.1	9.5	2.7	9.4
cable_FE_17	3.8	9.7	2.5	9.8
cable_FE_18	3.2	9.7	2.2	9.8

6.2.11Mooring lines

The mooring line response is given as characteristic maximum values, not including load factors.

Table 6-40 Axial force [MN] – ULS

	Max force
MooringLine1	3.86
MooringLine2	4.48
MooringLine3	4.36
MooringLine4	3.76
MooringLine5	4.08
MooringLine6	3.55
MooringLine7	3.73
MooringLine8	4.69
MooringLine9	5.62
MooringLine10	2.82
MooringLine11	4.70
MooringLine12	5.04

6.3 Coupled vs. uncoupled analysis

A comparison between ULS forces in the bridge girder have been made for coupled and uncoupled environmental load analyses. The uncoupled results have been used in the design development of the various bridge concepts. The environmental load conditions are given in Section 2.5. The uncoupled assessment uses the same environmental load cases but simulated separately and combined according to section 2.7.

Ten seeds are run for each of the coupled load cases. The AUR-method for extreme statistics [7] was used to get extreme values based on the time series of response data. The 90-percentile estimate has been calculated.

For uncoupled assessment all environmental loads except from wind are based on frequency domain simulation, and time series of the various responses were generated from these results. For wind, a time-domain simulation was applied using the worst of ten previously simulated wind seeds. The expected maximum response values were calculated.

The comparison has been performed for ULS3 and the key results are shown in Figure 6-7 to Figure 6-12 (sectional forces) and Figure 6-13 (von Mises stress). Note that the comparison is both expected max vs. 90-percentile and coupled vs. uncoupled response; the former was used in the design development, the latter is the more correct answer.

The uncoupled method is conservative for strong axis bending moment, while it is unconservative for axial force. The other force components have a similar level of magnitude. Torsional moment is observed to be slightly higher around Axis 3. The uncoupled strong-axis moment is governed by a swell condition (section 4.4.8.2) with around 17s Tp. For coupled simulations with the same swell period the other loads (wind sea and wind) cause sufficient disturbance to reduce the excitation of that mode considerably.

The uncoupled method is conservative for the calculated Von Mises stress. The basis for the design development thus far has been to use the maximum von mises stress from a single 1-hour realization with the uncoupled method. The comparison shows that this approach generally gives higher stresses than the 90 percentile values from the coupled analysis.

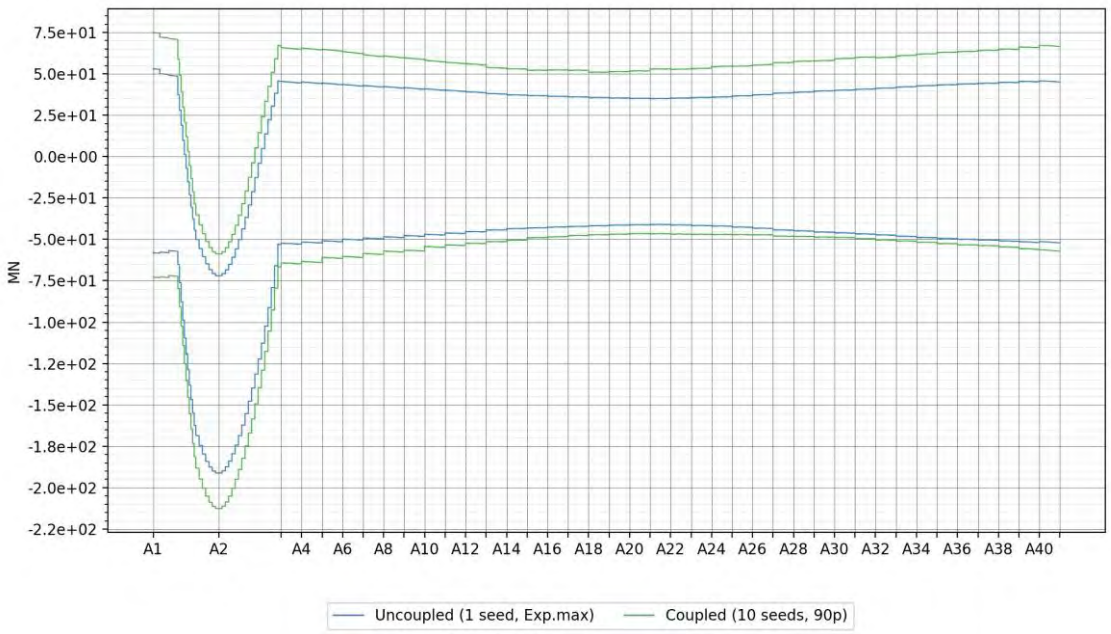

Figure 6-7 Coupled vs. uncoupled environmental loads for K12_07: Axial force

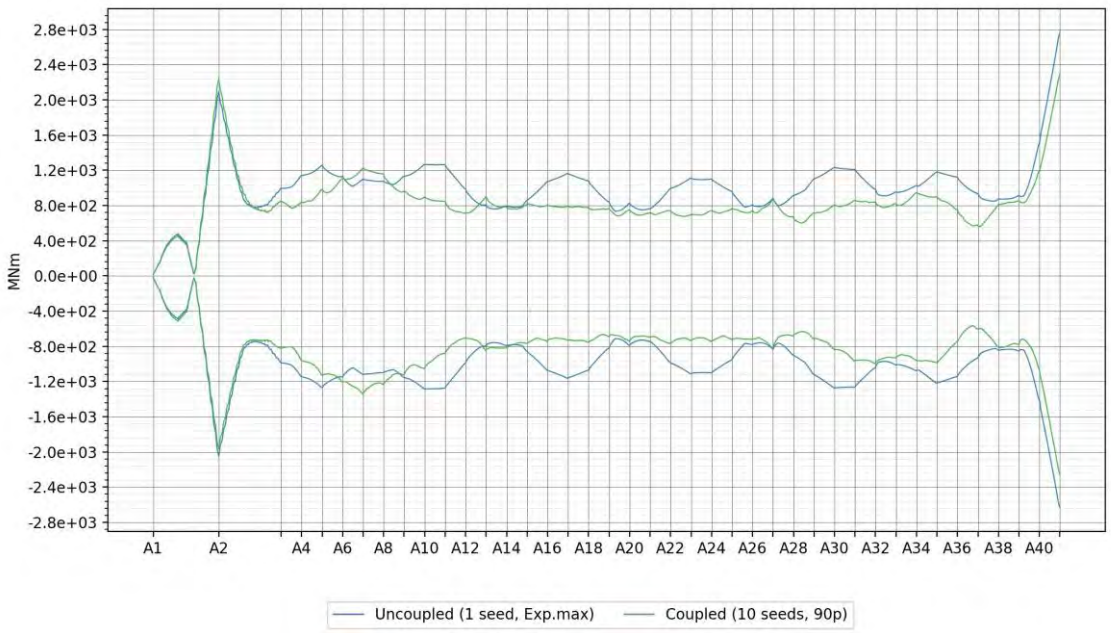

Figure 6-8 Coupled vs. uncoupled environmental loads for K12_07: Bending moment about strong axis

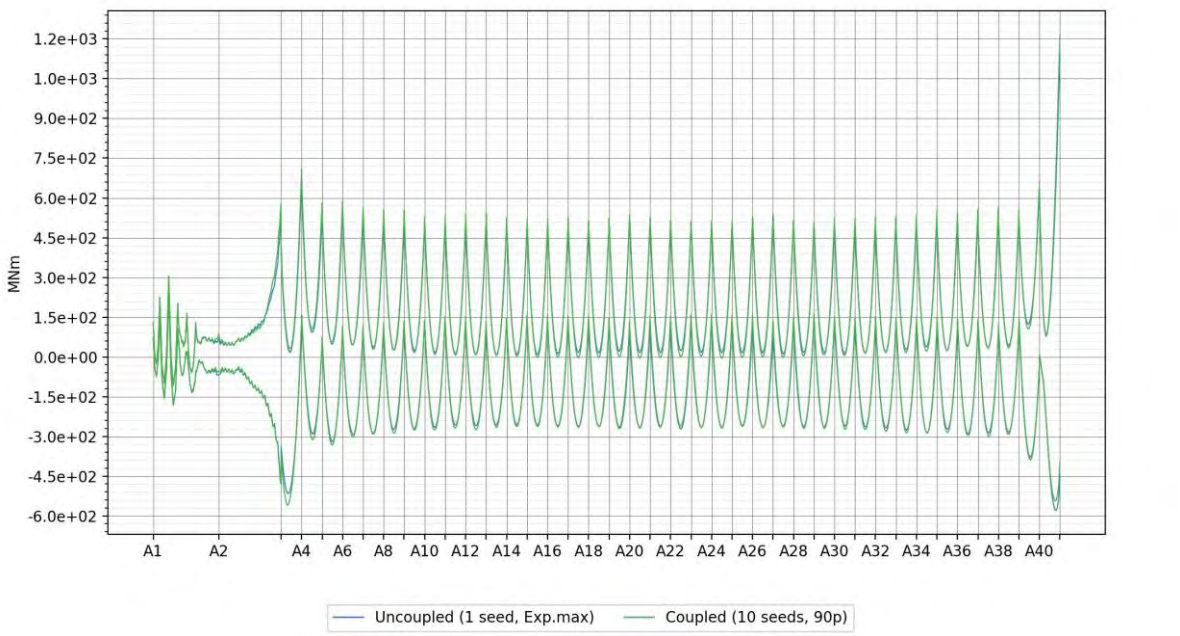

Figure 6-9 Coupled vs. uncoupled environmental loads for K12_07: Bending moment about weak axis

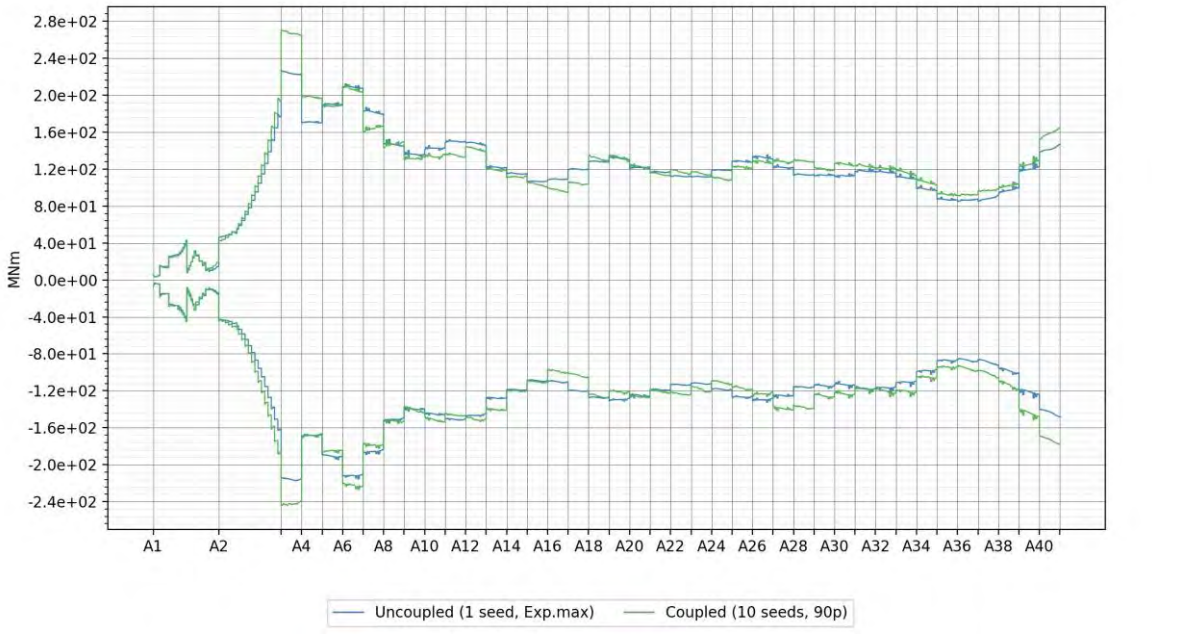

Figure 6-10 Coupled vs. uncoupled environmental loads for K12_07: Torsional moment

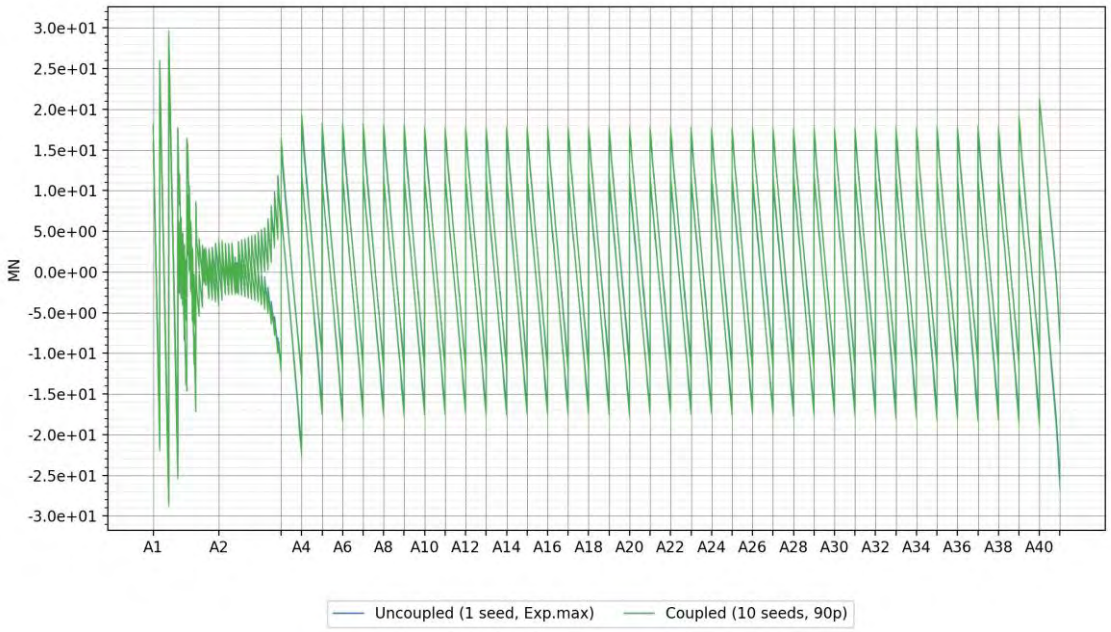

Figure 6-11 Coupled vs. uncoupled environmental loads for K12_07: Vertical shear force

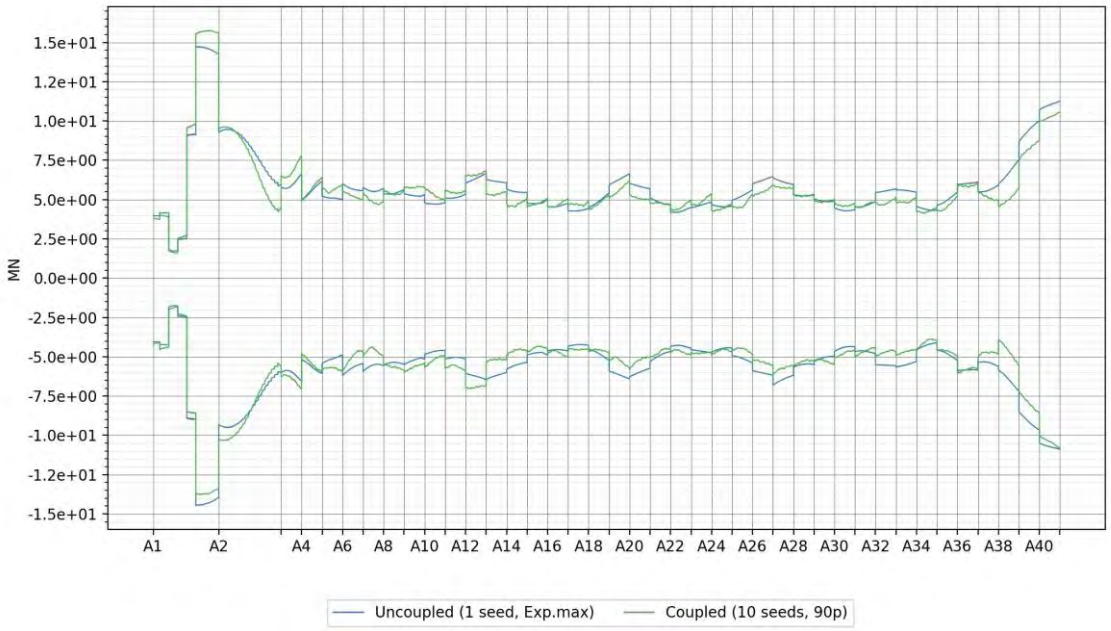

Figure 6-12 Coupled vs. uncoupled environmental loads for K12_07: Transverse shear force

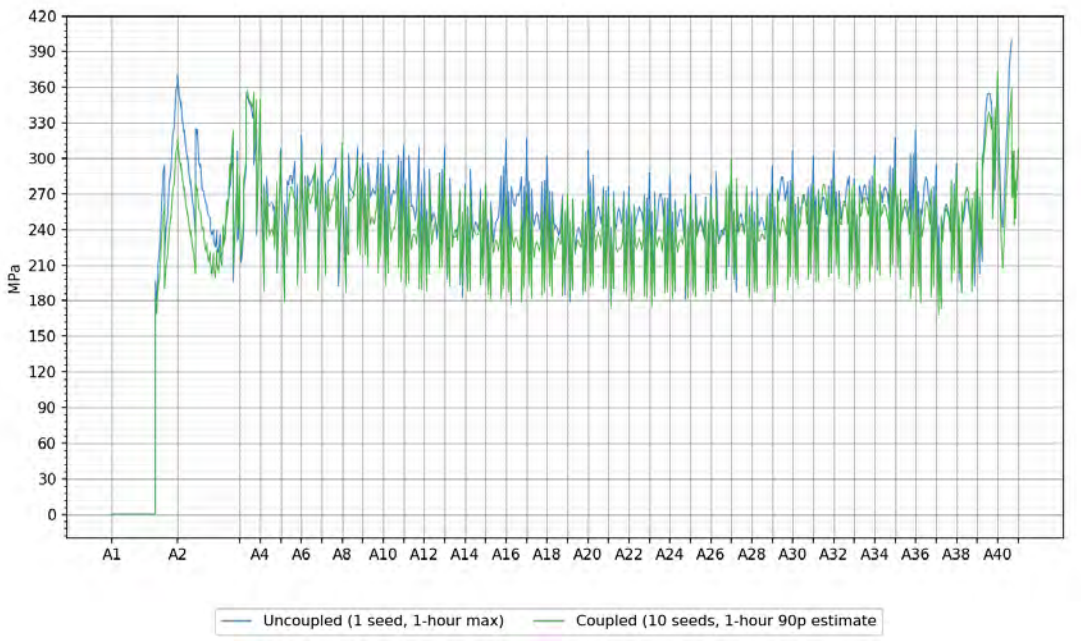

Figure 6-13 Coupled vs. uncoupled environmental loads for K12_07: Max Von Mises

7 Accidental limit state capacity

7.1 Intact condition

The response to 10 000-year environmental conditions was in Phase 3 of the project found to not be dimensioning as the increase in bridge response was below the load factor of 1.6 applied to the ULS loads. Similar assessments have been performed in this phase:

- Wind waves and swell cases are screened in frequency domain to identify a few governing environmental scenarios (section 2.2.2.3 and 2.6)
- Wind is assumed coming either from the west or east perpendicular to the main crossing direction
- Coupled dynamic simulations were performed in time-domain with 10 seeds for each environmental condition
- The response was evaluated at the required 95-percentile level using the AUR method and compared with the ULS response at the 90-percentile level
- The permanent and environmental load factor of 1.2 and 1.6 respectively was used for the ULS results, whereas a factor of 1.0 was used for both the for 10 000 year results.
- Note that the material factor also changes from 100 to 10 000 years, this should be considered when assessing the response.

The sectional responses are compared in Figure 7-1 to Figure 7-6. The sectional forces from 10 000 year environmental response is in general somewhat larger than the ULS response. It is not evaluated if this is due to the environment alone or the increased percentile level from 90 to 95. For stresses (Figure 7-7) the difference is less, and the 10 000 year 95-percentile and 100-year 90-percentile with load factors yields similar utilization of the bridge girder.

The design development has been performed with 100-year ULS results as a basis. The yield response is governed by the 100-year condition. As some of the sectional loads were higher for the 10 000 year response it is recommended to do a more comprehensive evaluation of the 10 000 year response during the next phase of the project, especially to evaluate that the buckling capacity of the structural elements are within the required margins.

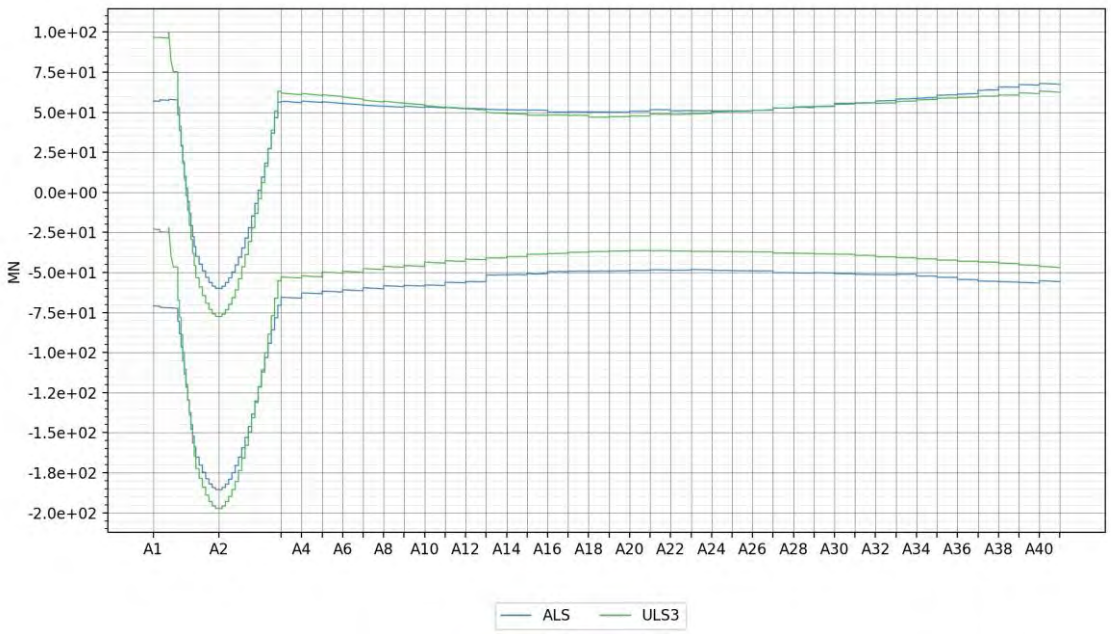

Figure 7-1 ALS (K12_06) vs. ULS (K12_07): Axial force

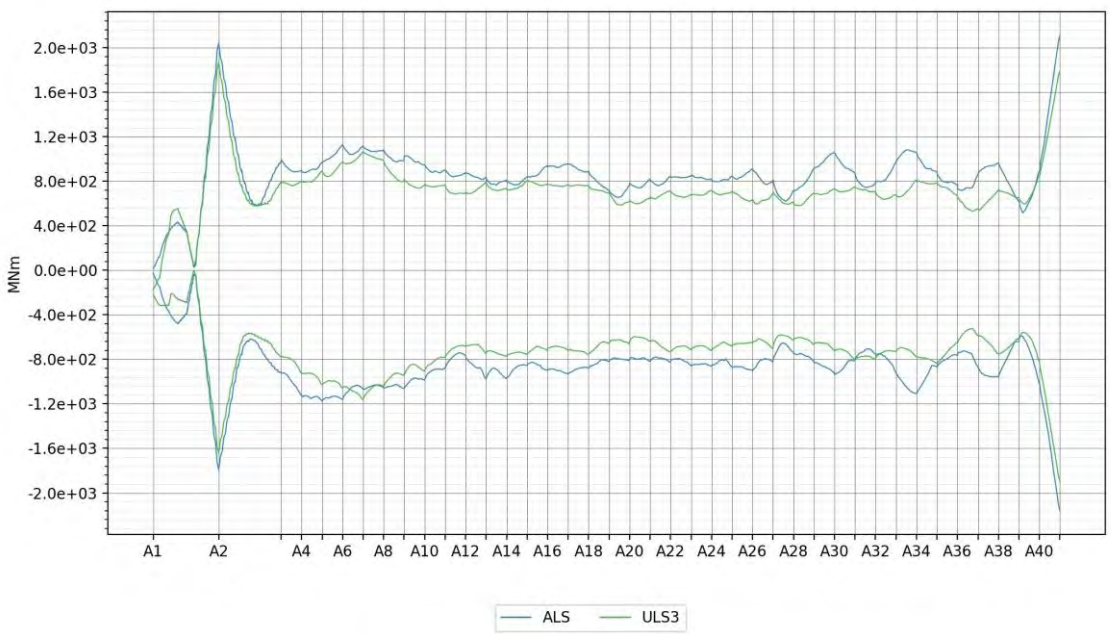

Figure 7-2 ALS (K12_06) vs. ULS (K12_07): Bending moment about strong axis

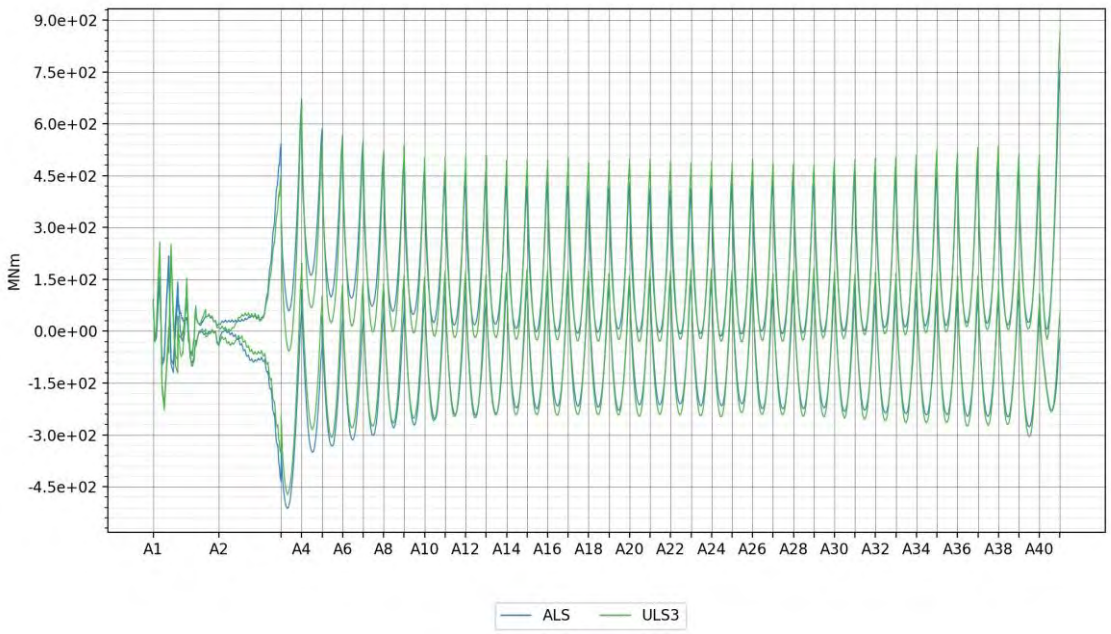

Figure 7-3 ALS (K12_06) vs. ULS (K12_07): Bending moment about weak axis

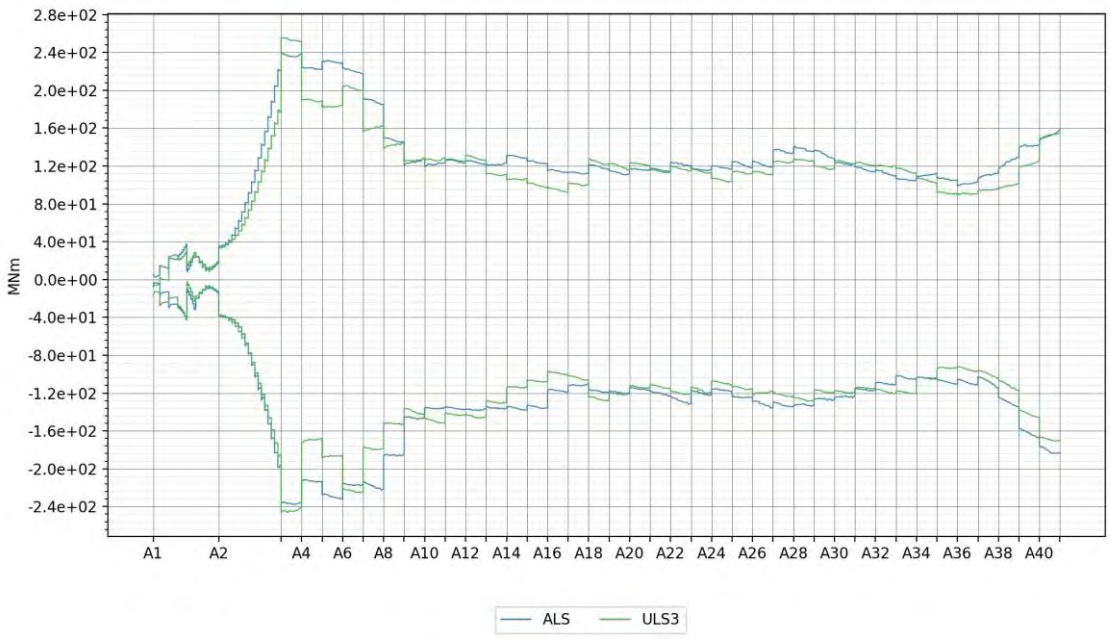

Figure 7-4 ALS (K12_06) vs. ULS (K12_07): Torsional moment

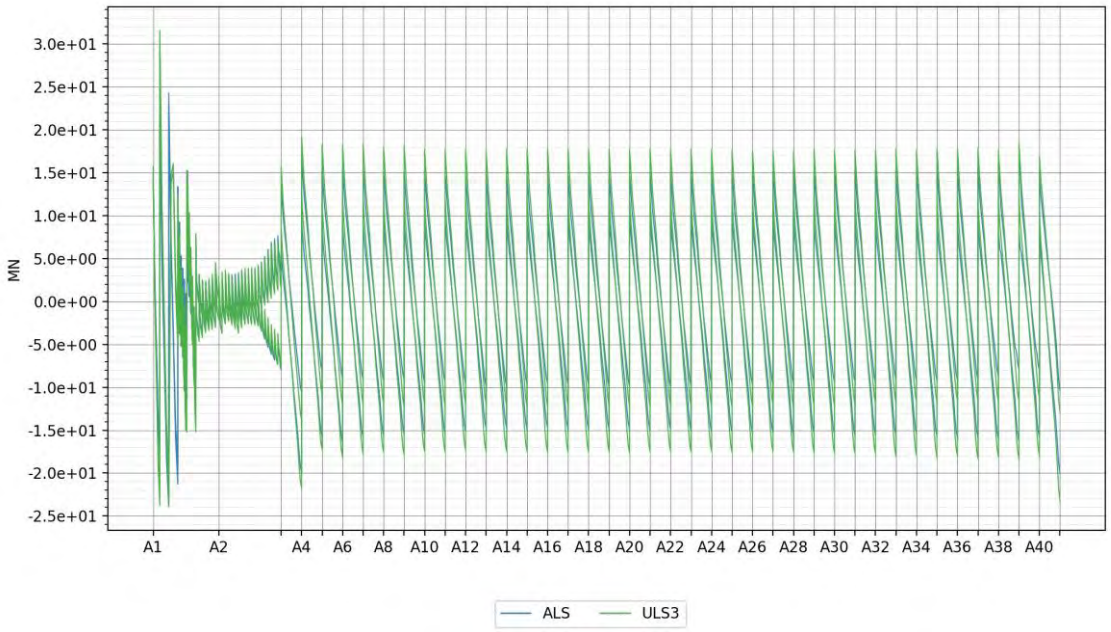

Figure 7-5 ALS (K12_06) vs. ULS (K12_07): Vertical shear force

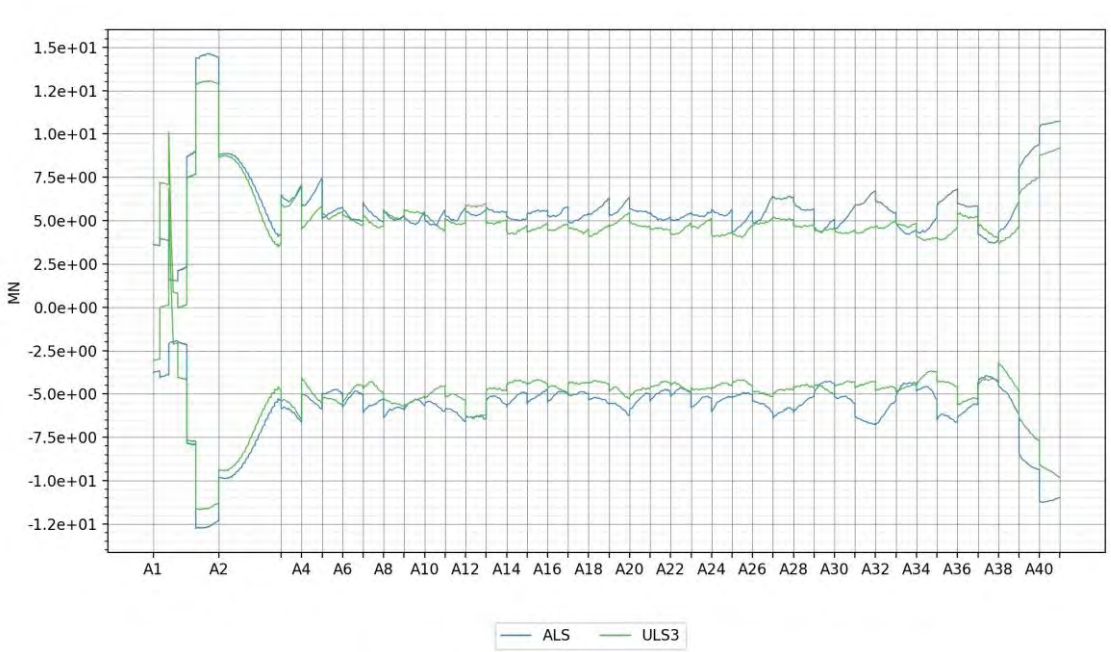

Figure 7-6 ALS (K12_06) vs. ULS (K12_07): Transverse shear force

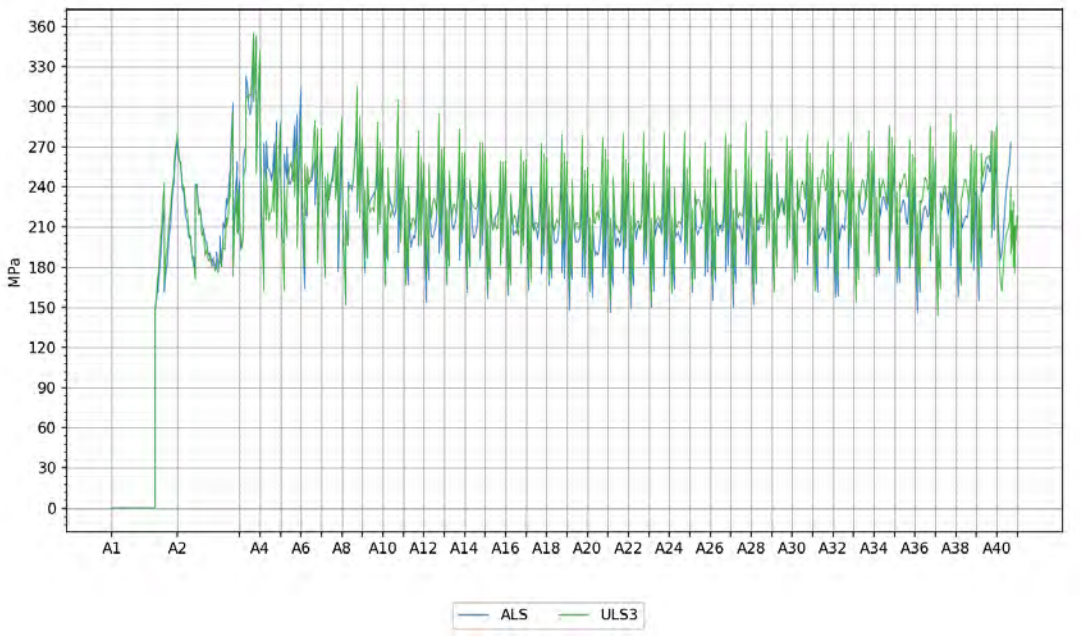

Figure 7-7 ALS (K12_06) vs. ULS (K12_07): Max Von Mises

7.2 Damaged condition

The design basis [9] specifies that the bridge is required to withstand a 100-year environmental condition after damage. Hence, the various variations of damaged bridge condition given in the following are simulated with coupled wind sea, swell and wind as shown in section 2.5. Only the seed with highest utilization in the ULS capacity check was used for the ALS checks (the worst of 10 seeds).

7.2.1 Setup

7.2.1.1 Loss of mooring lines

Removal of all anchor lines on one side of an anchor cluster was selected to investigate the consequence of loss of mooring lines. This is a conservative approach as the common assumption is loss of two mooring lines. It was selected as a risk mitigation measure to document the robustness of the bridge, capturing the possibility that all anchors on one side of a mooring group is lost due to e.g. underwater landslides.

The loss of one side of a mooring cluster (two lines, Figure 7-8) was considered for all moored pontoons, this is a required scenario according to the design basis. As a robustness check the loss of one side of two mooring clusters were evaluated (four lines, Figure 7-9), which is outside of the design requirements.

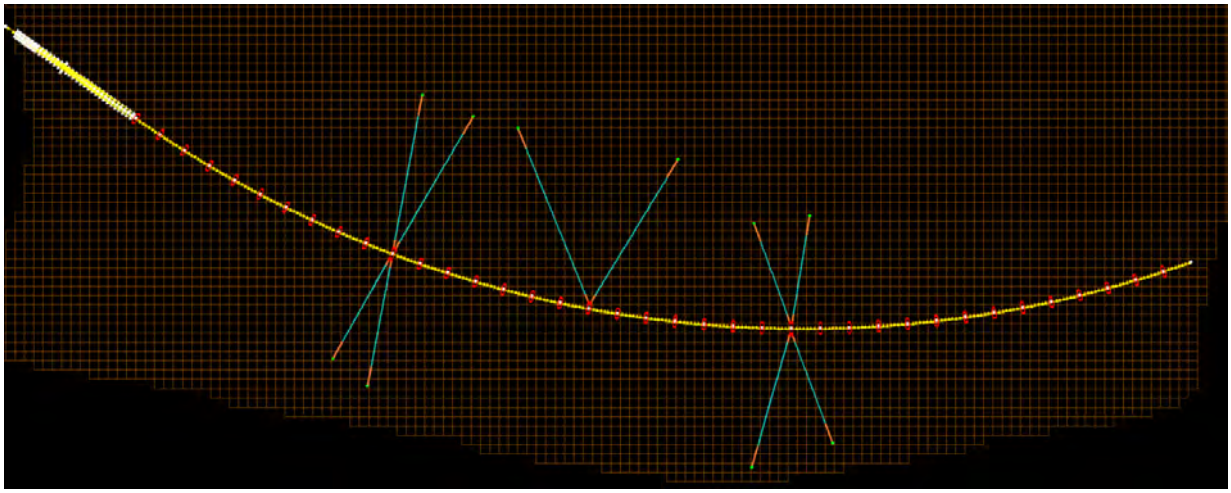

Figure 7-8 Example of loss of mooring group for K12-06 group 2.

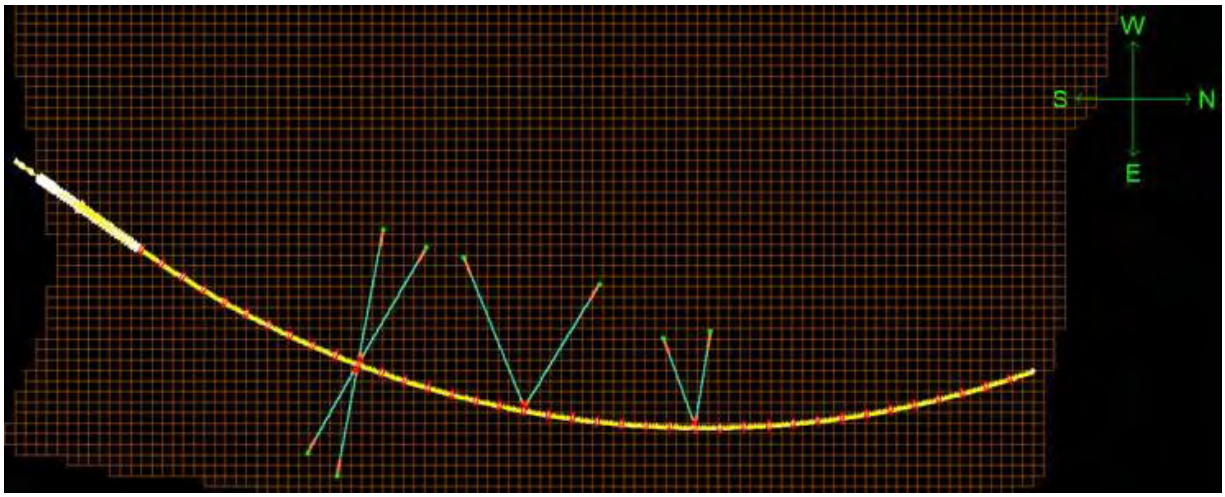

Figure 7-9 Example of loss of two mooring groups for K12_06.

7.2.1.2 Flooding of pontoons

Flooding of pontoons could occur due to leaks, faulty system operation or ship collision events. The latter is the more severe condition, and the local ship collision simulations [14] indicate that four-compartment damage may be possible. With the compartment layout in the pontoons this results in approximately 1380 m^3 of volume for a conventional pontoon and 2000 m^3 for a moored pontoon (due to its extra draught). The four outermost compartments were selected (Figure 7-10), and the waterplane stiffness in heave was reduced with 22% and the roll stiffness by 41% due to the flooding of 2000 m^3 volume. For simplicity, the shift in the center of buoyancy was neglected, and the roll stiffness reduction was assumed to be symmetrical.

A loss of mooring lines could occur due to local damage from the collision event. Loss of mooring lines will release a weight from the pontoon and thus partly counteract the flooding, thereby relieving the bridge girder for some weak axis moment. It was considered that it was sufficient to study these effects separately in order to obtain an upper bound; flooding and loss of hydrostatics as one case and loss of mooring lines as another.

The hydrodynamic parameters of the flooded pontoon was not altered except what is mentioned above, so drag, radiation and diffraction effects due to the increased submergence was not considered.

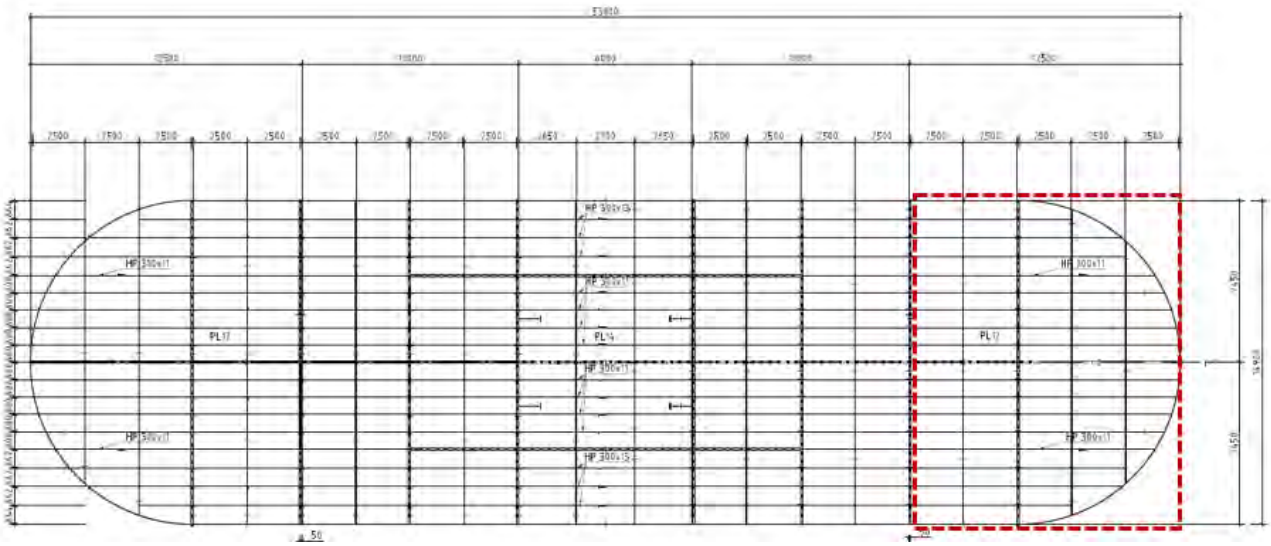

Figure 7-10 Illustration of damaged area for flooding

7.2.1.3 Damaged condition ship-bridge girder collision

NOTE : This section has not been updated with new model revisions as it was considered that the response was acceptable within large margins.

As a preliminary check the damage to a bridge girder following an impact is evaluated based on a phase 3 study from NTNU of deckhouse to bridge girder response. The results for D5 are used in the following as this is closest to the energy level obtained in the global ship collision simulations in [14].

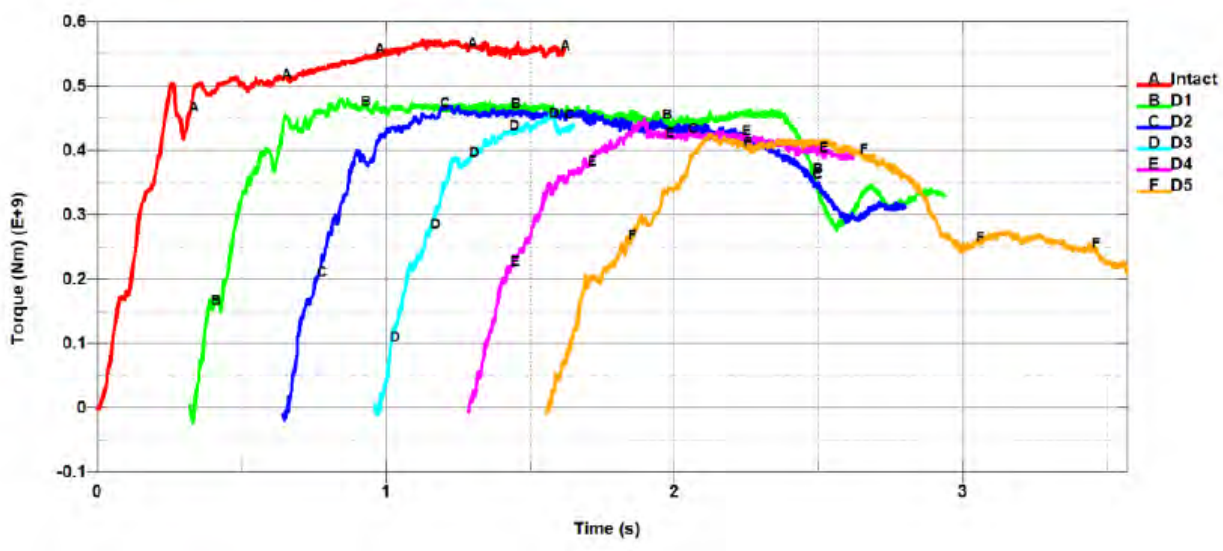

Figure 7-11 Reduction of torsional capacity in bridge girder due to ship collision.

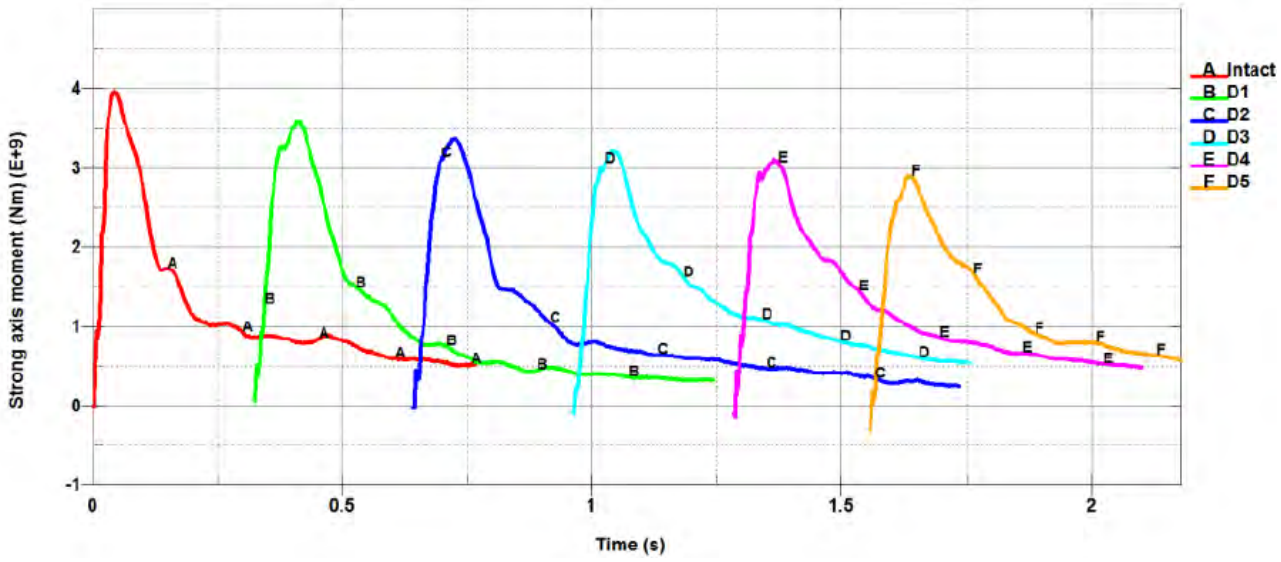

Figure 7-12 Reduction of strong-axis bending moment capacity in bridge girder due to ship collision.

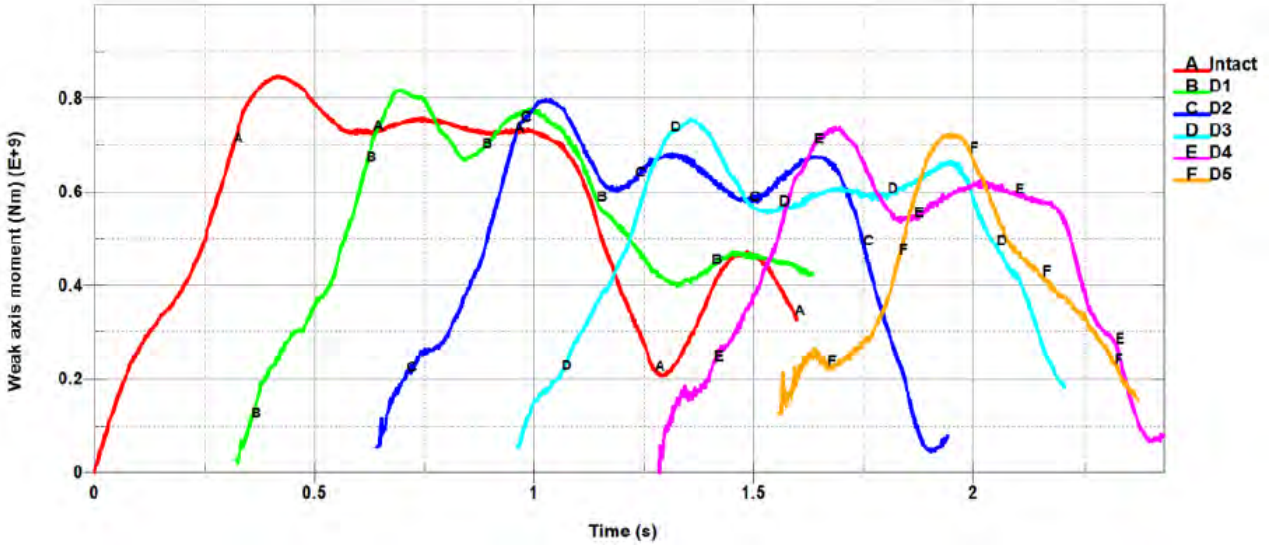

Figure 7-13 Reduction of weak-axis bending moment capacity in bridge girder due to ship collision.

As the simulation results shown above are based on a too weak material model for the deckhouse structure, the capacity reduction due to bridge girder damage is increased to a 30% loss for torsion and strong-axis moment and a 15% loss for weak-axis moment. Capacity reduction for axial force was not available but assumed to be 15%.

The weakness was introduced over a 24 m long span (in the range of deckhouse width) midway between pontoon A20 and A21 for all four concepts.

7.2.2 Results

In the following envelopes of the expected maximum response during a 1-hour simulation is presented. The results of the various damaged bridge concepts are compared against an intact bridge under the same loading, without load factors. For ULS a load factor of 1.6 is applied when the

dynamic load is dominating. Hence, if the response of the damaged bridge is less than 60% higher than the intact bridge the damage condition will not be dimensioning.

7.2.2.1 Loss of mooring lines

A significant increase in strong-axis bending moment when loss of mooring lines coincides with 100-year environmental conditions, shown in Figure 7-14 to Figure 7-16. The increase is larger than 60% in several sections of the bridge, but in general below the ULS capacity.

A 10% increase in weak-axis moment occurs around the pontoon that loose mooring lines. The transverse shear force also increases but is well within the capacity for all the concepts, see Figure 7-15.

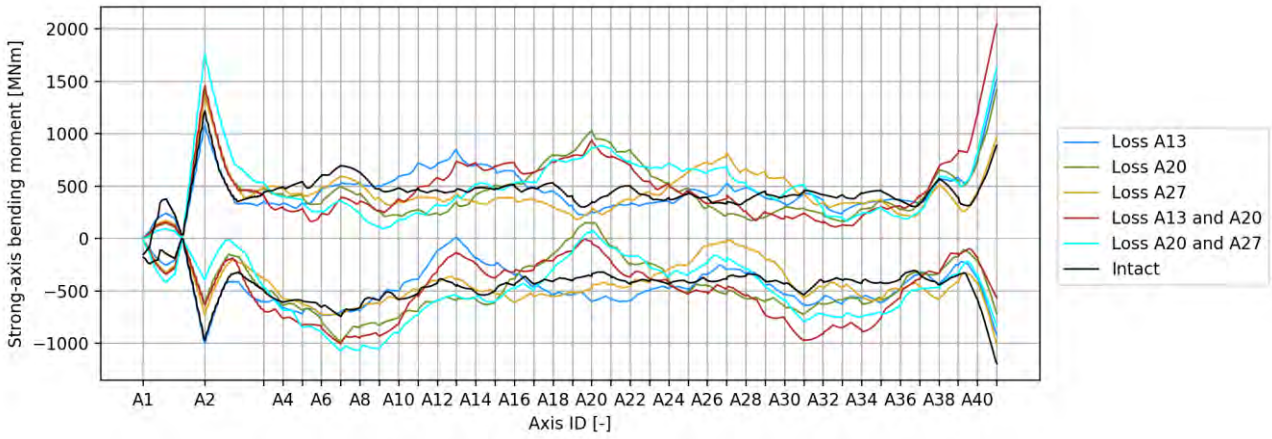

Figure 7-14 Envelopes of resulting strong--axis bending moment for K12_06 from loss of one side of one or two mooring groups in 100-year environmental conditions.

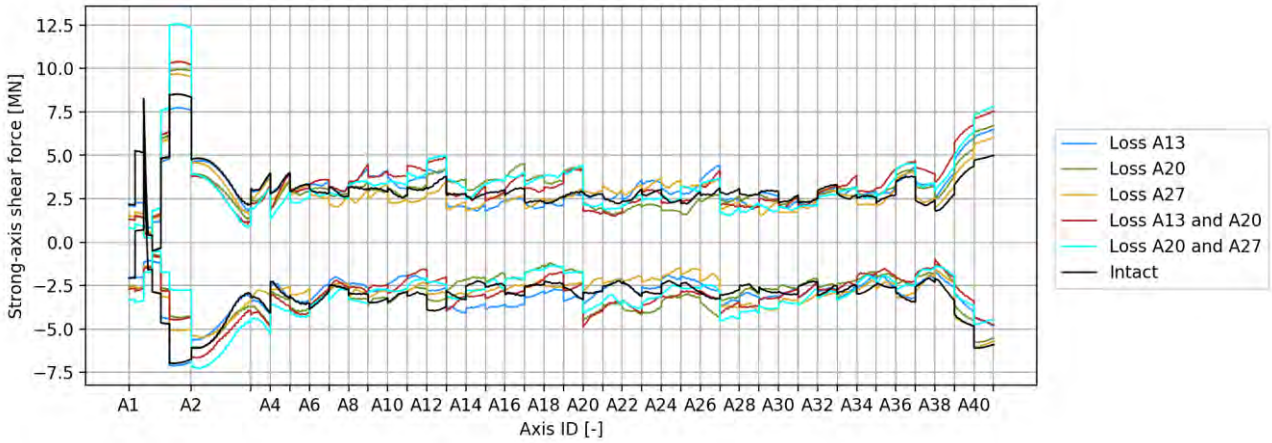

Figure 7-15 Envelopes of resulting strong--axis shear force for K12_06 from loss of one side of one or two mooring groups in 100-year environmental conditions.

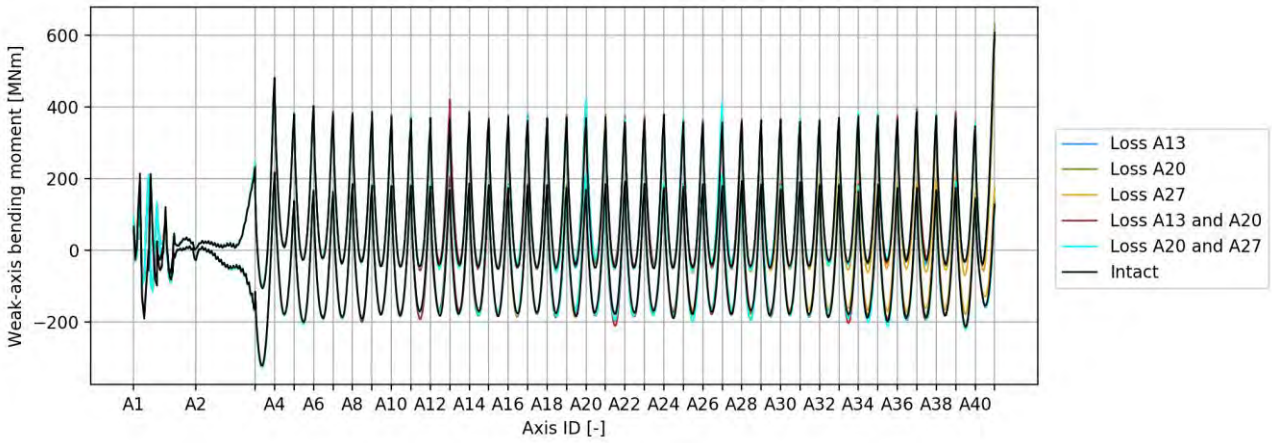

Figure 7-16 Envelopes of resulting weak--axis bending moment for K12_06 from loss of one side of one or two mooring groups in 100-year environmental conditions.

The resulting mooring line forces are shown in Table 7-1. Peak forces after line failure are below the breaking strength of the mooring lines, and progressive collapse is thus not of concern.

Table 7-1 Peak mooring line forces in an envelope of 100-year environmental conditions for intact bridge configuration and with loss of mooring lines.

	K12_06	
Line	**Intact**	**Mooringloss**
MooringLine1	2.9	3
MooringLine2	3.1	3.1
MooringLine3	3	3.9
MooringLine4	2.8	3.7
MooringLine5	3.2	3.3
MooringLine6	2.9	3
MooringLine7	3.2	3.3
MooringLine8	3.4	3.6
MooringLine9	3.4	3.1
MooringLine10	2.1	2.2
MooringLine11	3.2	4.3
MooringLine12	3.1	4.3

7.2.2.2 Flooding due to ship collision

The flooding event described in section 7.2.1.2 includes significant loss of buoyancy and waterplane stiffness in heave and roll. In a 100-year environmental condition the only significant bridge response is in weak-axis bending moment and shear force, shown in Figure 7-17 and Figure 7-18. The maximum weak-axis moment increases around 35%, and somewhat less for the shear force. The weak-axis moment in damaged condition is less than that in the ULS2 load combination and is primarily due to the static equilibrium, not dynamic effects.

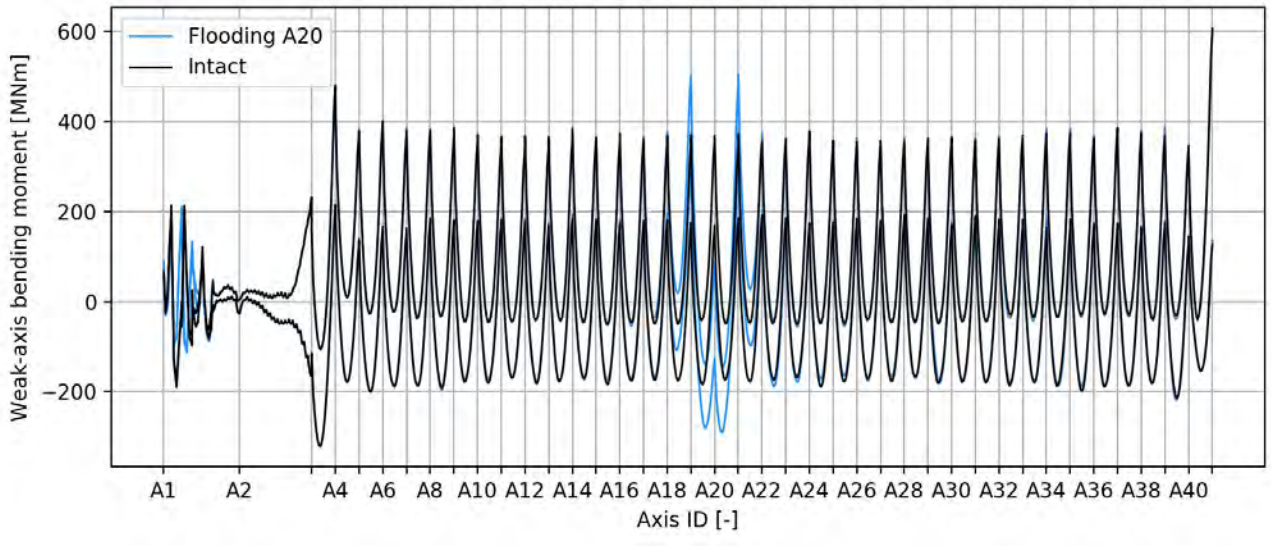

Figure 7-17 Envelope of weak-axis bending moment due to flooding of pontoon A20 for bridge K12_06.

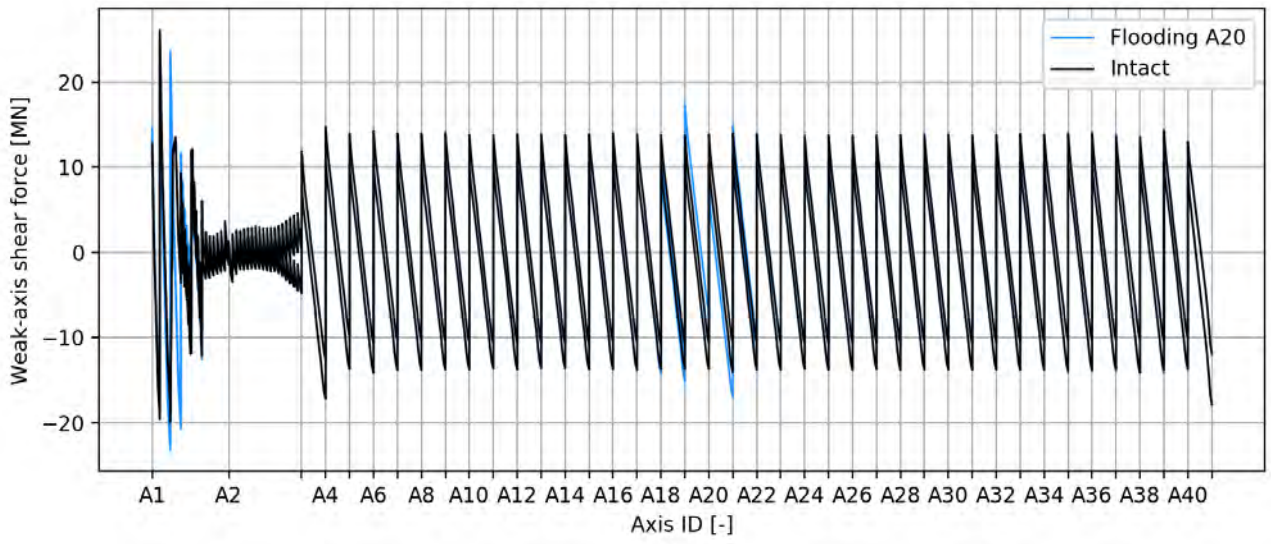

Figure 7-18 Envelope of weak-axis shear force due to flooding of pontoon A20 for bridge K12_06.

7.2.2.3 Response with damaged bridge girder

Overall, the global bridge behavior is not sensitive to local damages to the bridge girder cross-section in the order of magnitude as those assumed in section 7.2.1.3. An example is shown Figure 7-19. Hence, the acceptance criterium for local damage is that the damaged cross-section has enough local capacity to withstand the global response level of the intact bridge.

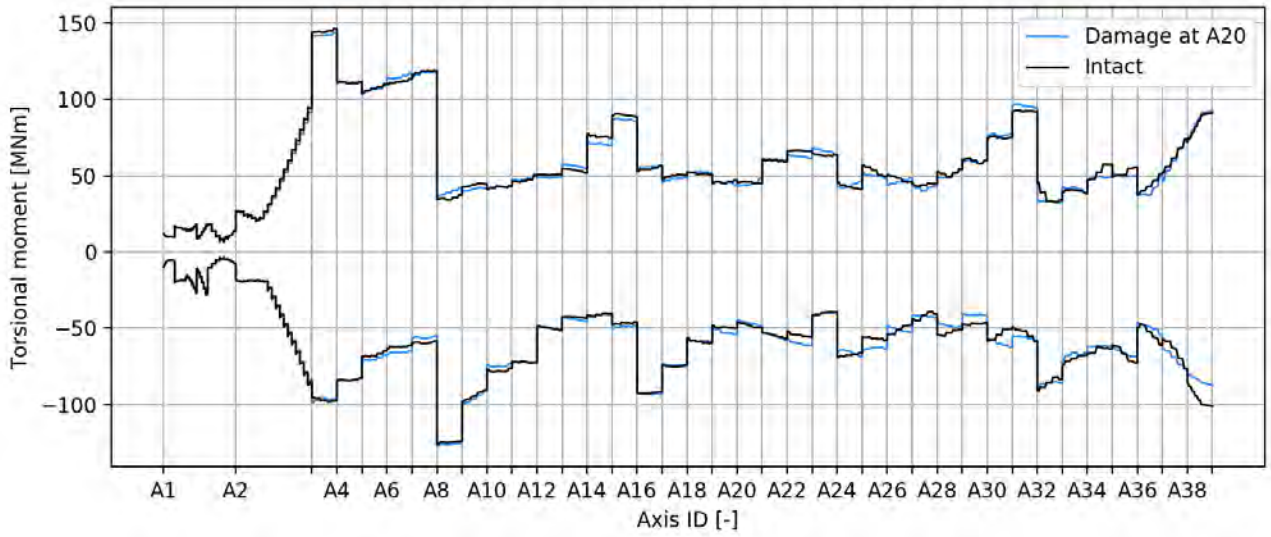

Figure 7-19 Envelope of torsional moment due to damage to the bridge girder close to A20 for bridge K13_06.

7.2.3 Discussion

The checks of residual capacity after a damage to the bridge or mooring system shows satisfactory response for all cases considered.

The increased response due to a damage event is either within the load factors used for ULS design (hence not dimensioning) or lower than the allowable limits for the relevant sectional loads. The bridge is as such considered robust against the specified damage events.

8 Sensitivities

Sensitivity studies were performed on all the four bridge concepts, and not rerun to be consistent with the K12_07 concept after it was selected as the preferred concept. The following show results for all four concepts.

8.1 Wave spectrum sensitivity

The wave spectrum sensitivity study was conducted for concepts K11_07, K12_06, K13_06 and K14_06. The conclusions are considered valid also for concept K12_07 as there are only minor stiffness changes from K12_06 to K12_07.

In a highly mode dependent problem like a floating bridge, it is important to make sure that the frequency dependent loading is properly discretized so that all eigen modes that lies within the range of the incident spectrum are triggered. Otherwise, the chances are that important modal responses are underestimated. This is especially important when estimating sensitive frequency dependent problems like parametric excitation.

There are many different approaches to discretization of the energy spectrum. In OrcaFlex, there are three methods; arithmetic progression, geometric progression and equal energy. To make sure that we cover the part of the spectrum with most energy the equal energy method is applied. In addition to the method, discretization is dependent on the number of frequency components. See [3] for a sensitivity study in the spectrum discretization.

The spectrum itself and the directional spreading are governed by parameters for which a range of possible values are given in the metocean design basis [5]. To evaluate the sensitivity of the bridge concept to changes in the parameters governing the wave modelling, full screenings of the characteristic response in the bridge girder – as outlined in section 2.2 - are run where one parameter is changed at a time; covering the range of possible values given in the metocean design basis as outlined in Table 8-1.

Table 8-1 Discretization parameters covered in sensitivity analysis

Wave	Gamma	ncos
Local wind waves	1.8, 2.3	3, 4, 8
Swell	3, 5	10, 20

Only bending moment about strong axis and axial loads in the bridge girder are checked in this sensitivity study, since these responses are most sensitive to changes in wave conditions. Only 10.000 year return period wave conditions have been screened. For the gamma value, the sensitivity analysis has been run for all bridge concepts. For ncos only K11 and K14 were analyzed.

The results show that the response from wind driven waves is not very sensitive to variation in wave parameters. This is probably due to a large number of eigen modes in the wind driven period regime. Therefore, there is no way to “turn the nobs” so that you avoid modes that you would otherwise trigger.

For swell the response is moderately sensitive to variation in wave parameters. In the swell period regime, only a few transversal eigen modes are triggered. Therefore, if the spectrum or direction is shifted slightly then another incident wave direction and spectrum will give the highest response.

A summary of the spectrum sensitivity study is shown in the following subsections. The resulting recommended discretization parameters are shown in Table 8-2.

Table 8-2 Recommended discretization parameters.

Wave	Gamma	ncos
Wind sea	2.3	8
Swell	5	20

8.1.1 Wind sea

Wind sea screenings for each concept were performed with variation of the gamma and ncos parameters. The results show that the characteristic response in the bridge girder is not very sensitive to changes in the discretization parameters. Further, the direction, period and height for which the characteristic response occurs are not changing with changes in the discretization parameters. An example of such a result is shown in Figure 8-1, where we see the same pattern repeated for three different values of ncos.

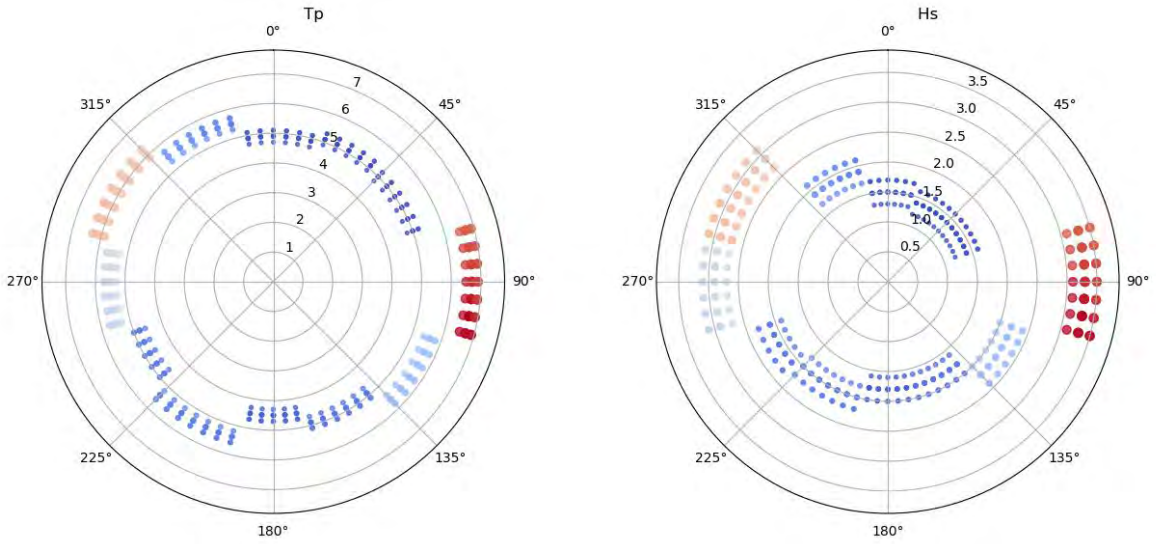

Figure 8-1: The contour of the wind sea conditions as given in [5]. For each wave direction there are three different dots, representing the same wave condition, but different discretization values. They are plotted together for visual comparison. The plot shows strong axis bending moment for K11_06 with variation of the ncos parameter.

Table 8-3 Strong axis bending moment and axial load variation with changing gamma values

	Max Bending moment about strong axis (Exp max)			Max Axial load (Exp max)		
Concept	γ=2.3	γ=1.8	diff	γ=2.3	γ=1.8	diff
K11_07	1112,3	1095	1,6 %	43,5	42,6	2,1 %
K12_06	828,4	836,4	-1,0 %	39,2	38,5	1,8 %
K13_06	1207	1164,4	3,5 %	26,5	26,3	0,8 %
K14_06	1011,3	982,3	2,9 %	40,8	39,5	3,2 %

Table 8-4: Strong axis bending moment and axial load variation with changing ncos values

	Max Bending moment about strong axis (Exp max)			Max Axial load (Exp max)		
Concept	ncos=3	ncos=8	diff	ncos=3	ncos=8	diff
K11_07	1033,3	1080,6	-4,6 %	42	40,7	3,1 %
K12_06						
K13_06						
K14_06	673,3	711,7	-5,7 %	29,7	27,5	7,4 %

8.1.2 Swell

Swell screenings for each concept were performed with variations of the gamma and ncos parameters. The results show that the characteristic response in the bridge girder is moderately sensitive to changes in the discretization parameters. Further, the direction, period and height for which the characteristic response occurs changes slightly with changes in the discretization parameters. An example of such a result is shown in Figure 8-2.

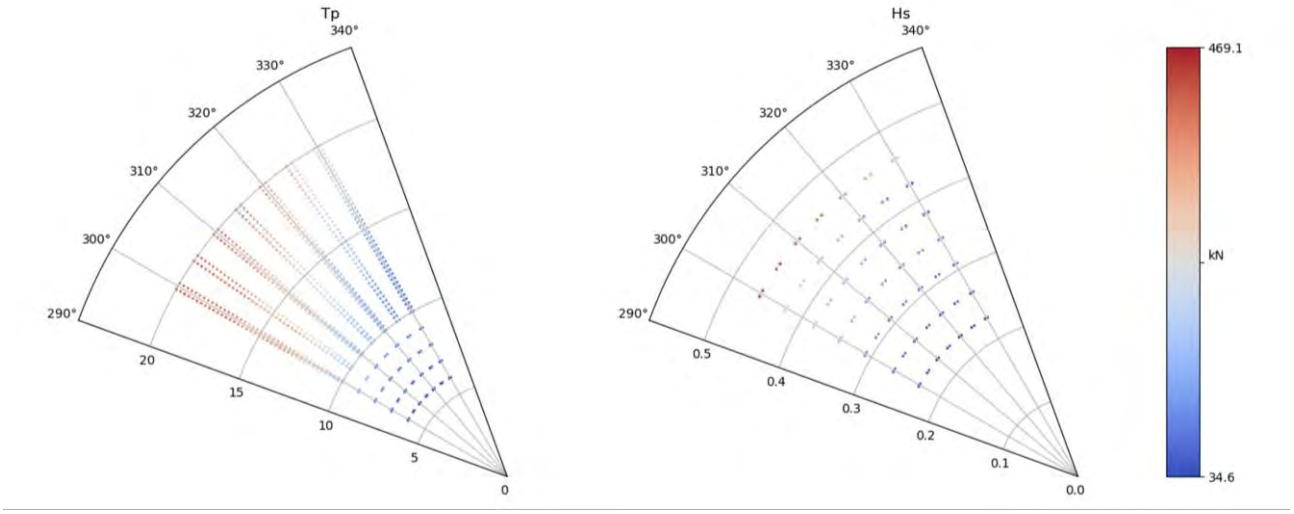

Figure 8-2 Bridge concept K14_05. The contour of the swell conditions, ref SBJ-01-C4-SVV-01-BA-001 rev_1, table 2. For each wave direction, height and period there are two different dots, representing the same wave condition, but different discretization values. They are plotted together for visual comparison.

Table 8-5: Strong axis bending moment and axial load variation with changing gamma values

	Max Bending moment about strong axis (Exp max)			Max Axial load (Exp max)		
Concept	γ=3	γ=5	diff	γ=3	γ=5	diff
K11_07	1043,9	1128,7	-8,2 %	33,7	35,3	-4,7 %
K14_06	418,3	398,3	4,8 %	11,6	12,1	-4,3 %

Table 8-6: Strong axis bending moment and axial load variation with changing ncos values

	Max Bending moment about strong axis (Exp max)			Max Axial load (Exp max)		
Concept	ncos=10	ncos=20	diff	ncos=10	ncos=20	diff
K11_07	1042,9	1087,0	-4,2 %	33,7	33,4	1,1 %
K14_06	418,3	439,6	-5,1 %	11,6	11,3	2,9 %

8.2 Sensitivities in the prediction of long-term response

The ultimate goal of a long-term response analysis is to identify the response value with a given return period. More specifically, we seek the characteristic response value r_q, which has a specified annual exceedance probability q. This is referred to as the q-probability response or the $1/q$-year response. For instance, the 100-year response has a probability $q = 0.01$ of being exceeded during any year, which means that it is exceeded in average once every 100 years.

The q-probability response is most accurately determined by a full long-term approach. However, due to the large computational cost associated with this approach, the environmental contour method is commonly used to obtain reasonable estimates of the q-probability response. Recently, methods have been developed which provide more accurate estimates of the q-probability response at a significantly reduced computational cost [15, 16]. These methods are referred to as inverse reliability methods. The relation between the full long-term approach, the environmental contour method and the inverse reliability methods is explained in detail in Enclosure 15.

In the Bjørnafjorden project so far, environmental contour lines have been applied to identify which sea states that give rise to the q-probability response. An assessment of the validity of the contour line approach is carried out in Enclosure 15 for K12_07. The 100-year response due to wind waves was calculated by an inverse reliability method, using joint distributions of H_s and T_p for each directional sector which were provided by the client. The provided (H_s, T_p)-distributions were the same distributions that the environmental contours reported in the metocean design basis [5] are based on. However, the environmental contours that are reported therein have been adjusted in order to give more correct 100-year H_s values. The difference in the 100-year environmental contours is shown in Figure 8-3. Thus, the environmental model used with the inverse reliability method was not validated for direct use in a long-term response analysis. Still, the model was used to give an indication of the uncertainty of the contour line approach.

In Enclosure 15 the 100-year response due to wind waves was calculated for 20 different responses along the K12_07 concept using an inverse reliability method. The results were compared with the 100-year response estimates from the contour line approach. An example of a 100-year response value and the corresponding design point obtained by the inverse reliability method is given in Figure 8-4. Even if the results in Enclosure 15 are based on an environmental model that is not validated for use in long-term response estimation, they give an indication that the estimates of the long-term response produced by the contour line approach might be too rough in some cases. It is however not possible to draw any definite conclusion without a comparison with a full long-term approach. Further studies on the long-term response are therefore recommended. An environmental model suited for use in long-term response analyses should be established, and full integration of the long-term response formulation should be carried out for some selected cases.

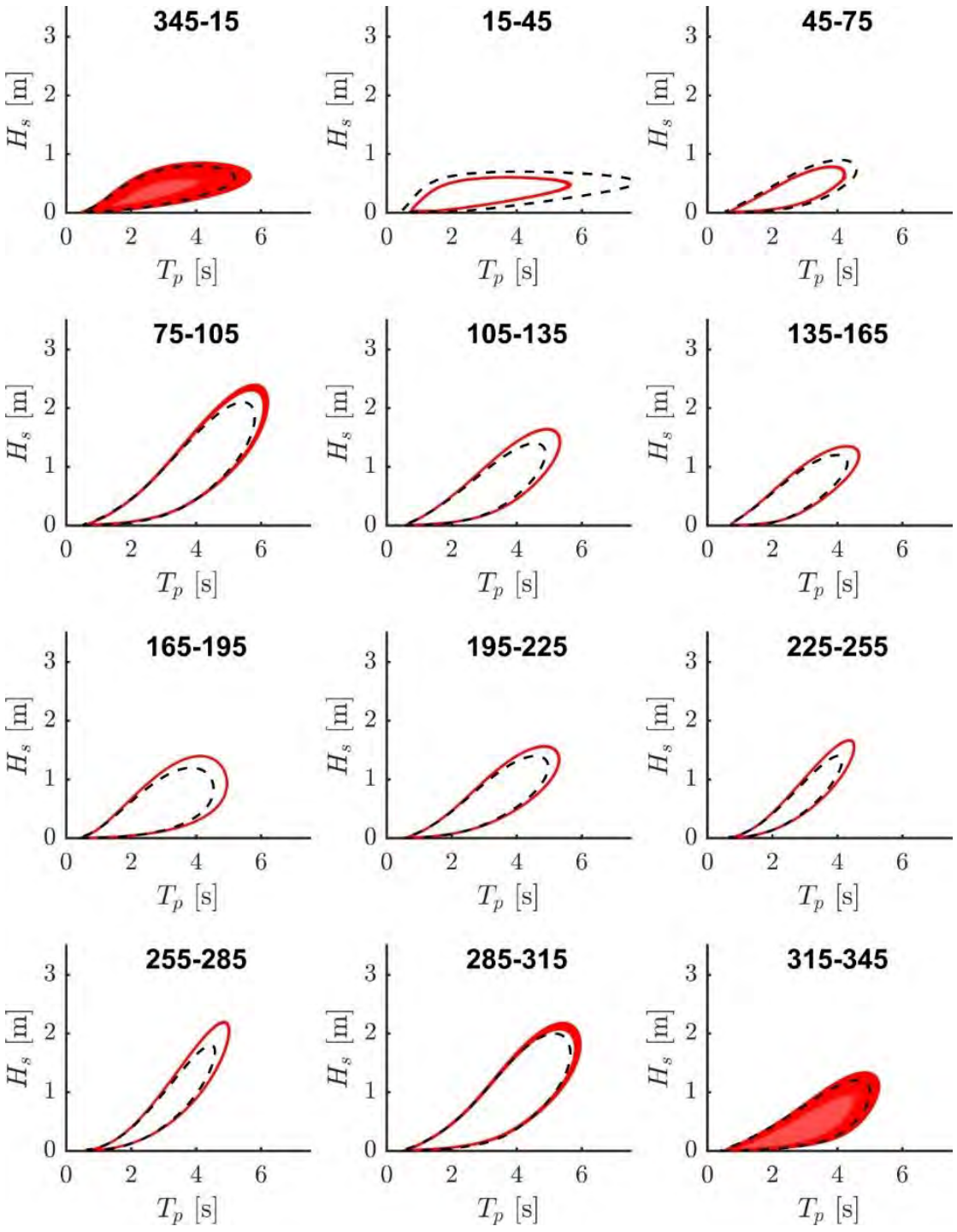

Figure 8-3 The 100-year environmental contours for the model applied with the inverse reliability method (red solid lines) and the directional contours given in the metocean design basis (black dashed lines).

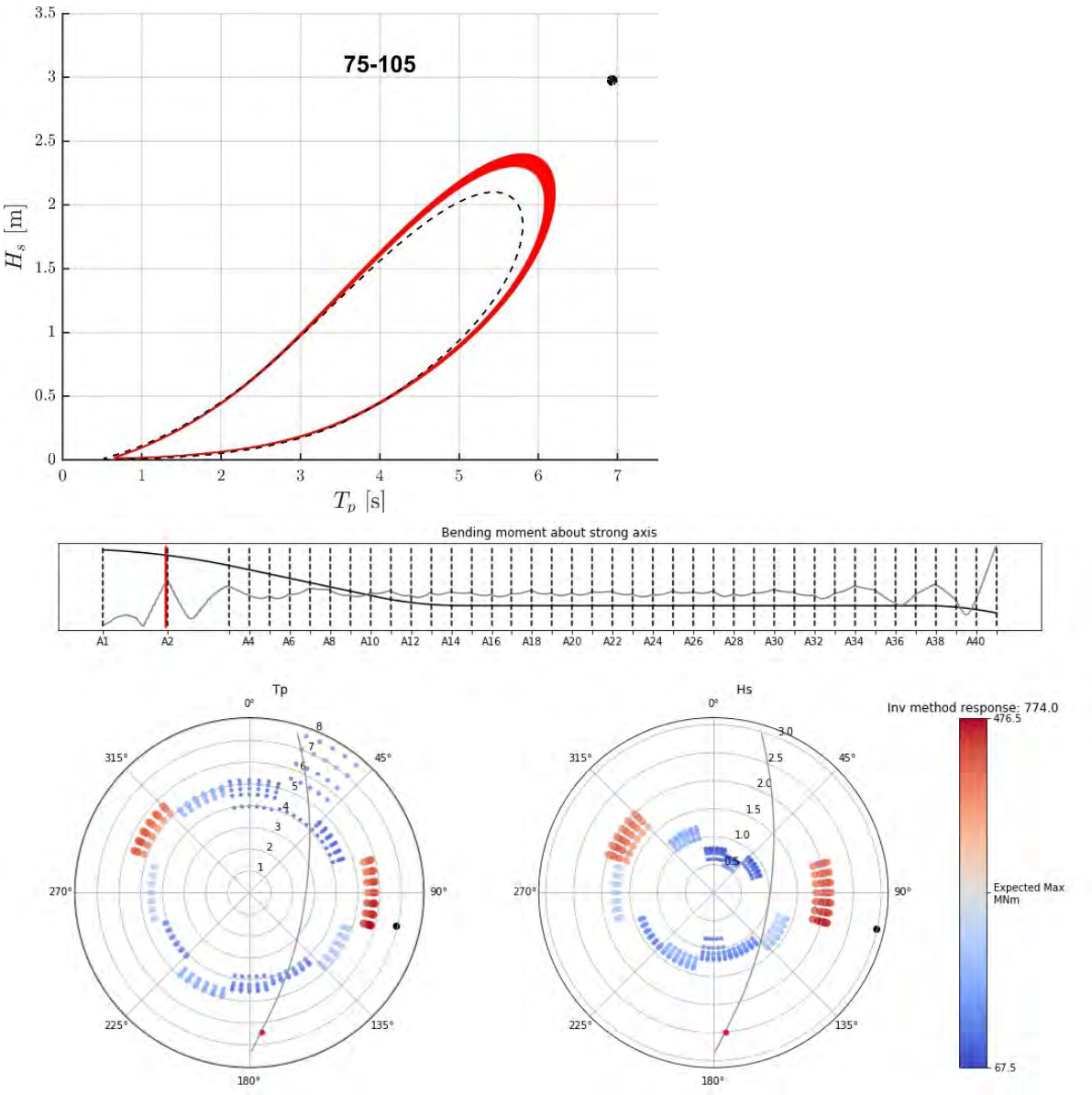

Figure 8-4 Bending moment about strong axis in the bridge girder at the south side of axis 2 (the tower) of K12_07 for 100-year return period sea states along the contour (dashed line in the top plot), plotted together with the inverse reliability method design point (black dot). The inverse reliability method gives a 100-year response of 774 MNm, whereas the largest value of the expected 1-hour max along the contour is 477 MNm.

8.3 Evaluation of mooring system's sensitivity to static load effects

8.3.1 Introduction

The analyses for ULS have been performed by combining the individual load groups, such that deformations and forces from other load groups are not accounted for.

The static load effects (tide, temperature, current, static wind, mean drift) will affect the individual damping). In [17], the pretension is plotted versus the sway damping coefficient, illustrating a peak value for the sway damping coefficient at 3000 kN (note that this peak value is only correct for the analysed mooring system in the memo and may be somewhat different for the mooring systems for K12-K14). Variations of the viscous damping contribution from mooring lines is particularly important

when investigating the dynamic response for swell, which is significantly affected by the mooring system's damping.

8.3.2 Comparison K12 / K14

The mooring systems for the K14 bridge concept are more affected by the horizontal load effects than the K12 bridge concept, as the static horizontal loads mainly acts in the mooring system for the K14 concept while the arch action contributes to significant horizontal stiffness for the K12 concept. The resulting transverse displacement from current and temperature are compared in Table 8-7, where K11 is included to illustrate the displacement for the concept where the horizontal stiffness only results from arch action.

Table 8-7: Comparison of transverse displacement from static load affects, giving an indicative comparison of the deflection for the bridge concepts. The displacement from current is evaluated including the cases defined in [18] (shear flow, linearly increasing flow etc).

	K11	K12	K14	Unit
Current$_{10\,000\,year}$	4.5	0.9	1.8	m
Temperature$_{30\,deg}$	3.6	2.9	2.7	m

The static and dynamic mooring line responses are reported separately in [19], where it is reported that K14 has approx. 80% higher mooring line loads from the static load effects, which is due to the static horizontal loads (current, mean wind). The mooring line response from temperature and tide are similar for K12 and K14.

8.3.3 Evaluation K12

Three static cases / configurations have been evaluated for the K12 concept to evaluate how the static load effects affect the mooring system configurations:

- Basecase: only permanent loading
- 100 yr Case: permanent, -1.5m sea level and 30 degrees temperature increase
- Tide -5m: -5m sea level to trigger a large reduction of pretension (far above the 10 000 year tidal range).

The resulting line tensions, cluster quadratic damping coefficients and cluster stiffness are presented in Table 8-8, Table 8-9 and Table 8-10.

An approx. 1/3 reduction of pretension (axis 28, Tide -5m) results in a 60% reduction of cluster quadratic damping and a 70% reduction of horizontal stiffness.

Table 8-8: Resulting mooring line pretension for each mooring line for the evaluated static cases.

Line Pretension		Line1 [kN]	Line2 [kN]	Line3 [kN]	Line4 [kN]	Line1	Line2	Line3	Line4
Axis 13	Basecase	1976	1995	2086	1933	100 %	100 %	100 %	100 %
	100yr Case	1774	1742	1918	1797	90 %	87 %	92 %	93 %
	Tide -5m	1488	1420	1656	1579	75 %	71 %	79 %	82 %
Axis 20	Basecase	2583	2274	2541	2638	100 %	100 %	100 %	100 %
	100yr Case	2430	2141	2344	2373	94 %	94 %	92 %	90 %
	Tide -5m	2155	1906	2021	1968	83 %	84 %	80 %	75 %

Axis 27	Basecase	2172	1693	2076	2035	100 %	100 %	100 %	100 %
	100yr Case	1870	1586	1753	1749	86 %	94 %	84 %	86 %
	Tide -5m	1487	1406	1384	1397	68 %	83 %	67 %	69 %

Table 8-9: Resulting horizontal quadratic damping coefficient for each cluster for the evaluated static cases.

Quadratic Damping Coeff.		**Sway [kN/m/s]**	**Sway**
Axis 13	Basecase	1891	100 %
	100yr Case	1463	77 %
	Tide -5m	828	44 %
Axis 20	Basecase	2771	100 %
	100yr Case	2504	90 %
	Tide -5m	1850	67 %
Axis 27	Basecase	1882	100 %
	100yr Case	1439	76 %
	Tide -5m	749	40 %

Table 8-10: Resulting horizontal stiffness for each cluster for the evaluated static cases.

Resulting Stiffness		**Sway [kN]**	**Sway**
Axis 13	Basecase	540	100 %
	100yr Case	387	78 %
	Tide -5m	215	40 %
Axis 20	Basecase	628	100 %
	100yr Case	506	82 %
	Tide -5m	328	52 %
Axis 27	Basecase	792	100 %
	100yr Case	517	67 %
	Tide -5m	254	32 %

The strong axis moment dynamic response from swell has been compared for the Basecase and the "Tide -5m" case for K12_06. The results are presented in Figure 8-5. The critical eigenperiod is shifted from approx. 17s to 17.1s by the change of horizontal stiffness and has been accounted for by shifting the peak period correspondingly. The results from the analyses show that there is approx. a 10% increase in the response for the "Tide -5m" case as compared to the basecase model when accounting for the 70% decrease in mooring line damping.

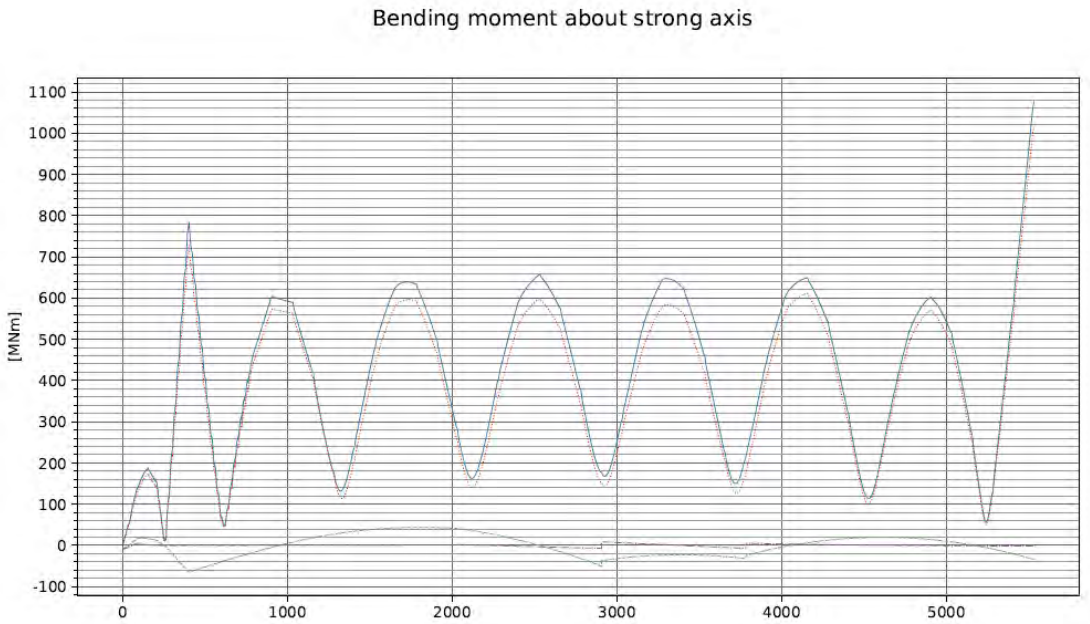

Figure 8-5: Comparison of strong axis moment for the 100 year swell condition for the Basecase labelled in red, and the "Tide -5m" labelled in blue. The purple and green lines illustrate the static value for Basecase and "Tide -5m", respectively.

As the mooring system characteristics is greatly affected by the pretension, this topic should be investigated further to ensure that all critical combinations of static forces and dynamic responses are evaluated, including evaluation of parametric resonance. A design mitigation, if this turns out to be a challenge, is to modify the permanent pretension such as designing for a lower or higher pretension at mean sea level. Hence, this is something to keep in mind during detailed design of the bridge but not a cause of great concern. In further work a design philosophy that accounts for this uncertainty should be developed.

8.4 Sensitivity of abutment modelling

In the global analysis the abutment is modelled as a fixed connection to ground / constraint. The connection may be somewhat compliant due to the large ultimate forces acting about the vertical axis. To evaluate this, eigenvalues analyses have been performed for the K11 concept, where the abutment flexibility is modelled by a rotational spring. The resulting horizontal eigenmodes and eigen periods are presented in Figure 8-6 - Figure 8-9.

The rotational stiffness for the northern abutment is calculated to be in the range of $1x10^{9}$ - $1x10^{11}$kNm/deg. The sensitivity analysis show that the eigenmodes are not greatly affected by this rotational stiffness, and the global response is as such not affected.

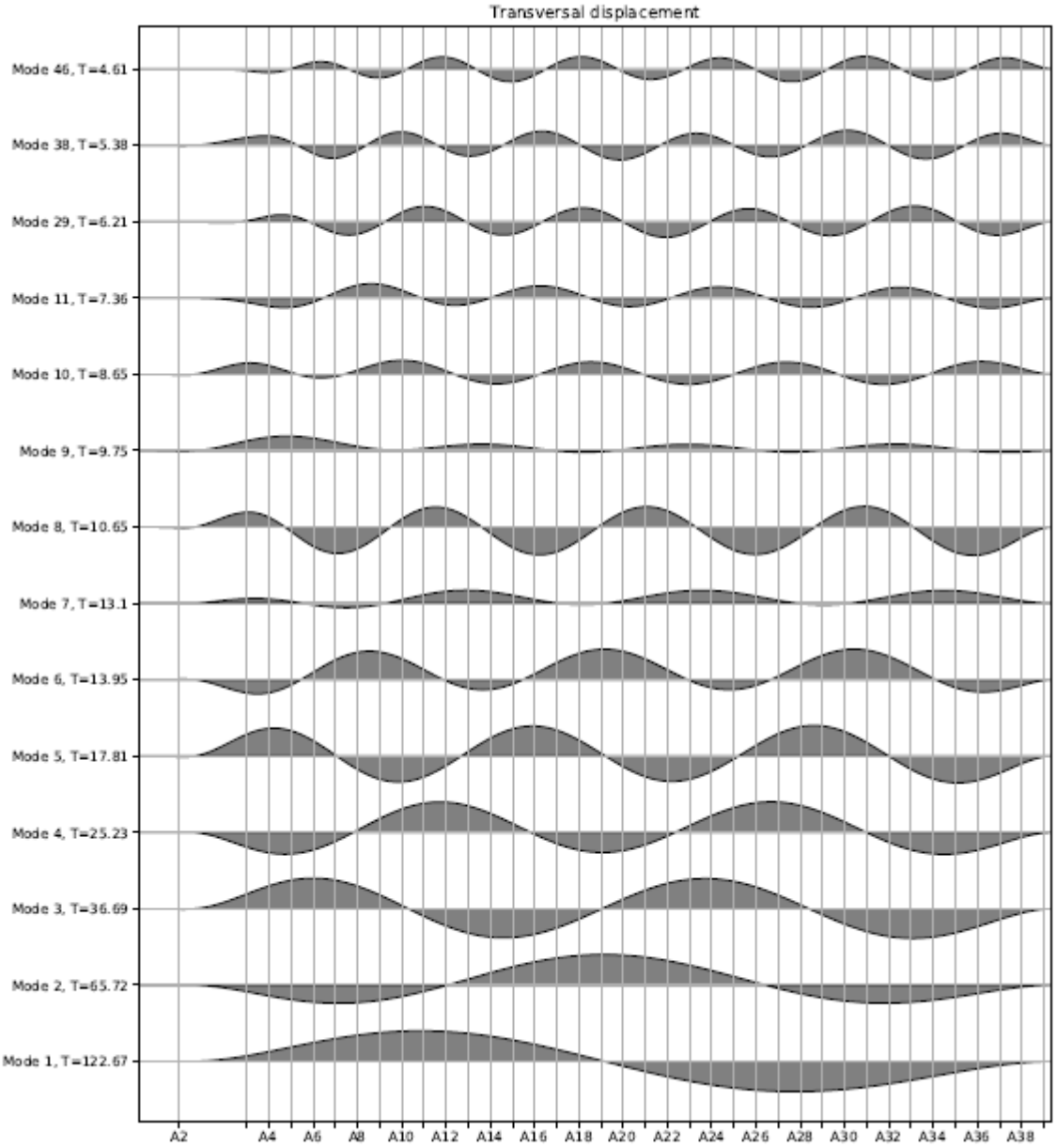

Figure 8-6: K11-06 Fixed Northern Abutment

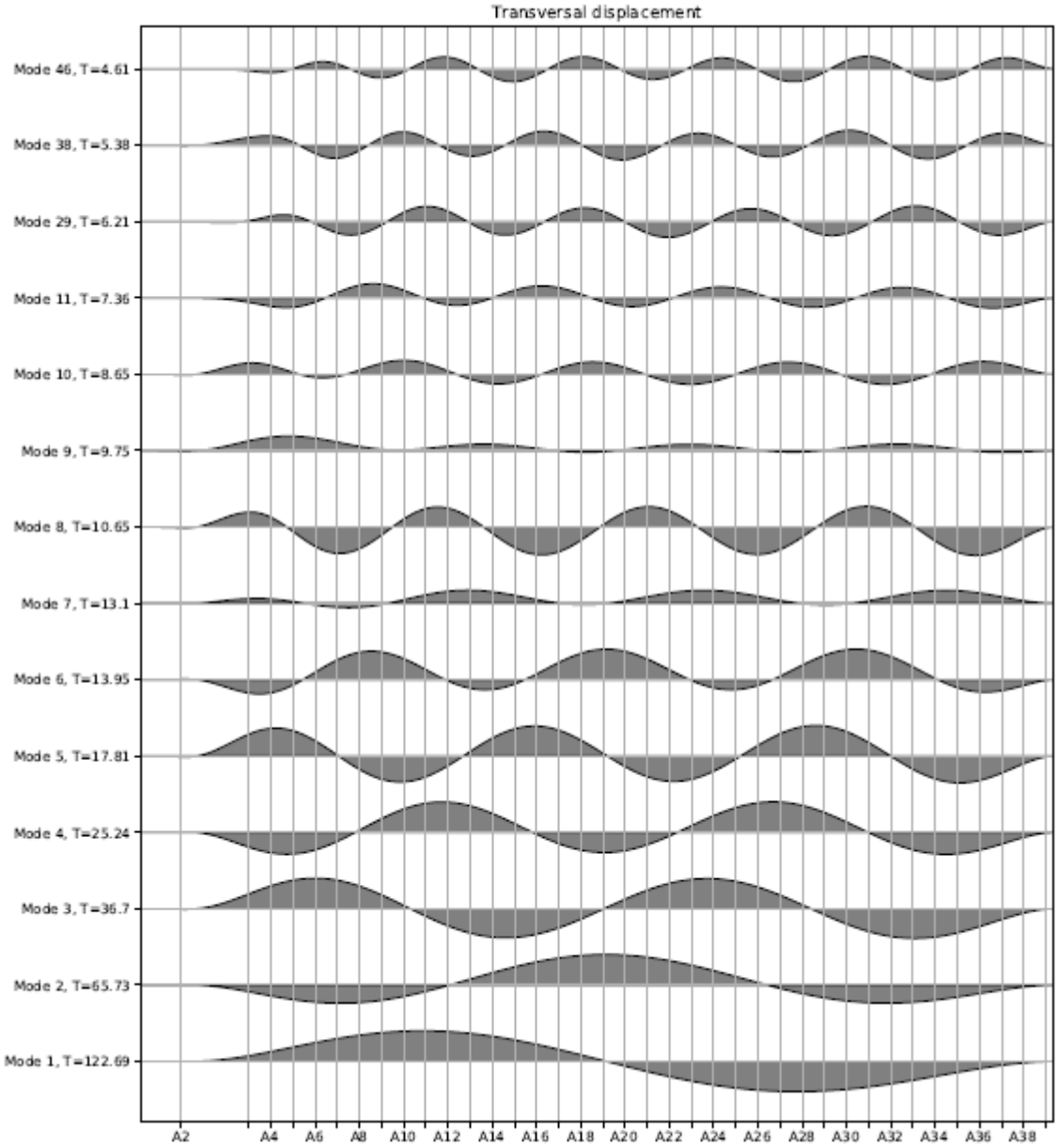

Figure 8-7: K11-06 Rotational spring in Northern Abutment, 1E9 kNm/deg.

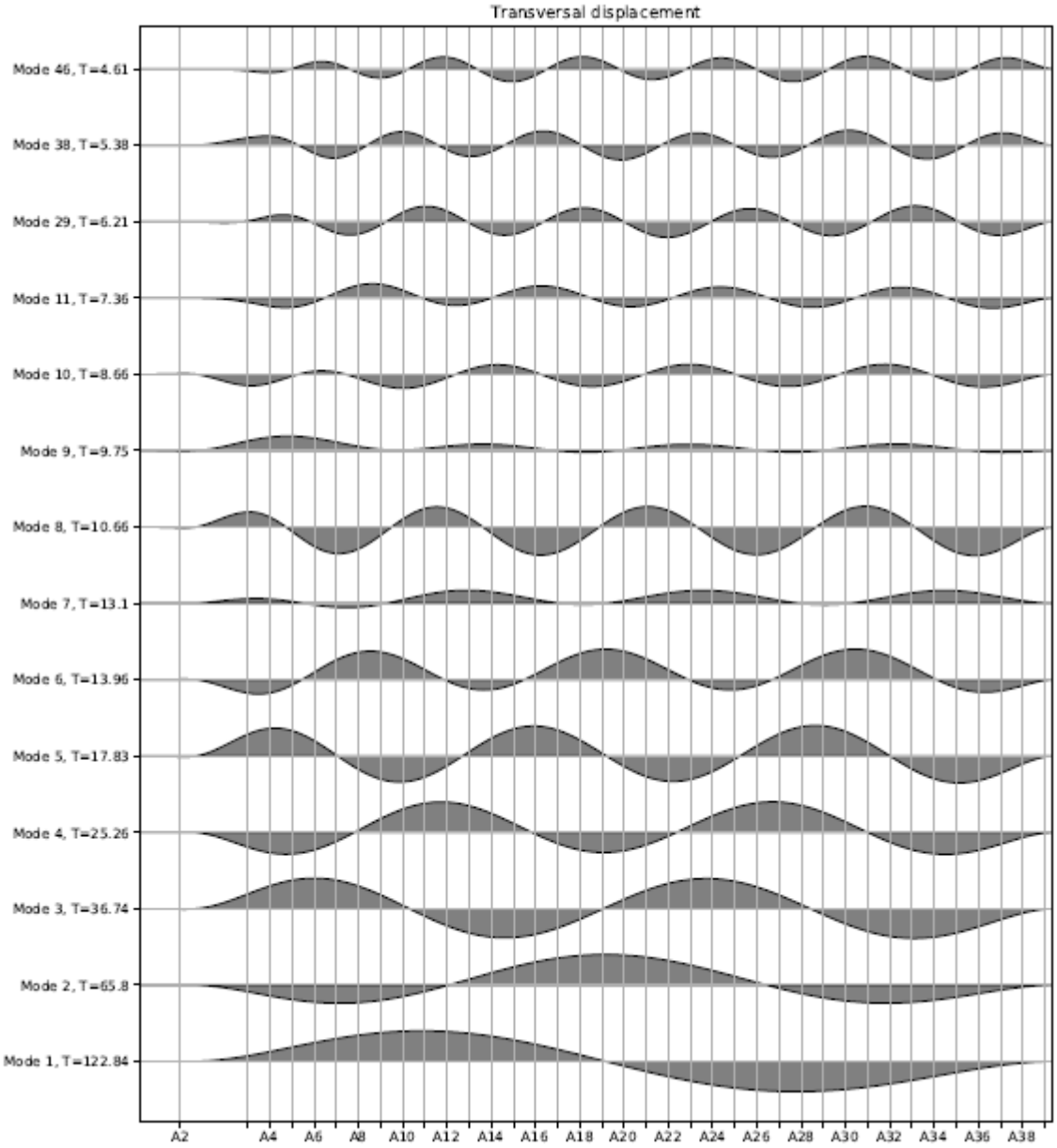

Figure 8-8 K11-06 Rotational spring in Northern Abutment, 1E8 kNm/deg

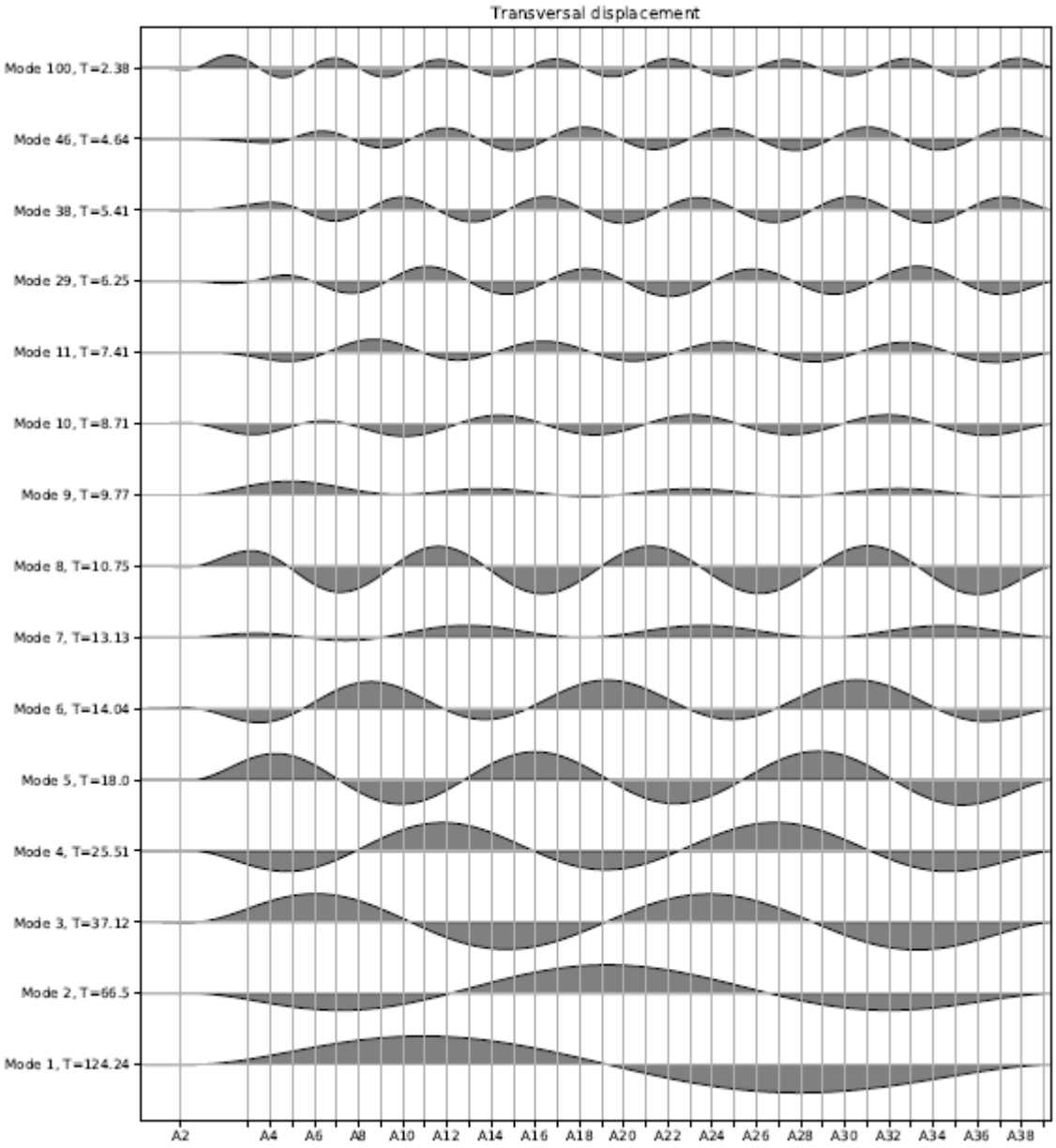

Figure 8-9 K11-06 Rotational spring in Northern Abutment, 1E7 kNm/deg

8.5 Sensitivity to traffic

The bridge is open for 1-year environmental conditions, and some traffic is to be expected. The ULS load combinations in section 6.2 include the effect of the weight of traffic with 60 kN/m over a section of the bridge combined with other environmental loads. However, the effect of wind loading directly on the vehicle was not accounted for.

As a sensitivity study, a version of the K12_06 model was modified to include the following effects:

- A traffic load of 2 tons/m
- Updated hydrodynamic parameters accounting for the increased draught (about 0.3 m) due to the traffic load.
- Updated aerodynamic parameters for mixed traffic on the bridge (listed in [20])

Two load scenarios were defined; traffic along the entire bridge length (termed *even traffic* in the following) and traffic along the southern half of the bridge (termed *south traffic* in the following). For simplicity the traffic was assumed centered in the bridge cross-section. For even traffic along the entire bridge girder the longest eigenmode increases from 56 to 58 s. The environmental load cases were not tuned towards the new eigenperiods for the bridge with increased mass, rather the same load cases were simulated for the bridge with and without traffic.

Compared to the ULS2 results in section 6.2 this sensitivity scenario captures fully the increased wind load, but the traffic weight along the bridge and thus the weak-axis moment will be somewhat lower than those reported for ULS2. The various effects are included simultaneously, and the contribution from each individual component is not separated.

The updated bridge model is simulated using coupled time-domain simulations of the five environmental conditions with 1-year return period as given in section 2.4, and compared to the same bridge but without the effects of traffic using the expected maximum response levels. Figure 8-10 to Figure 8-13 show key results. A slight increase in all response components is observed.

The weak-axis response is worse for the conventional ULS2 approach than the sensitivity study shown below (due to 60 vs 20 kN/m traffic load). The effect of increased hydrodynamic loads due to increased draught is believed to be minor, but this has not been checked separately. The dynamic weak axis bending moment shows a small increase when considering coupled traffic, due to the modified hydrodynamic coefficients and the modified aerodynamic parameters. The increase in axial force and strong-axis moment when considering coupled traffic is assumed to primarily be caused by the aerodynamic drag force from traffic. Traffic on only the southern part of the bridge yields a somewhat higher response for strong-axis moment and axial force than the even traffic on the entire bridge girder.

ULS2 is dominated by weak-axis bending moment, and the strong-axis response is of lesser importance. For ULS3 the strong-axis response is more important. Hence, it is considered that the conventional ULS2 approach as used in section 6.2 will be governing for the 1-year response evaluation (weak-axis), and an additional check with traffic on the bridge including wind loading will not exceed the strong-axis response that is found in ULS3.

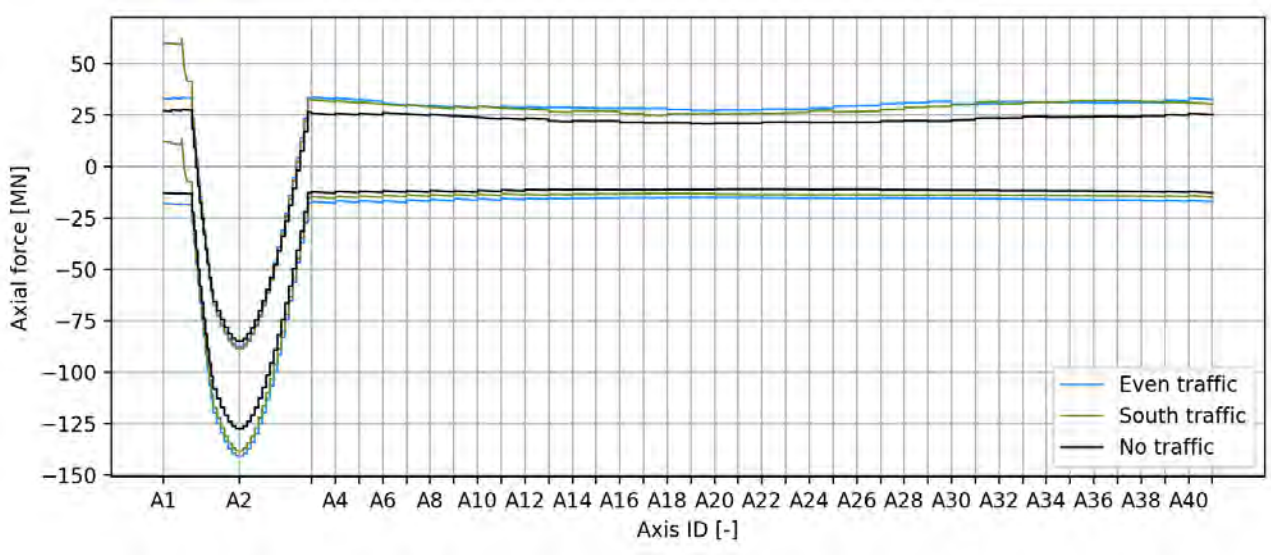

Figure 8-10 Envelope of axial force in a sensitivity check of bridge response with and without effect of traffic in 1-year environmental conditions.

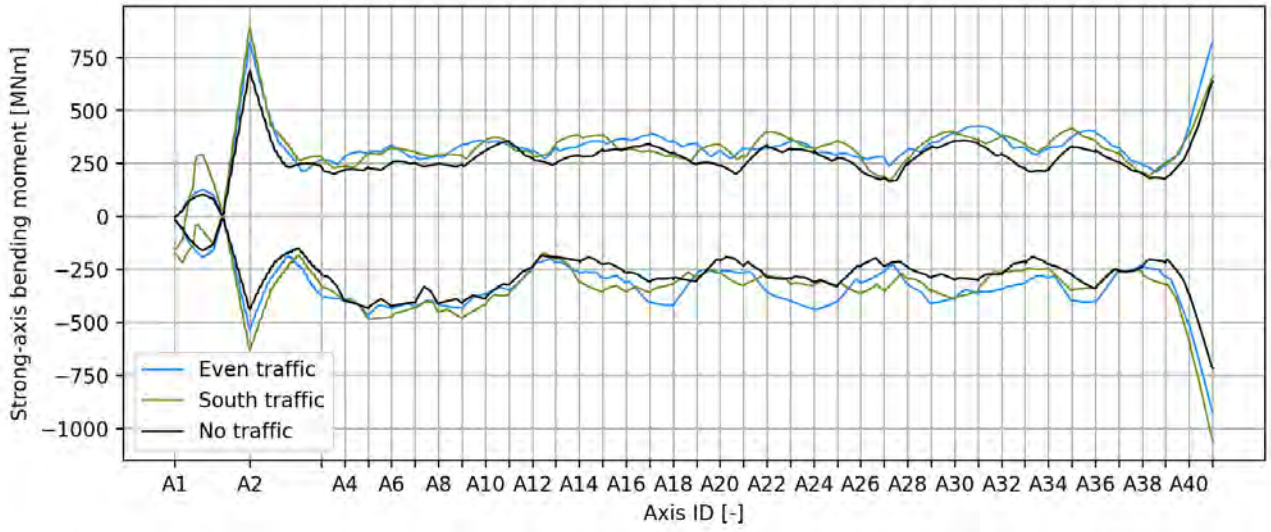

Figure 8-11 Envelope of strong-axis bending moment in a sensitivity check of bridge response with and without effect of traffic in 1-year environmental conditions.

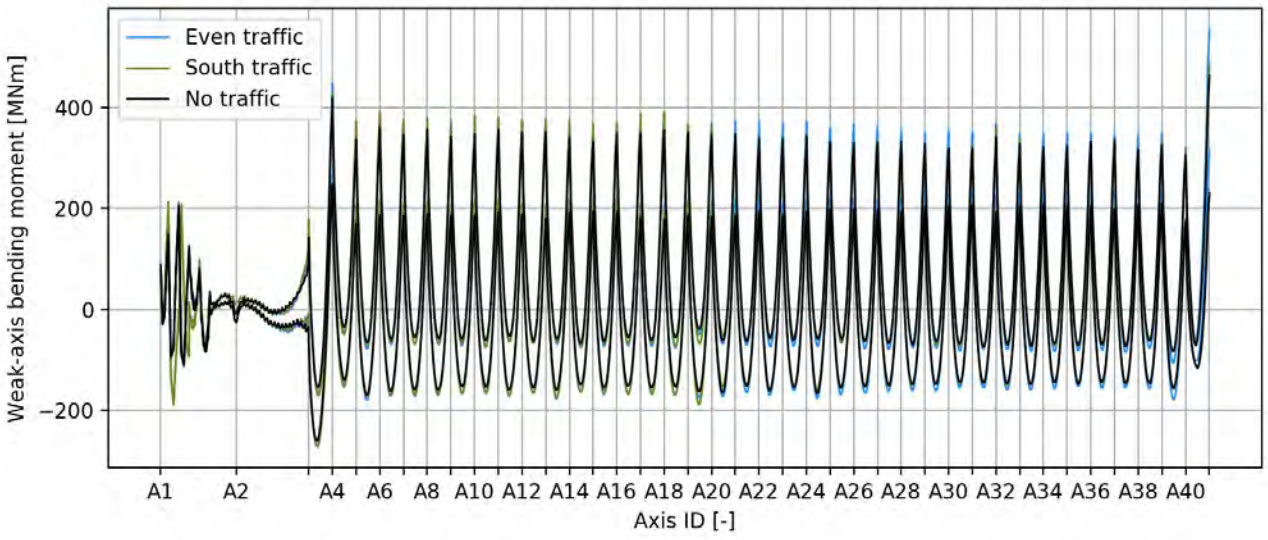

Figure 8-12 Envelope of weak-axis bending moment in a sensitivity check of bridge response with and without effect of traffic in 1-year environmental conditions.

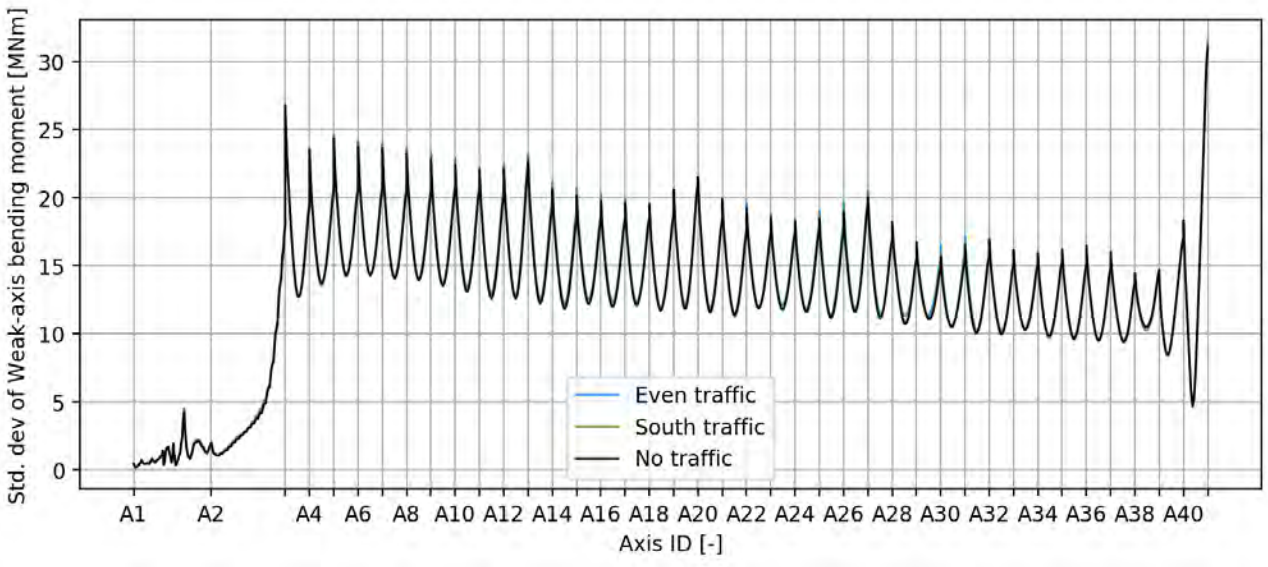

Figure 8-13 Standard deviation of weak-axis bending moment in a sensitivity check of bridge response with and without effect of traffic in 1-year environmental conditions.

8.6 Second order wave loads – wave drift forces

The second order wave loads – wave drift forces study was conducted for concepts K11_07, K12_05, K13_06 and K14_06. The conclusions are considered valid also for concept K12_07.

The response from wind driven waves with and without the effect of second order drift included are compared for the four concepts, using wind sea wave states outlined in Table 8-11. Dynamic effects of drift are marginal for all concepts. For the mean bending moment about the bridge girder strong axis the effect of including mean drift is quite large. For K11_07 the moments are reduced quite substantially. For K12_05 the moments are reduced somewhat. For K13_06 and K14_06 the bending moment about the strong axis in the bridge girder increases somewhat when including drift forces.

None of the effects seen have any significant effect on the stresses in the bridge girder and the effect of drift forces are seen as negligible with respect to design.

Table 8-11: The effect of wave drift is analysed for all concepts using the following 100 year return period wave states

Concept	Run	Hs [m]	Tp [sec]	Direction [deg]
K11_07	0	2.10	5.50	105
K11_07	1	1.40	4.60	195
K11_07	2	2.00	5.20	295
K11_07	3	2.00	5.20	315
K12_05	0	2.10	5.50	95
K12_05	1	1.40	4.60	195
K12_05	2	2.00	5.20	295
K12_05	3	2.00	5.20	315
K13_06	0	2.10	5.50	95
K13_06	1	1.40	4.60	195
K13_06	2	2.00	5.20	295
K13_06	3	2.00	5.20	315
K14_06	0	2.10	5.50	95
K14_06	1	1.40	4.60	195
K14_06	2	2.00	5.20	295
K14_06	3	2.00	5.20	315

8.6.1 Results

In the following axial force and bending moment about strong axis in the bridge girder are plotted for simulations with and without drift forces included. The run with the largest discrepancy is shown for all bridge concepts.

8.6.1.1 1-hour expected maximum

K11_07

Axial force (Run 3)

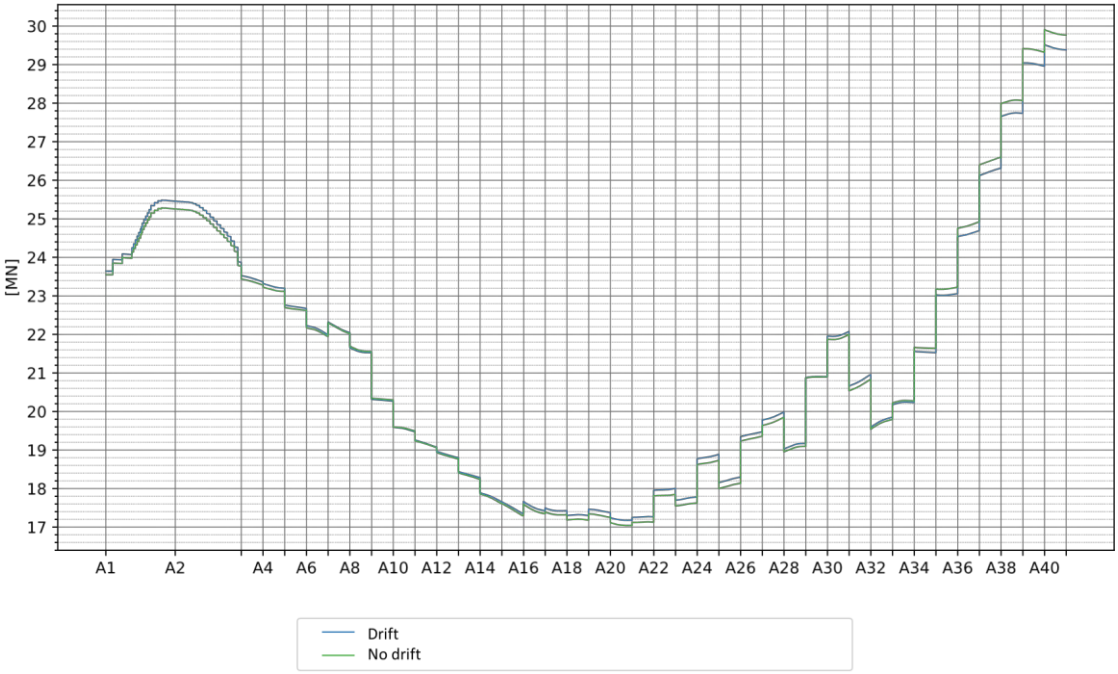

Figure 8-14 Comparison of Axial force for simulations with and without second order drift

Bending moment about strong axis (Run 3)

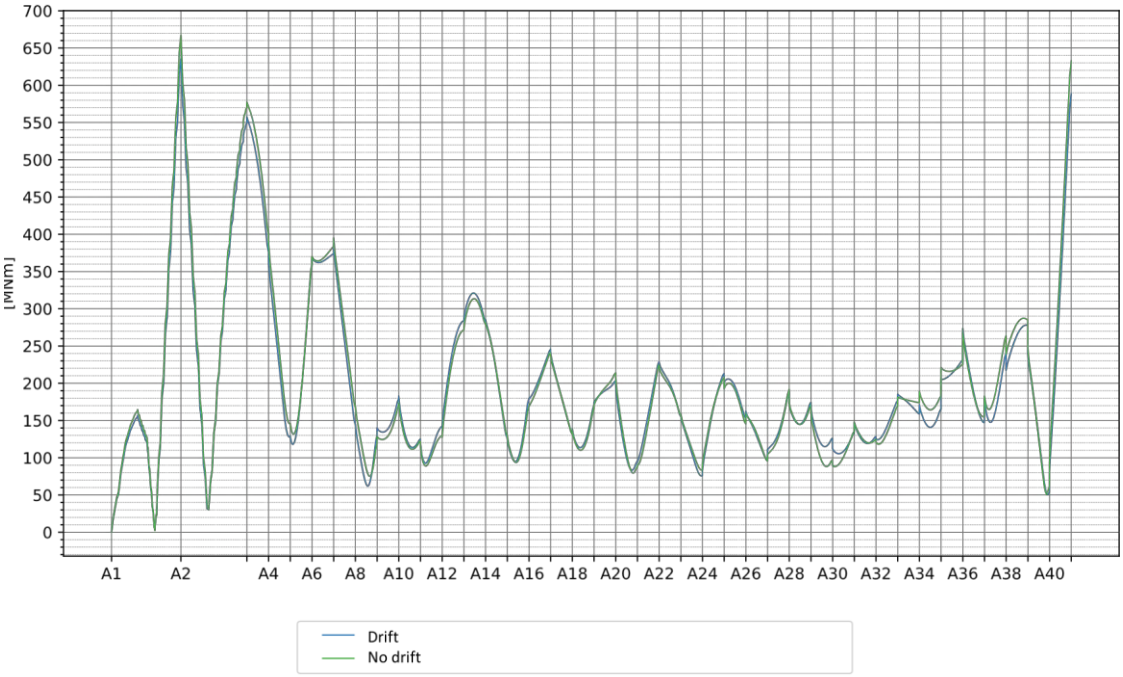

Figure 8-15 Comparison of Bending moment about strong axis for simulations with and without second order drift

K12_05

Axial force (Run 3)

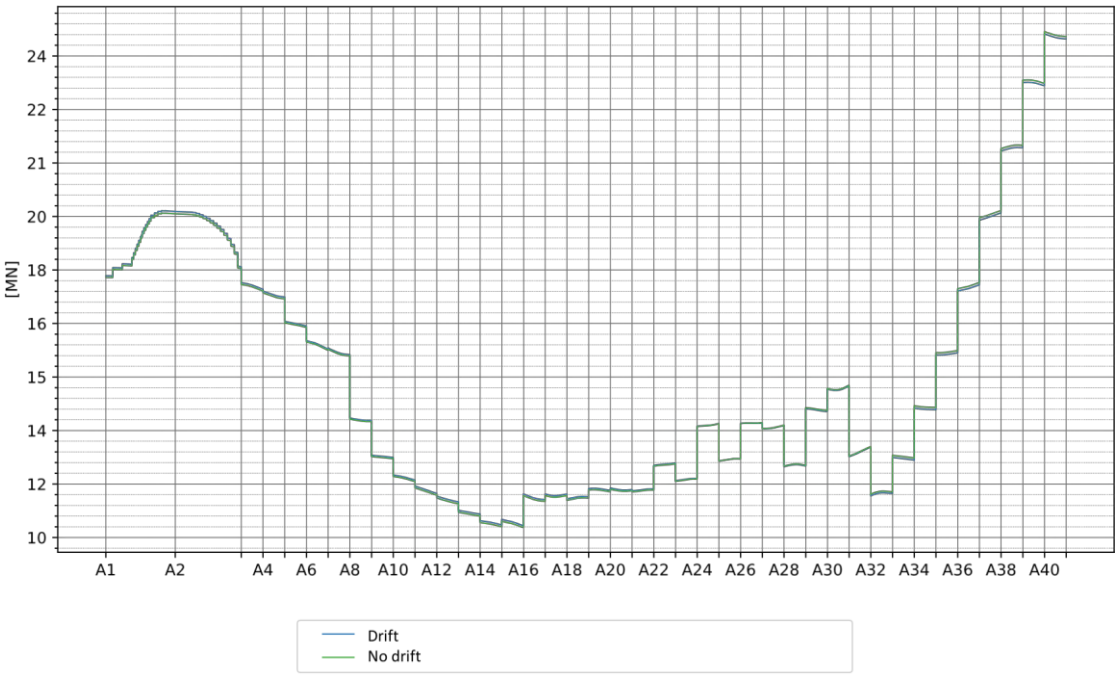

Figure 8-16 Comparison of Axial force for simulations with and without second order drift

Bending moment about strong axis (Run 3)

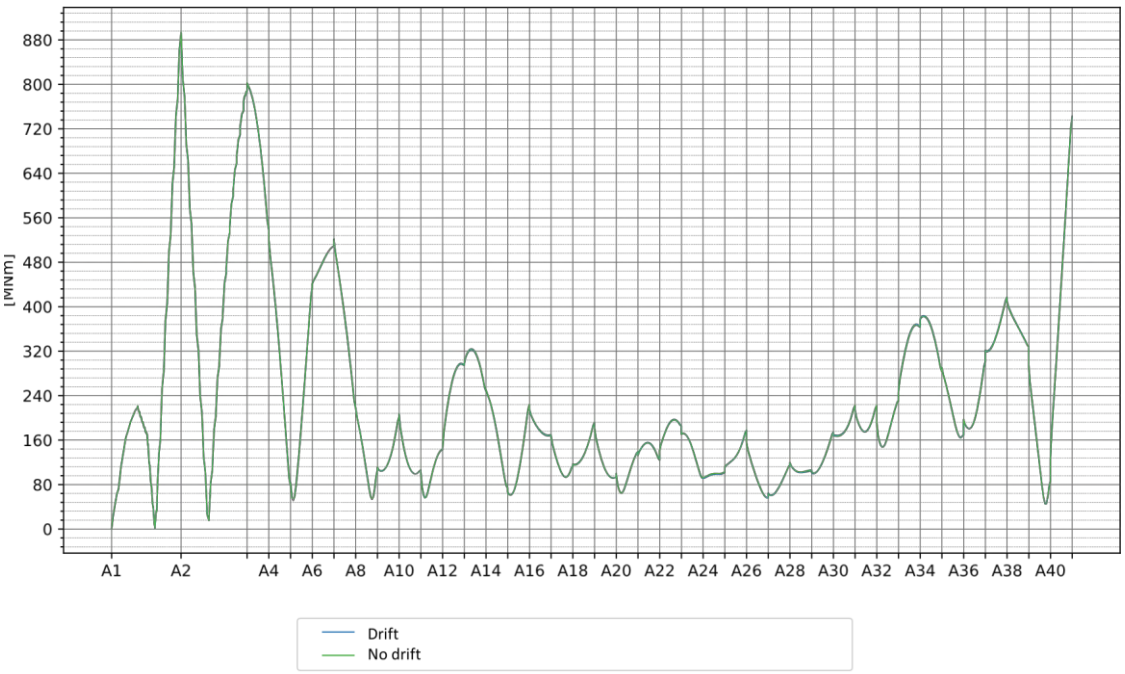

Figure 8-17 Comparison of Bending moment about strong axis for simulations with and without second order drift

K13_06

Axial force (Run 0)

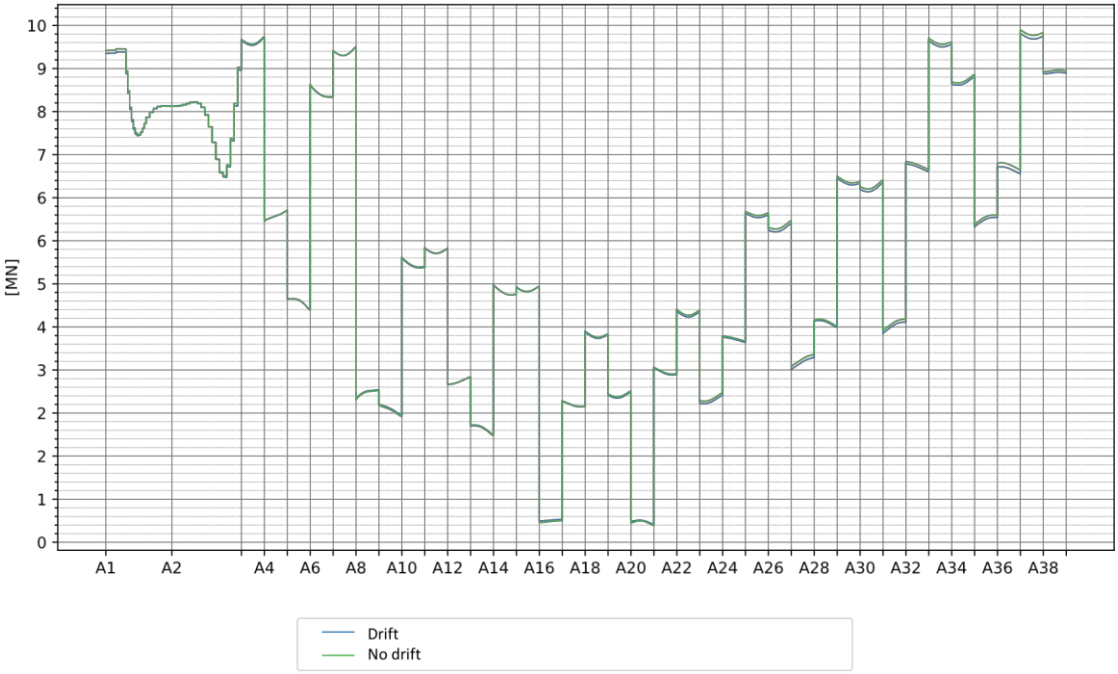

Figure 8-18 Comparison of Axial force for simulations with and without second order drift

Bending moment about strong axis (Run 0)

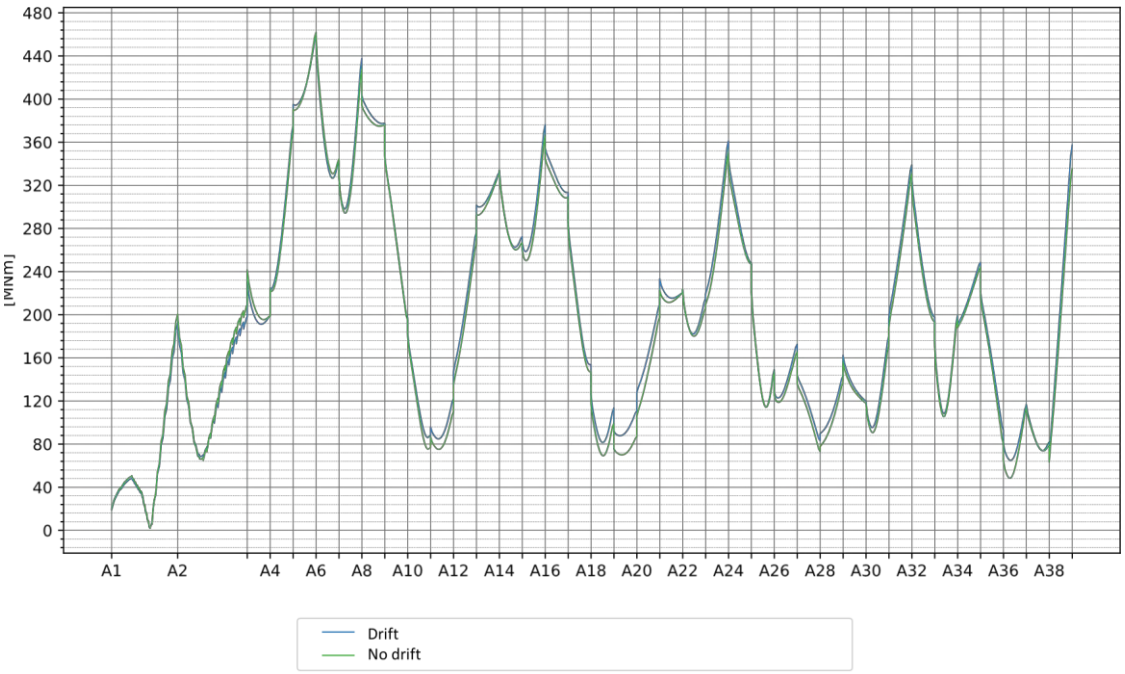

Figure 8-19 Comparison of Bending moment about strong axis for simulations with and without second order drift

K14_06

Axial force (Run 0)

Figure 8-20 Comparison of Axial force for simulations with and without second order drift

Bending moment about strong axis (Run 0)

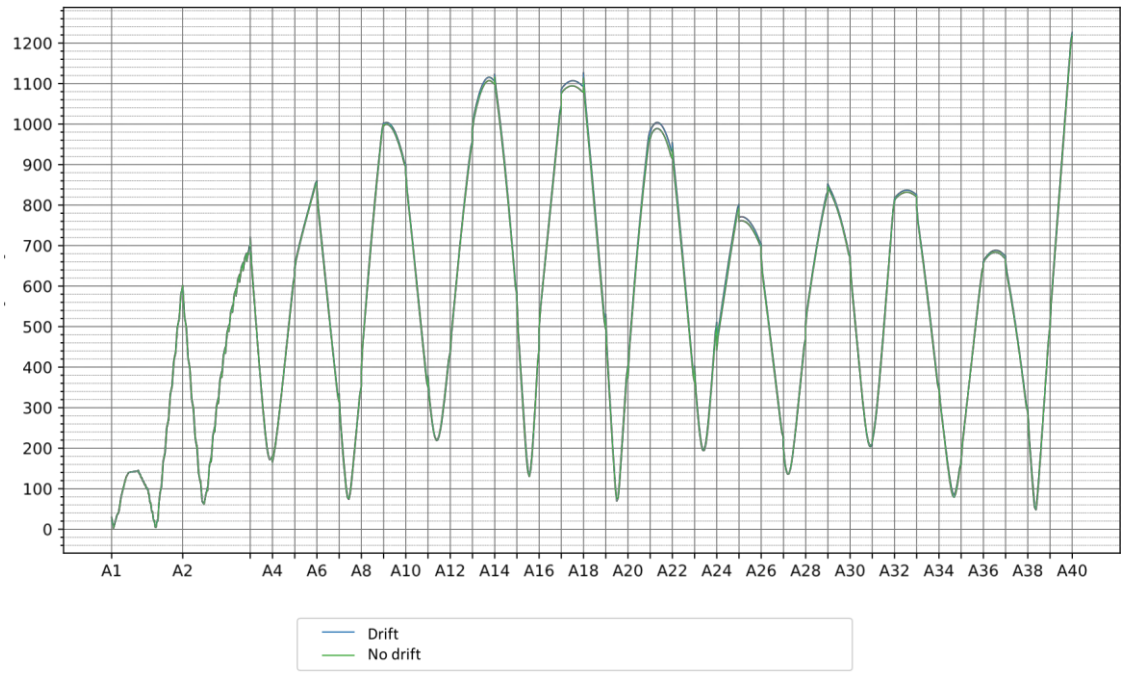

Figure 8-21 Comparison of Bending moment about strong axis for simulations with and without second order drift

8.6.1.2 Mean

K11_07

Axial force (Run 0)

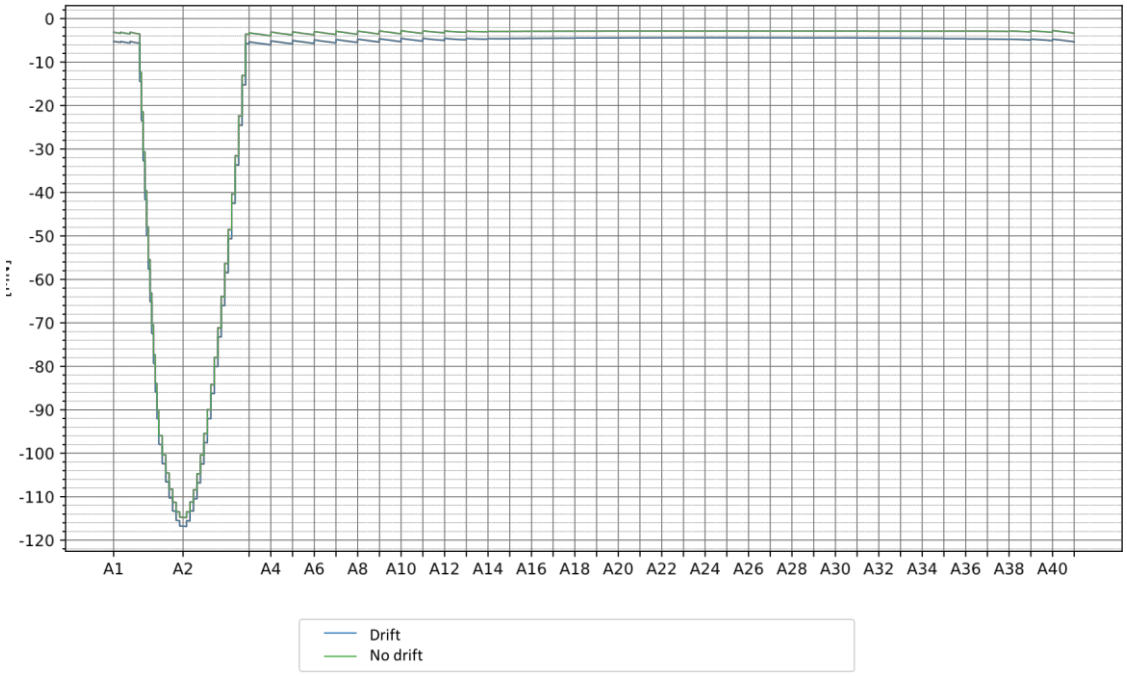

Figure 8-22 Comparison of Axial force for simulations with and without second order drift

Bending moment about strong axis (Run 3)

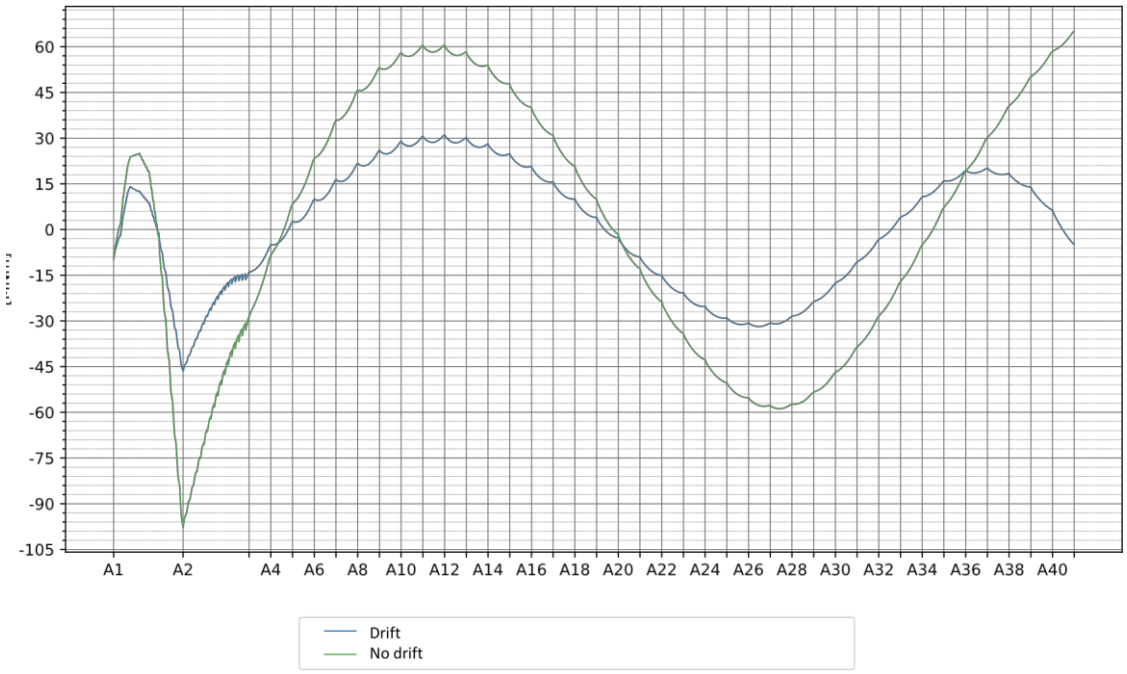

Figure 8-23 Comparison of Bending moment about strong axis for simulations with and without second order drift

K12_05

Axial force (Run 0)

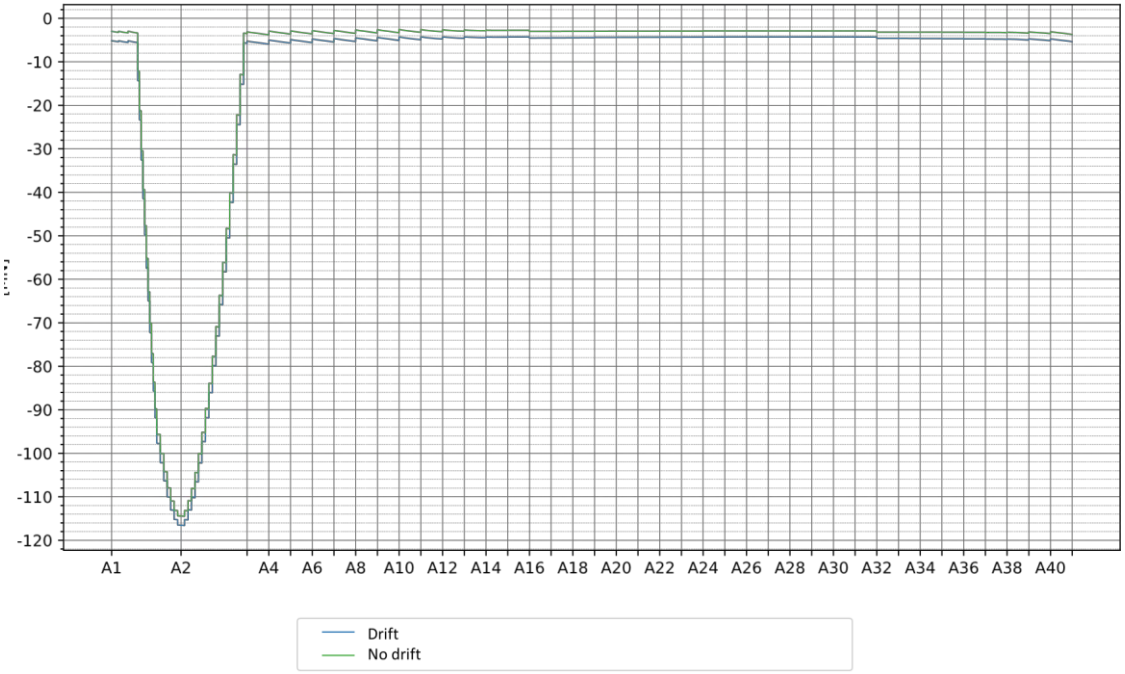

Figure 8-24 Comparison of Axial force for simulations with and without second order drift

Bending moment about strong axis (Run 3)

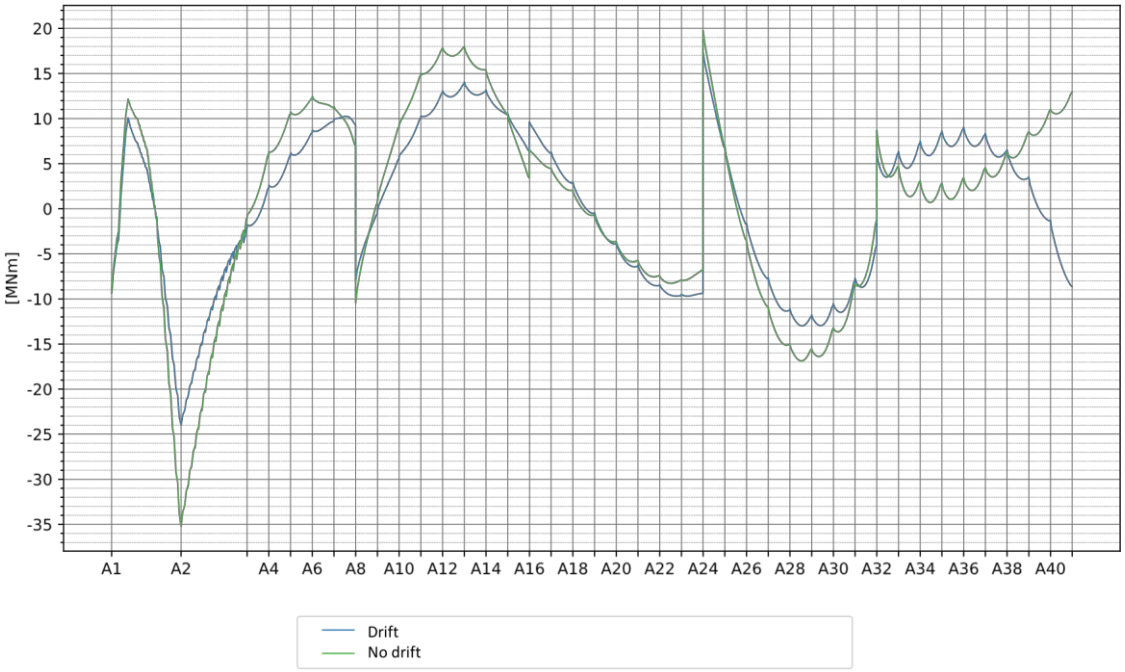

Figure 8-25 Comparison of Bending moment about strong axis for simulations with and without second order drift

K13_06

Axial force (Run 1)

Figure 8-26 Comparison of Axial force for simulations with and without second order drift

Bending moment about strong axis (Run 0)

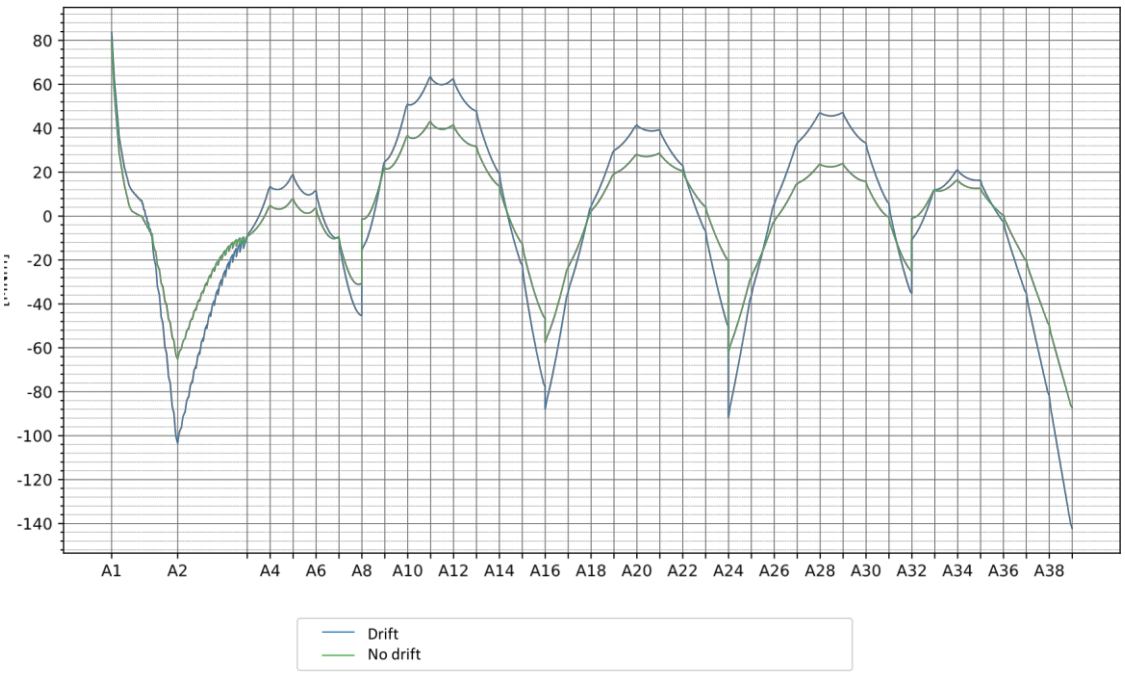

Figure 8-27 Comparison of Bending moment about strong axis for simulations with and without second order drift

K14_06

Axial force (Run 3)

Figure 8-28 Comparison of Axial force for simulations with and without second order drift

Bending moment about strong axis (Run 0)

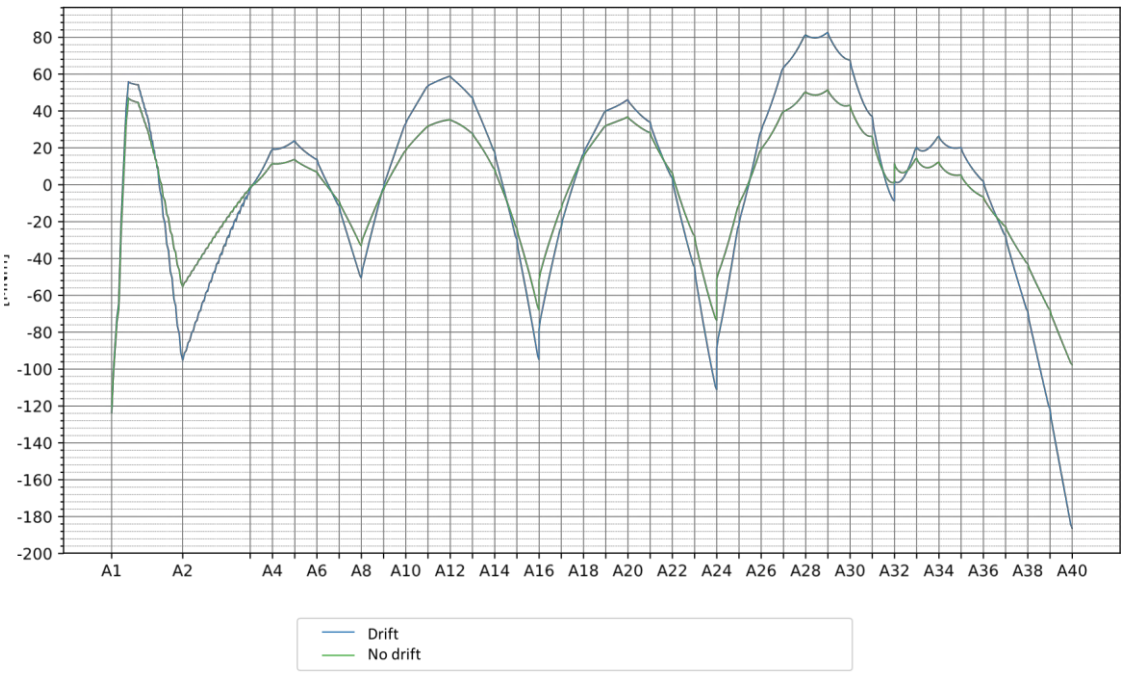

Figure 8-29 Comparison of Bending moment about strong axis for simulations with and without second order drift

9 References

[1] AMC, "SBJ-32-C5-AMC-90-RE-100 : Concept evaluation - main report Rev. 0," 24.05.2019.

[2] AMC, "SBJ-33-C5-AMC-90-RE-100 : Preferred solution, K12 - main report Rev. 0," 15-08-2019.

[3] AMC, "SBJ-33-C5-AMC-90-RE-106 : Appendix F: Global Analyses - Modelling and assumptions Rev. 0," 15-08-2019.

[4] AMC, "10205546-11-NOT-088 : Variable static loads," 29.03.2019.

[5] Statens Vegvesen, "SBJ-01-C4-SVV-01-BA-001 MetOcean Design basis Rev. 1," 30.11.18.

[6] DNVGL, "DNVGL-RP-C103 Column-stabilized units," July 2015.

[7] AMC, "10205546-11-NOT-059 Estimation of extreme response using the AUR method. Rev. 0," 29.03.2019.

[8] Orcina, "https://www.orcina.com/SoftwareProducts/OrcaFlex/Documentation/Help/Content/html/Dynamicanalysis, Frequencydomainsolution.htm#Statistics," 2019. [Online].

[9] Statens Vegvesen, "SBJ-32-C4-SVV-90-BA-001 Design basis. Rev. 0," 19.11.2018.

[10] 2631-1, ISO, "Mechanical vibration and shock - Evaluation of human exposure to whole body vibration - Part 1: General requirements," 1997.

[11] Statens Vegvesen, "Vehicle properties for comfort evaluation," 04.02.2019.

[12] SVV, "304624-1-A-0021 Egenskaper kjøretøy, eRoom," 18 Dec 2018.

[13] SVV, "304624-1-A-0035 - Kjøretøy oppdatert med koeffisienter vind og sideveis dempning," 4 Feb 2019.

[14] AMC, "SBJ-33-C5-AMC-27-RE-110 : Appendix J: Ship collision Rev. 0," 15-08-2019.

[15] F.-I. G. Giske, "Long-Term Extreme Response Analysis of Marine Structures Using Inverse Reliability Methods," Norwegian University of Science and Technology (NTNU), Trondheim, 2017.

[16] F.-I. G. Giske, K.-A. Kvåle, B. J. Leira and O. Øiseth, "Long-term extreme response analysis of a long-span pontoon bridge," *Marine Structures,* vol. 58, pp. 154-171, 2018.

[17] AMC, "10205546-11-NOT-095 Rev1. Analytical mooring line damping," 2019.

[18] SVV, "SBJ-01-C3-SVV-01-BA-001 Design Basis MetOcean rev C," 2017.

[19] AMC, "SBJ-33-C5-AMC-26-RE-113 : Appendix M: Anchor systems Rev. 0," 15-08-2019.

[20] AMC, "SBJ-33-C5-AMC-20-RE-105 : Appendix E: Aerodynamics Rev. 0," 15-08-2019.

[21] L. D. Zhua and Y. Xub, "Buffeting response of long-span cable-supported bridges under skew winds. Part 1: theory," *Journal of Sound and Vibration ,* vol. 281, p. 647–673, 1995.

10 Enclosures

The following documents are enclosed to this report, containing more details on bridge response. The direct method is described in section 2.7.1 and the factorized method in section 2.7.2. Eigenmodes are extracted from models with mooring represented as linear springs, so local eigenmodes in the mooring system are not shown.

Enclosure 1. K12_07 Eigenmodes

Enclosure 2. K12_07 Load combinations direct method

Enclosure 3. K12_07 Load combinations factorized method

Enclosure 4. K12_07 Load combinations AUR method 100 year

Enclosure 5. K12_06 Load combinations AUR method 10 000 year

Enclosure 6. K12_07 screening windsea 1yr

Enclosure 7. K12_07 screening windsea 100yr

Enclosure 8. K12_07 screening windsea 10 000yr

Enclosure 9. K12_07 screening swell 1yr

Enclosure 10. K12_07 screening swell 100yr

Enclosure 11. K12_07 screening swell 10 000yr

Enclosure 12. K12_07 Load combination motions

Enclosure 13. AMC, “10205546-11-NOT-088 : AMC status 2 - Variable static loads,” 29.03.2019.

Enclosure 14. AMC, “10205546-11-NOT-059 : AMC status 2 - Estimation of extreme response using the AUR method. Rev. 0,” 29.03.2019.

Enclosure 15. AMC, “10205546-11-NOT-193 : Long-term wave response,” 15.08.2019.

Enclosure 16. AMC, “10205546-11-NOT-196 : Uncertainty assessment” 15.08.2019

Enclosure 17. K12_07 Current response with 100-year return period

Concept development, floating bridge E39 Bjørnafjorden

Appendix G – Enclosure 1

Eigenmodes

Plot of modes for K12_07_linkmodel

June 13, 2019

Contents

1 Mode maps

1.1 Vertical displacement Mode map 0

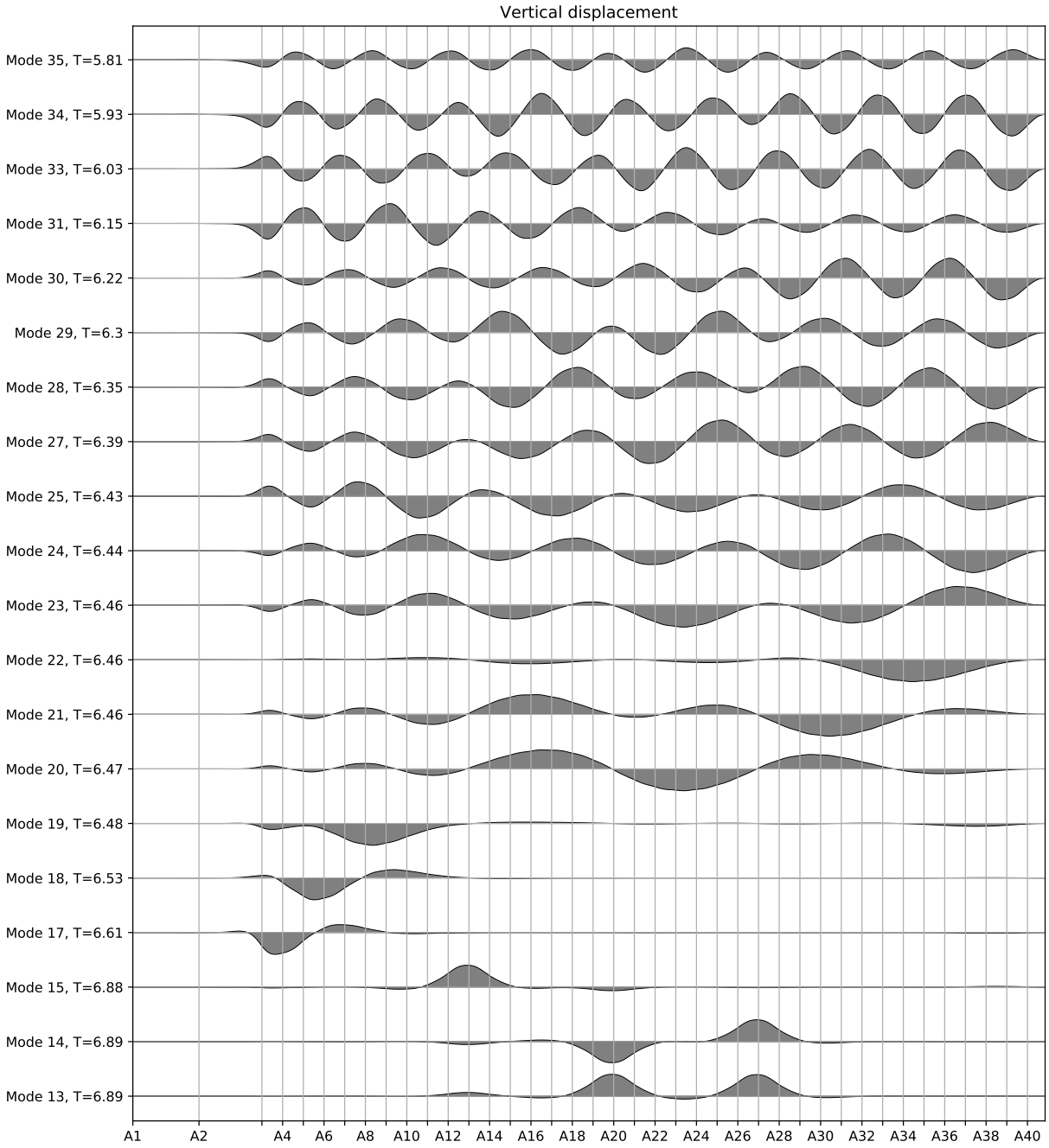

1.2 Vertical displacement Mode map 1

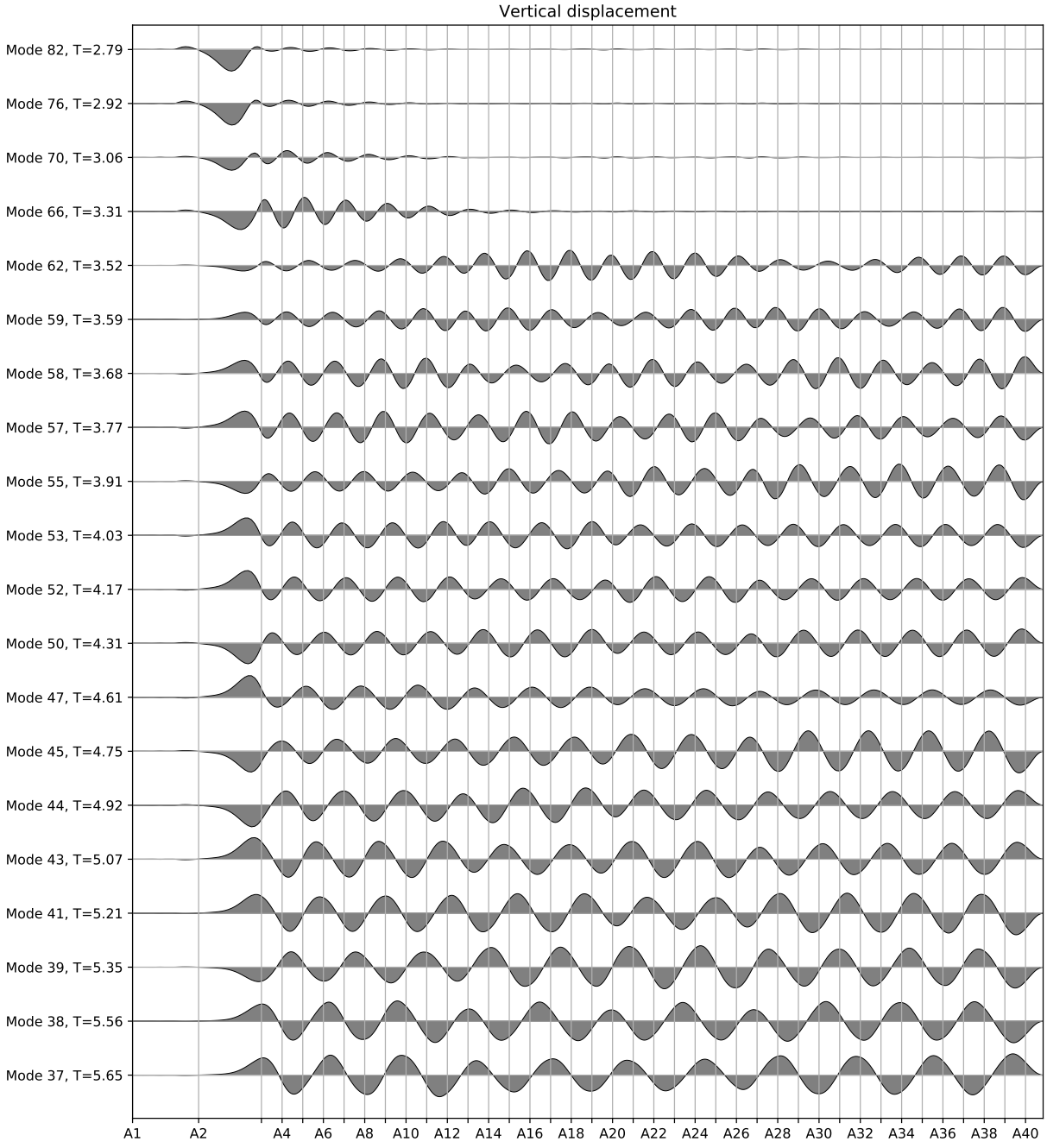

1.3 Vertical displacement Mode map 2

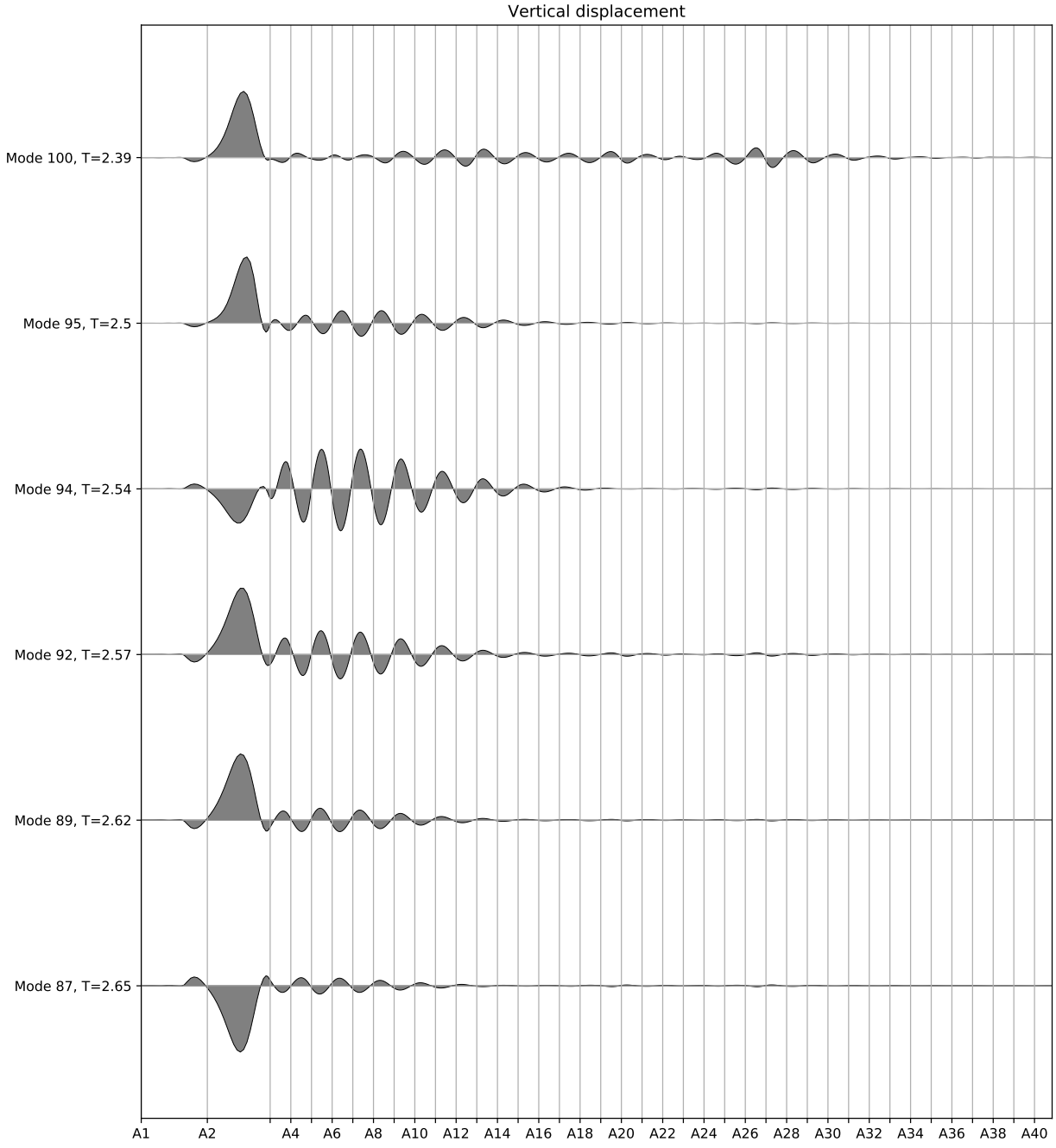

1.4 Transversal displacement Mode map 0

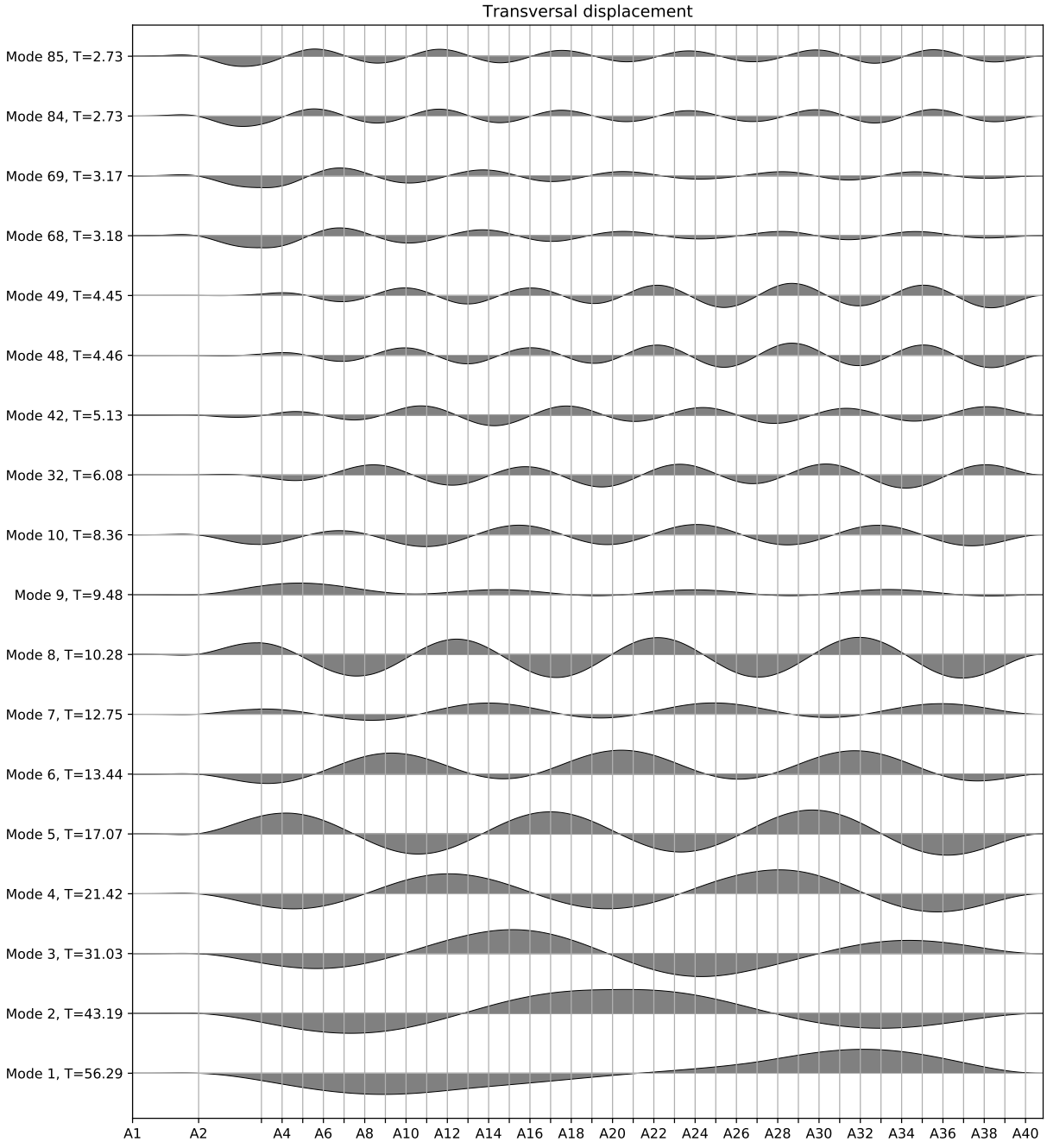

1.5 Longitudinal displacement Mode map 0

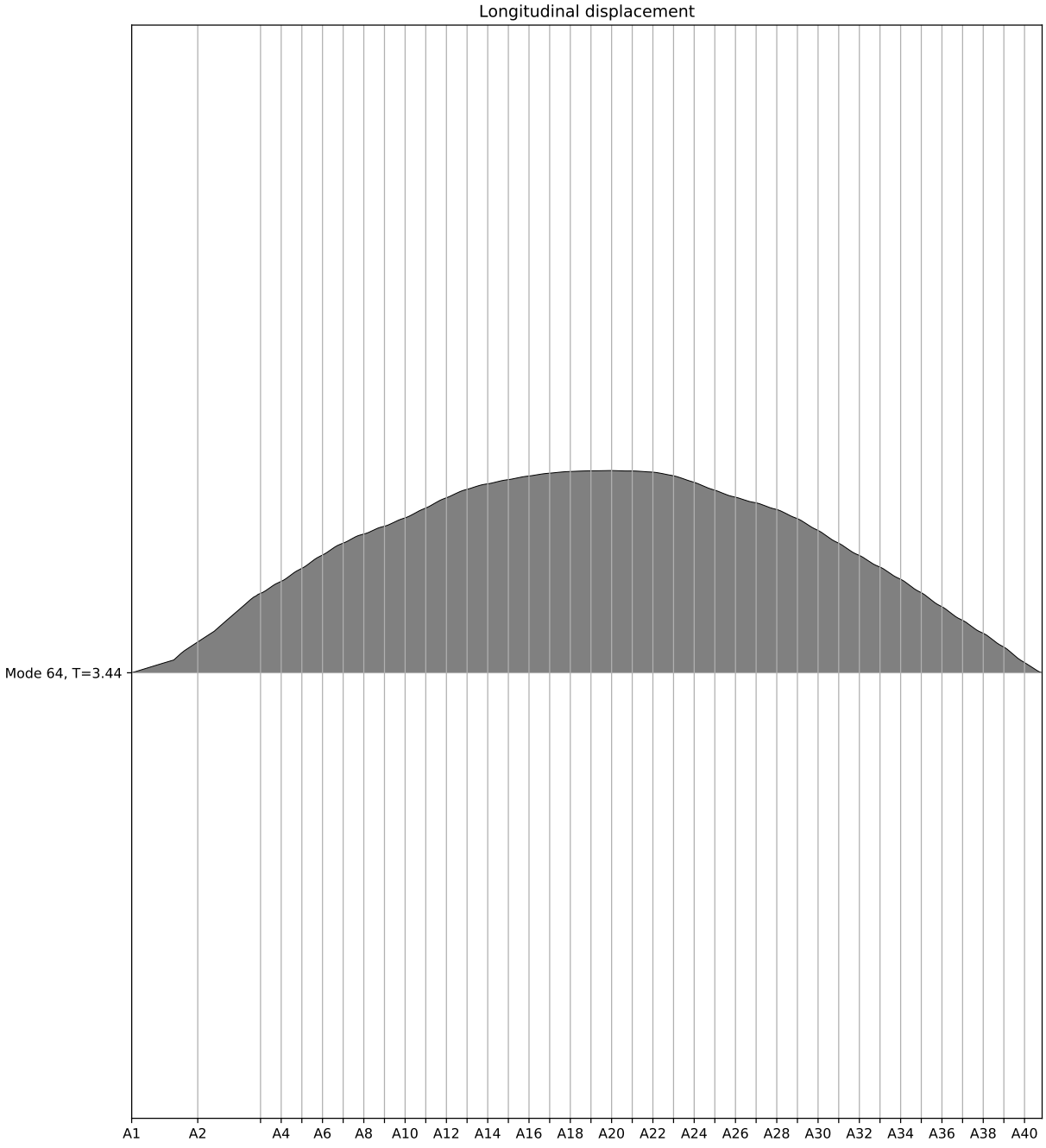

1.6 Tranverse Rotation Mode map 0

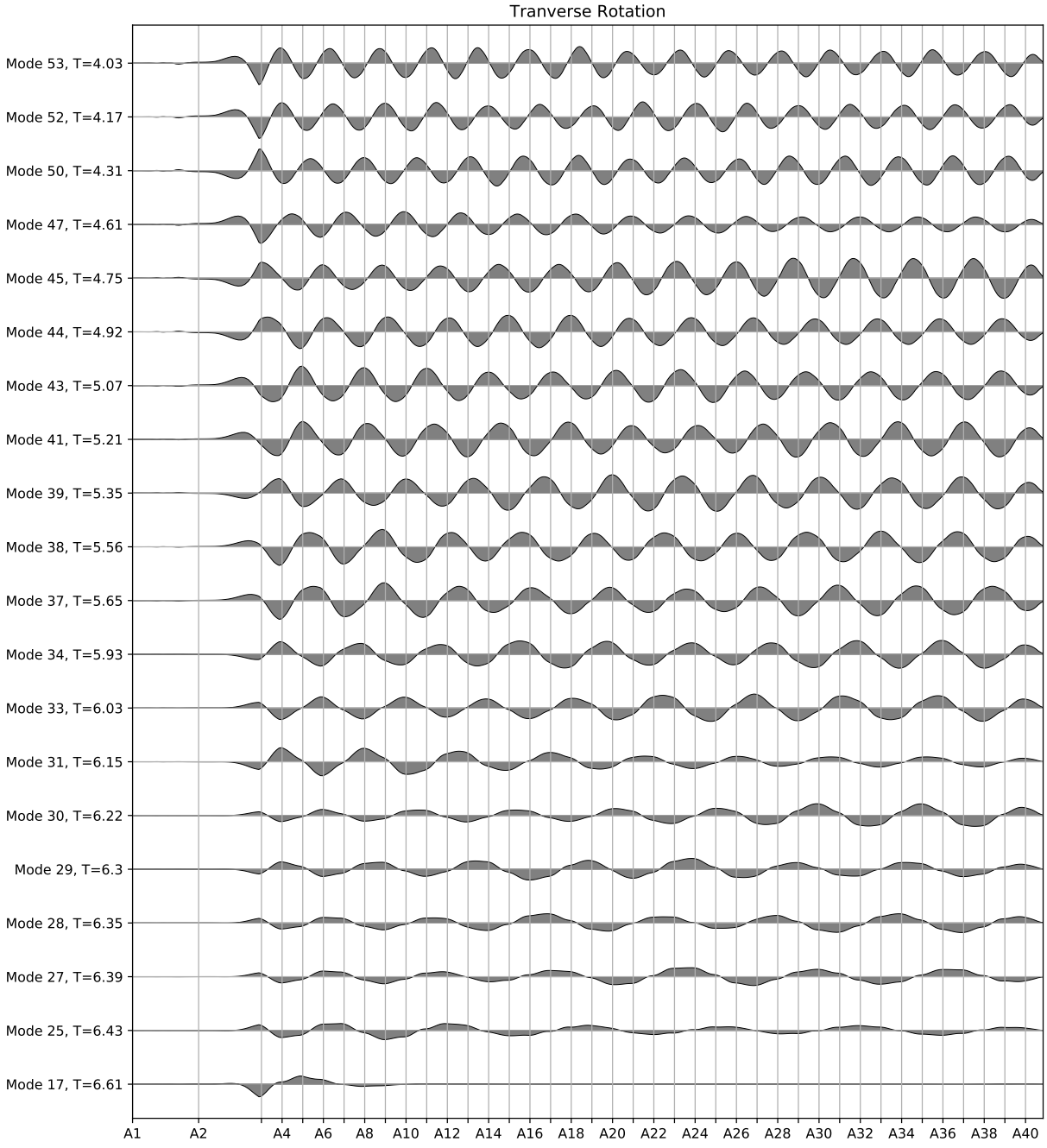

1.7 Tranverse Rotation Mode map 1

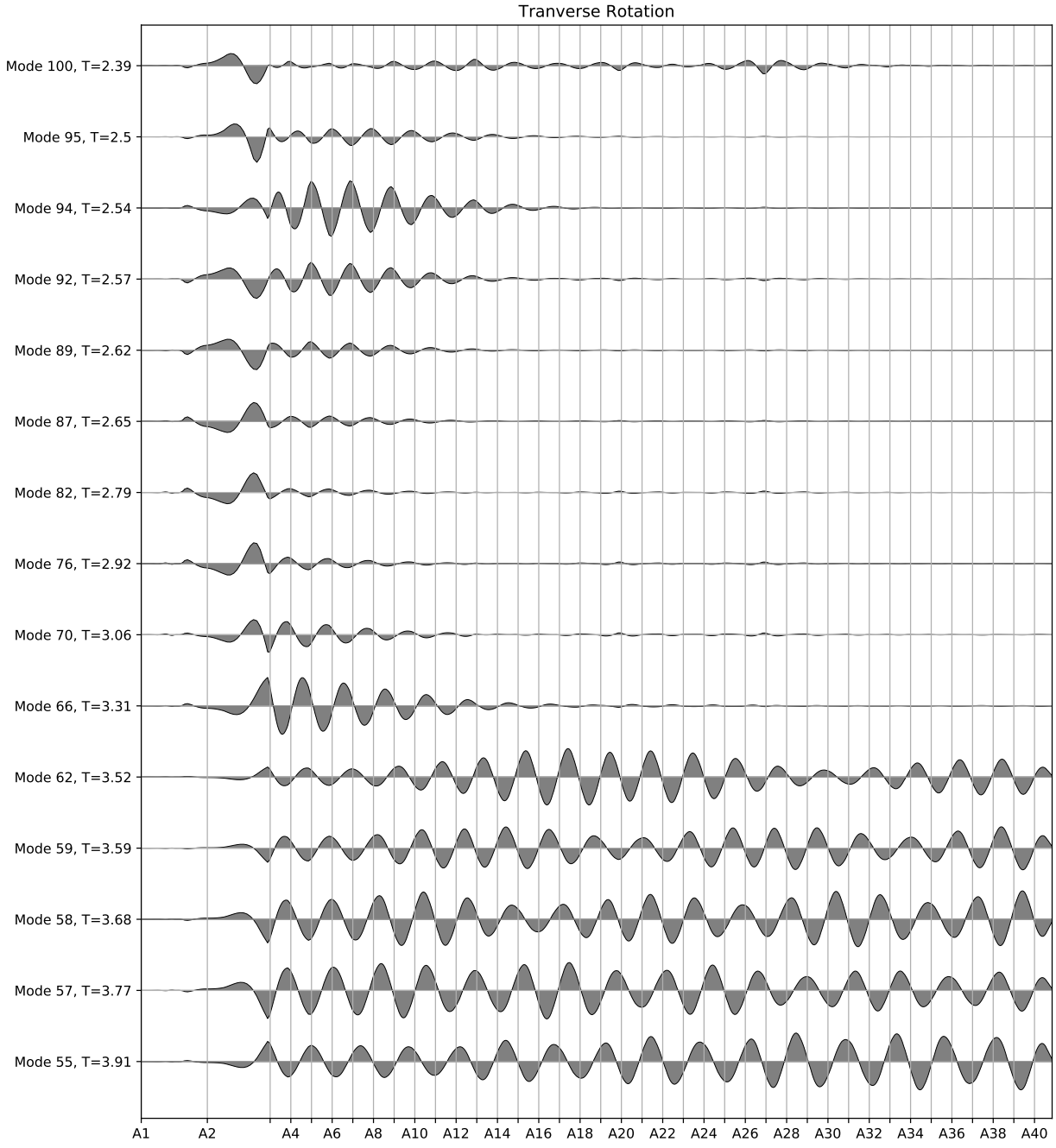

1.8 Longitudinal Rotation Mode map 0

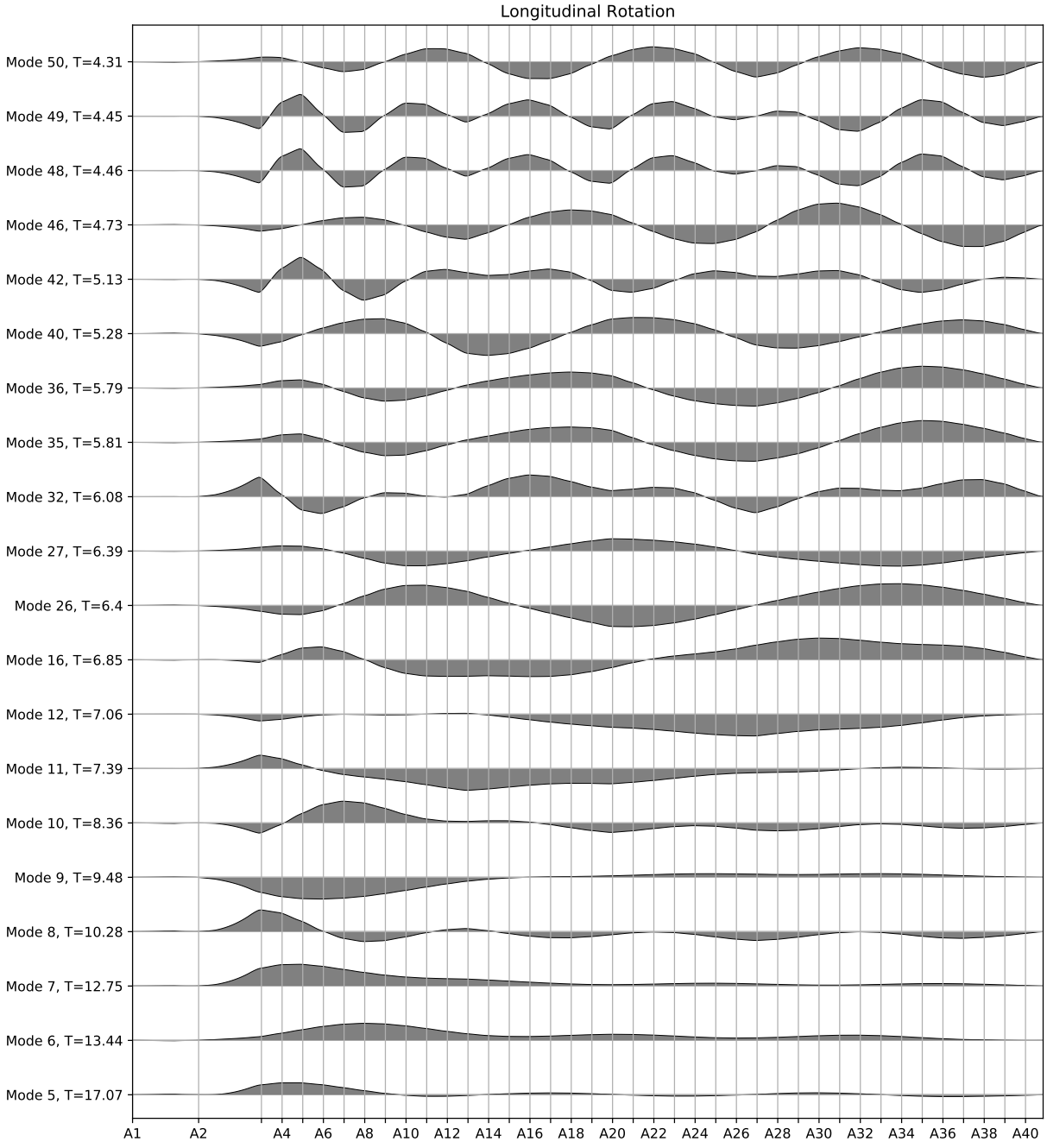

1.9 Longitudinal Rotation Mode map 1

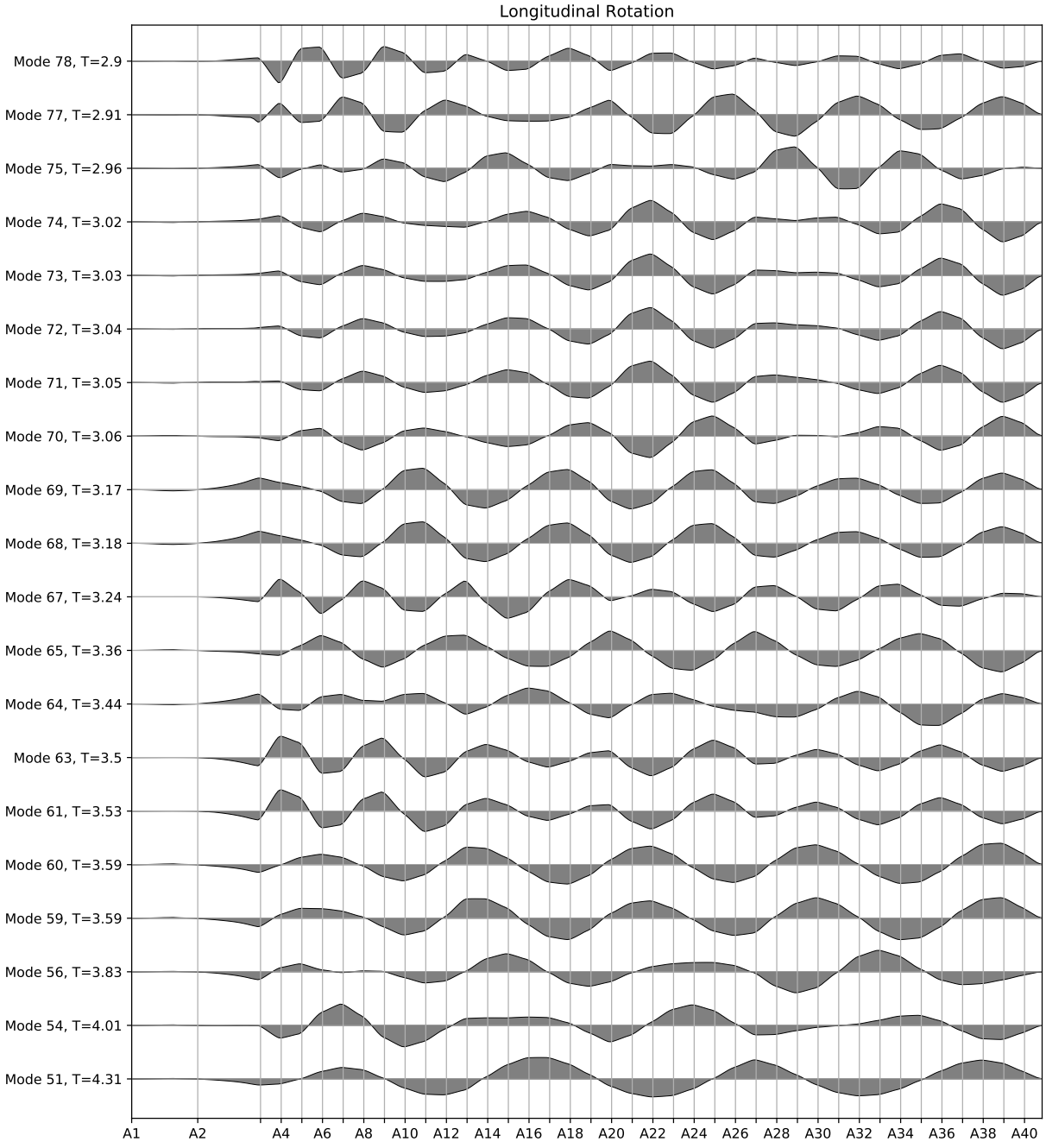

1.10 Longitudinal Rotation Mode map 2